ELECTRON PRECIPITATION AND IONOSPHERIC DISTURBANCE.

A THESIS SUBMITTED FOR THE DEGREE OF MASTER OF SCIENCE AT RHODES UNIVERSITY.

BY:

MARSHA R. TORR.

JANUARY, 1966.

Except where it is clear from the text that I am describing the work of others, the work described in this Thesis is my own.

Marsha R. Torr

ACKNOWLEDGEMENTS.

I am extremely grateful to Professor J.A. Gledhill, the Supervisor of this research, for numerous valuable discussions and suggestions. Secondly, I would like to thank Douglas Torr, in conjunction with whom the work presented in section 4.5 of this Thesis was carried out. The Alouette electron flux data, which proved invaluable, was supplied by Dr. I.B. McDiarmid of the Canadian National Research Council. I am also indebted to the many ionospheric stations mentioned in this Thesis for their data. The data for Sanae is used with the permission of the South African Department of Transport. Part of this research was performed with the support of a grant from the Council for Scientific and Industrial Research.

C O N T E N T S.

ELECTRON PRECIPITATION AND IONOSPHERIC DISTURBANCE.

Introduction:

The minimum in the scalar magnitude of the geographic total field, which lies off the coast of Brazil, allows the mirror points of trapped particles to dip low into the atmosphere over the South Atlantic Ocean, resulting in two regions of maximum intensity of preciptated particles in that region, one from the inner belt and one from the outer. High charged particle fluxes have been observed at low altitudes over these regions by satellites Sputnik 5 and 6 (Ginsburg et al, 1961) and Discoverer 31 (Seward and Kornblum, 1963) amongst others. The more southerly of these two regions acts as a sink for electrons from the outer radiation belt and will be referred to in what follows as the Southern Radiation Anomaly.

Gledhill and van Rooyen (1963) predicted that the energy deposited in the upper atmosphere by these charged particles would be sufficient to give rise to enhanced geophysical effects such as auroral emission, X-rays and ionization and heating of the upper atmosphere in this region.

Although some of these effects have been correlated with precipitated electrons, no definite relation had until now been established between ionospheric effects and precipitated particles. The aim of this thesis was to investigate such a relationship and the results were extremely

2/.....

successful. It will be shown conclusively in what follows, that the precipitation of electrons can account for the ionospheric disturbances defined by a disturbance criterion at all stations around L=4.

Part I describes the exploration of the radiation belts and the magnetosphere with rockets and satellites. The resulting theoretical models based on the observations are discussed. A brief review is given of the work that has been done to date to derive equations for the loss and replenishment of particles in the belts. Because of the complexity of these and the number of doubtful factors involved, a simple model of injection of electrons into the outer belt is devised, giving average values of trapped and precipitated electron fluxes at any point around L=4.

In Part II, this model is employed together with the disturbance criterion of Gledhill and Torr (1965) to examine the relationship between ionospheric disturbances and electron fluxes. Also the energy range of the precipitated particles is examined.

3/.....

CHAPTER I.

THE MAGNETOSPHERE.

1.1 Introduction.

In the past the geomagnetic field of the earth has been approximated to by the field of a magnetic dipole placed at the centre of the earth with its axis at an angle of 11.4° to the axis of rotation. In the absence of external influences, this field would extend indefinitely (becoming weaker with increasing distance from the earth) into interplanetary space. However, since 1958 direct measurements of the outer geomagnetic field by means of rocket probes and artificial satellites have drastically revised this picture.

Streams of charged particles from the sun together with electrical currents in the radiation belts distort the symmetrical dipole field, confining it to an elongated drop-shaped volume in space. This region is called the magnetosphere.

It was noticed that large solar flares were often followed, with a delay time of one to three days, by geomagnetic storms, generally beginning with sharp increases in the geomagnetic field strength over large areas of the earth's surface. In the light of such observations, Chapman and Ferraro, (1931, 1933, 1940) proposed a theory of magnetic storms in which the increase in the field strength was

4/.....

caused by compression of the geomagnetic field by a plasma cloud from the sun. On encountering the geomagnetic field, electric currents would be induced in the cloud in such a way that the resulting magnetic field would cancel the normal geomagnetic field in the cloud and strengthen the normal field in the region between the cloud and the earth. The cloud would then continue to advance until its forward momentum was expended in compressing the geomagnetic field, the resultant boundary remaining in the same position while the flow of plasma in the cloud was constant.

Observations on the tails of comets (Biermann, 1957) showed that the streams of particles formed a continuously blowing 'wind' which, although it might intensify when the sun was very active, was continually present. Chapman found that the solar corona, although extremely thin at this distance (100 to 1000 hydrogen atoms per c.c.), extended as far as the earth. Parker then showed that the solar corona and the solar wind were the same thing. The corona, expanding with increasing distance from the sun, streams past the earth with a velocity of $\sim$400 Km/sec. The boundary of the magnetosphere, the magnetopause, would fluctuate due to increases in the solar wind caused by solar flares and other solar activity.

5/.....

The theory of Chapman and Ferraro (1931 - 1940) predicted that the magnetosphere should be compressed on the sunward side and swept back on the right side by the solar wind. Calculations showed that the magnetopause should lie between 5 to 10 earth radii on the sunward side.

1.2 Satellite Exploration:

A number of magnetomer carrying satellites have now been launched and the trajectories of some of these are shown in Figure 1.

Pioneer 1 (Sonett et al, 1960) provided the first direct data concerning the outer magnetosphere. These indicate an inverse-cube field decrease over the interval 3.7 to 13.6 R_E (earth radii), with a sudden decrease in the field at 13.6 R_E from 50 γ to 5 γ. The field over the region 12.3 to 14.8 R_E was found to be very fluctuating. Similarly Pioneer 5 (Coleman et al, 1960) observed a gradually decreasing field out to $\sim$ 8 R_E, a strongly fluctuating field beyond 10 R_E and a sharp decrease between 15 and 20 R_E.

Explorer 10 was launched with the specific objective of obtaining vector magnetic field and plasma measurements, (Heppner et al, 1963). Beyond 8 R_E the field lines appeared to be pulled away from the earth and the field strength was

6/.....

FIGURE 1.

Diagram of the trajectories of a number of Magnetometer carrying satellites, compiled from diagrams by Cahill (1964), and Ness et al, (1965).

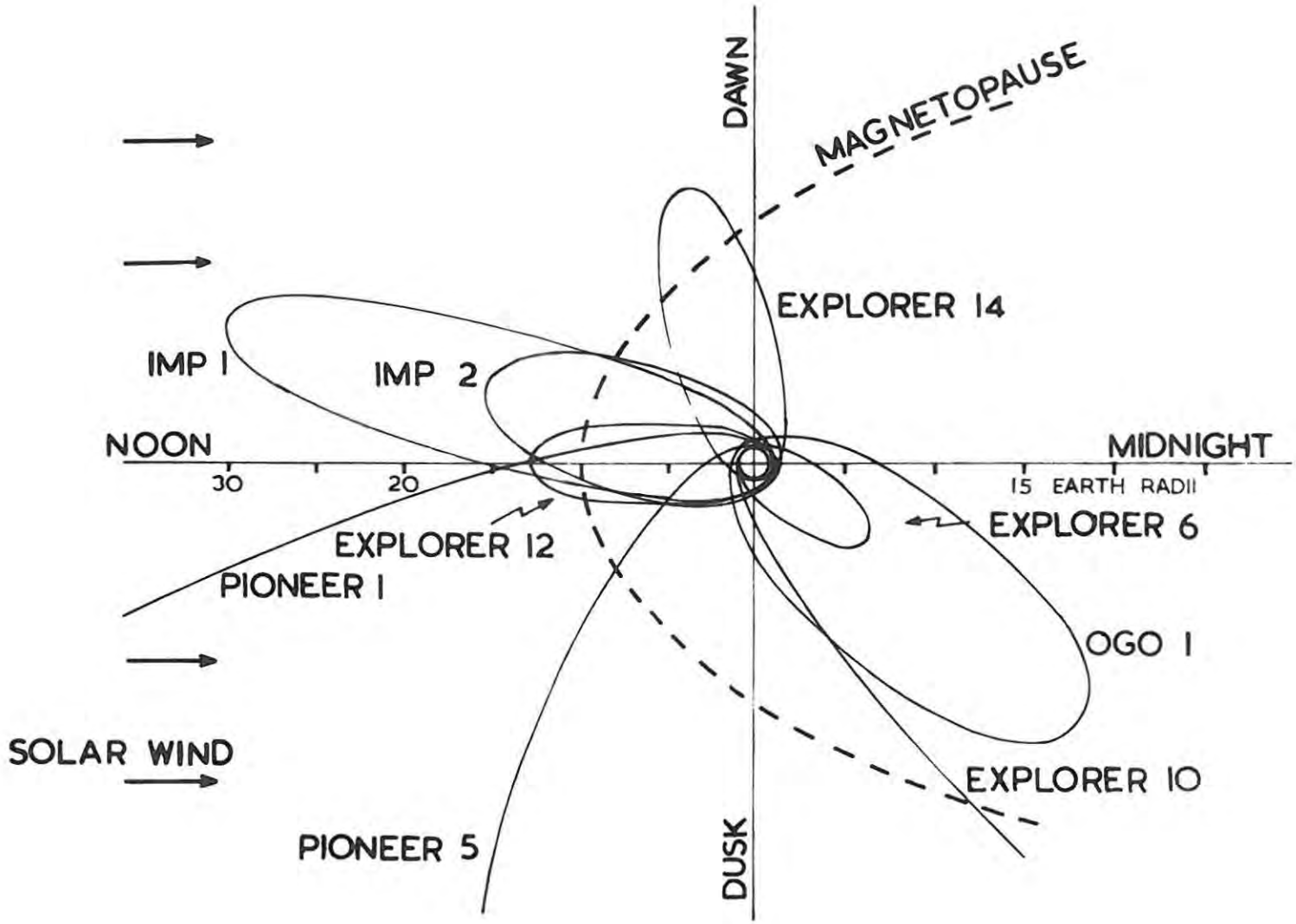
DAWN
MAGNETOPAUSE
EXPLORER 14
IMP 1
IMP 2
NOON
MIDNIGHT
30
20
15 EARTH RADII
EXPLORER 12
EXPLORER 6
PIONEER 1
OGO 1
SOLAR WIND
EXPLORER 10
PIONEER 5
DUSK

higher than predicted. From 8 to 22 R_E the field dropped gradually in strength from ~30 γ to 20 γ. At 22 RE it dropped sharply to 10 γ and the direction of the field changed abruptly. Also high-velocity plasma was detected for the first time at this point. The strength and direction of the field showed large fluctuations beyond 22 R_E indicating that the satellite passed through the magnetopause at ~22 R_E. Beyond 22 R_E the satellite at times found periods of plasma alternating with plasma-free periods, suggesting that the magnetopause was moving back and forth across the trajectory of the satellite.

Explorer 12 (Cahill and Amazeen, 1963) provided magnetic vector measurements for several months on the sunlit side of the earth. Again the most striking feature of the observations was the termination of the earth's magnetic field shown by the abrupt change of direction. During magnetically quiet periods, the boundary at the sub-solar point was at ~10 R_E. The magnitude of the field just inside the boundary was ~125 γ, whereas for the dipole field it would be 60 γ, i.e. the field magnitude was doubled by solar wind pressure. The thickness of the magnetopause was found to be ~100 to 1000 km. (The satellite also observed a discontinuity in intensity of geomagnetically trapped electrons having energies $\geq$40 kevat the boundary (Freeman et al, 1963)).

7/.....

Explorer 14 (Frank et al, 1963) was launched with an apogee of 16 R_E. However, as the earth rotated round the sun, and the satellite moved round into the tail of the magnetosphere, it ceased to observe the magnetopause which was then presumed to be beyond 16 R_E.

The first really accurate measurements of the strength field were provided by the Interplanetary Monitoring Platforms, IMP 1 and 2, and the Orbiting Geophysical Observatory, OGO 1, (Ness et al, 1964; Wolfe et al, 1965) which greatly elaborated on the earlier findings.

1.3. DeductionsConcerning the Magnetosphere:

In the light of all the above information the following picture of the magnetosphere may be drawn (see Figure 2). It extends to approximately 10 RE at the sub-solar point and at least as far as 30 RE on the dark side. The magnetosphere is bounded by the magnetopause which is ~100 to 1000 km thick. Beyond the magnetopause, satellites have detected a transition region, a turbulent region associated with the interaction of the solar wind with the geomagnetic field, in which the strength and direction of the magnetic field is very fluctuating and which has two characteristic boundary surfaces. One is

FIGURE 2.

A summary of the results from the Imp 1 magnetic field experiment (Ness et al, 1965), showing the main features of the magnetosphere.

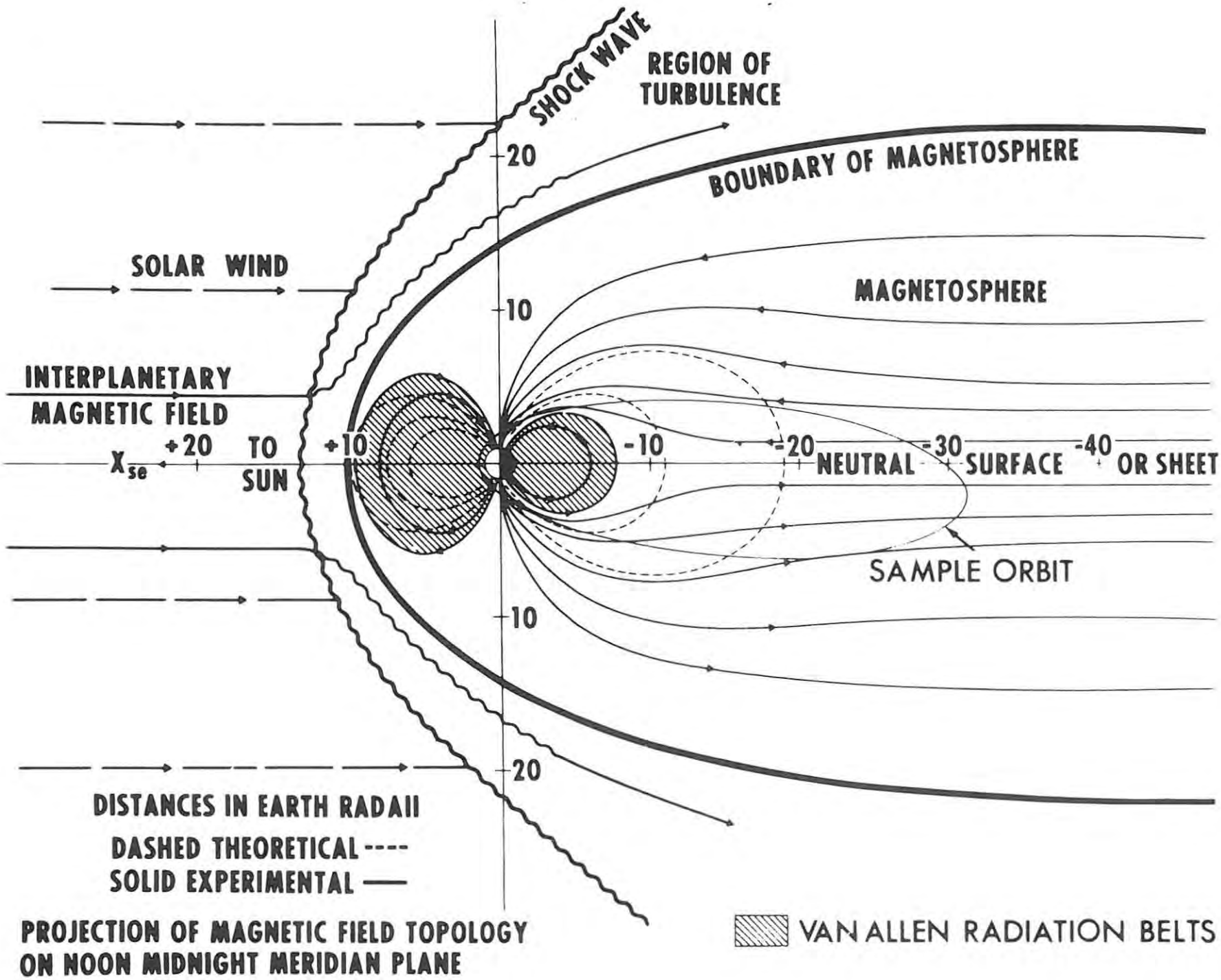
SHOCK WAVE
REGION OF TURBULENCE
BOUNDARY OF MAGNETOSPHERE
SOLAR WIND
MAGNETOSPHERE
INTERPLANETARY MAGNETIC FIELD
X_{se}
+20
TO SUN
+10
-10
-20
-30
-40
NEUTRAL SURFACE OR SHEET
SAMPLE ORBIT
20
10
10
20
DISTANCES IN EARTH RADAII
DASHED THEORETICAL ----
SOLID EXPERIMENTAL ——
PROJECTION OF MAGNETIC FIELD TOPOLOGY
ON NOON MIDNIGHT MERIDIAN PLANE
VAN ALLEN RADIATION BELTS

the magnetopause and the other is the collisionless magnetohydrodynamic shock wave surface (at ~13.4 RE in the solar direction) which separates the undisturbed interplanetary medium from the transition region (Axford, 1962; Kellogg, 1962).

The interplanetary magnetic field has been estimated by various methods to be approximately 1 to 10 γ average value, although steady periods might be infrequent.

The dynamics of charged particle motion in the magnetopause are dominated by the magnetic field of the earth (Alfvén, 1950). Deviations of direction and magnitude of the observed magnetic field when compared with theory do not become significant until ~10 RE. The directional distortion is consistent with the fields being orientated approximately tangential to the surface of the magnetopause and the magnetic fields are oppositely directed on either side of this boundary.

The shape of the magnetosphere is roughly cylindrical, with diameter ~44 RE. Detailed observations of the geomagnetic field on the right side reveal that while those field lines on the right side corresponding to L values less than ~8 do appear to co-rotate with the earth, (Dessler and Juday, 1965), the magnetic tail does not co-rotate.

1.4. Models of the Magnetosphere:

The sunward side of the magnetosphere has been relatively well defined but the polar regions and the distant tail remain comparatively unexplored and it is in these respects that the various models differ. There is also considerable speculation as to the way in which particles from the solar wind enter the magnetopause.

Chapman and Ferraro were the first to describe the effects of a neutral, ionized gas striking and deforming the earth's field and confining it to a hollow. According to their model, the field lines form loops around the ring current (see Appendix I), giving rise to neutral points at the centre of the loops where the magnetic field is zero. Because the field lines near the neutral points emerged from the auroral zone, they suggested that particles from the solar wind enter at these neutral points.

Johnson (1960) proposed the simplest form of the 'closed tail' model. (See Figure 3a). In this the high latitude field lines form closed loops although Johnson mentions the possibility of hydromagnetic waves (see Appendix I) opening the tail of the tear-drop shaped magnetosphere. Piddington (1960) discussed a similar model for periods of geomagnetic storms, and Beard (1960) has studied some details of its formation.

10/.....

Dungey (1961) suggested a closed tail model in which under certain conditions, the interplanetary magnetic field may join the earth's field (viz. when the interplanetary field is opposite to the earth's field at the nose of the magnetosphere). In this model the polar field lines carry the plasma towards the rear of the magnetosphere and the plasma then returns to the front along the auroral zone field lines.

Axford and Hines (1961) also proposed a closed tail model in which they examined convection patterns in the magnetosphere due to distant forces. They envisaged a driving mechanism consisting of a viscous-like interaction between the outer magnetosphere and the interplanetary gas beyond, where again the plasma returned along auroral field lines, (see Figure 3c). Such models however, do not predict an auroral zone confined to a narrow band of latitude.

Dessler and Juday (1965) criticized the neutral point theories on the grounds that they could not explain the occurrence of night-time aurorae. Also the auroral zone field lines, because they are embedded deep in the magnetosphere, are not differentiated (on the right side) from field lines on either side of the auroral zone.

They proposed an 'open-tail' model in which the field lines are dragged out to perhaps 20 to 50 a.u. in length.

11/.....

FIGURE 3.

Diagramatic representations of various models of the magnetosphere.

(a) 'Closed-tail' model (Johnson, 1960)
(b) 'Open-tail' model, (Dessler and Juday, 1965.)
(c) 'Closed-tail' model, (Axford and Hines, 1961).

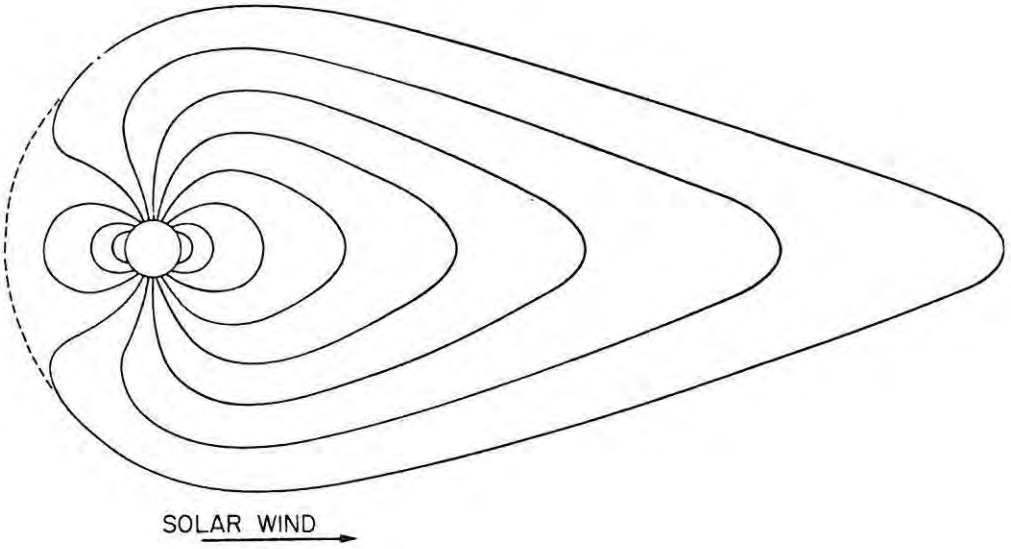
SOLAR WIND

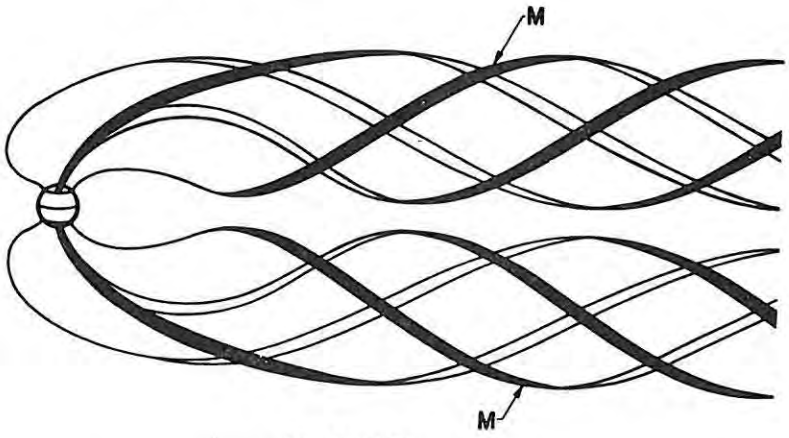
M
M

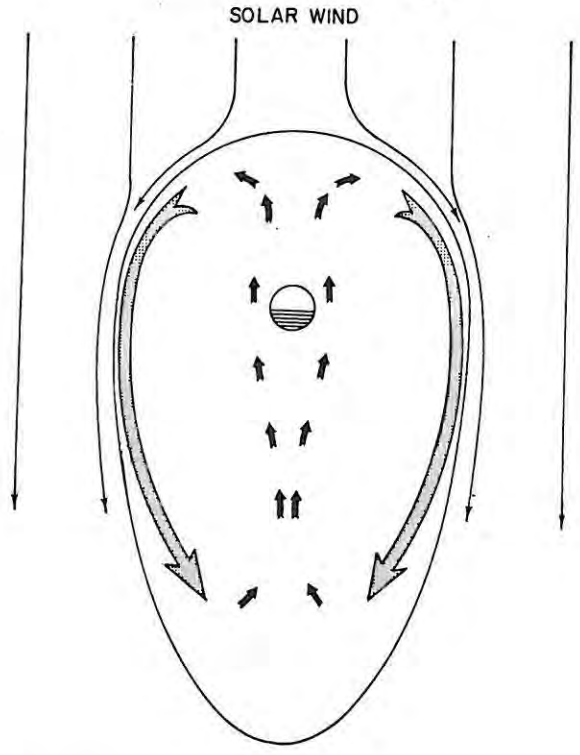
SOLAR WIND

The tail is defined by two tubes of flux emerging from the solar caps, approximately circular in cross-section due to the transverse pressure of the solar wind, thus forming a θ-shaped region in cross-section. Lines on the surface of the tail (the magnetopause) emerge from the auroral zone field; lines closer to the poles will be embedded in the tail. They postulated that auroral particles are energized along the magnetopause, so that particles on field lines closer to the poles will not be energized by this mechanism. The 24-hour rotation of the earth results in a spiralling of the field lines down the tail, (Figure 3b). Two complete auroral zones will only be mapped out if all the auroral zone field lines reach the magnetopause, which will happen if the length of the tail is at least equal to the pitch of the spiral. Using the hydromagnetic wave velocity and the solar wind velocity, they have shown that $4 \times 10^{2} R_E < \lambda < 7 \times 10^{3} R_E$ in order for all field lines to reach the magnetopause.

In the Dessler and Juday model, the high-latitude boundary of closed field lines on the day side, is defined by the latitude of the lines that go to the neutral points. Mead (1964) determined this critical latitude to be between 80° and 85°, depending on the density of the solar wind, i.e. $\sim$10° above the auroral zone. However, Dessler and Karplus (1961) have shown that a ring current causing a 90γ decrease on the earth's surface, can move a field line from

12/.....

$6R_E$ to 8.4 R_E, which would result in a lowering of the critical latitude if the magnosphere were to remain fixed. Akasofu (1963) has shown that a ring current may lower the surface latitude of the neutral point to $\sim 60^\circ$. Also changes in the shape of the magnetosphere would result in movement of the neutral point and hence the critical latitude. By this means, field lines that were closed on the sunward side may be swept back over the poles on the surface of the magnetosphere, thus becoming part of the trapping boundary, and vice versa, depending on the shape of the magnetosphere.

One of the most recent models proposed to date is that by Taylor and Hines (1965), who believe that auroral events occur on magnetic lines of force which close in the tail of the magnetosphere within 50 R_E of the earth. They vary the strength of an image dipole, its distance from the dipole of the earth and the strength of the magnetic field caused by the current sheet to fit magnetometer measurements of the real field.

1.5. The Radiation Belts:

After the discovery of the belts, the outer zone was regarded as a reservoir or 'bucket' which occasionally spilled out electrons to cause aurorae - hence the name, the 'leaky bucket' model. However, O'Brien (1962) showed

that the observed particle population of the outer belt would be depleted in a few minutes if the belts were to provide in this manner the electron fluxes necessary to sustain the aurorae. Using the data obtained from satellites Injun 1 and 3, O'Brien postulated and verified the 'splash-catcher' model. In this model the precipitated particles are 'fresh' particles and the outer belt acts rather as a bucket that catches some of the electrons that splash back from the precipitating mechanism.

Studies of satellite observations (O'Brien and Laughlin, 1962, O'Brien, 1964) have shown that precipitated particles have highly fluctuating characteristics, as would be expected if these are 'fresh' particles because of the large variations in the solar wind. Precipitation has at times been found to be fairly uniform over as much as 80° longitude and at others, very limited in longitudinal extent, while the latitudinal extent of precipitation varies from $\Delta L \sim 1$ to $\Delta L \sim 20$.

Balloon observations (Winckler et al, 1962) have shown that time variations as rapid as periods of $\frac{1}{10}$ second can occur in the electron flux. No systematic variation in the intensity of the electron precipitation over periods as long as a day could be found by O'Brien (1964) from Injun 1 and 3 data.

14/.....

The magnitudes of the precipitated electron fluxes together with pitch angle distributions and energy spectra will be discussed in later chapters.

1.6. Motion of Particles in L - Space:

If particles may only enter the magnetosphere along that part of the tail lying at the magnetopause i.e. the auroral zone field lines, the mechanism by which they reach field lines of lower L values must be considered. The motion of a particle trapped in the geomagnetic field is governed by 3 adiabatic invariants (see Appendix II) each connected with one of the 3 types of motion of the particle viz. the spiralling of the particle about the field line, the bouncing of the guiding centre of the particle back and forth between northern and southern hemispheres, and the longitudinal drift of the guiding centre.

Each of the invariants has associated with it a characteristic time t, such that, if a geomagnetic field change occurs in a period of time less than t, the particle motion will be non-adiabatic.

For the first invariant the period of one radius of gyration is $\sim 10^{-5}$ seconds at 3 RE and decreases as the particle moves towards high latitudes. The second adiabatic invariant is preserved provided that field changes

do not occur in a time comparable to or less than the transit time between mirror points, which for a 100 kev electron mirroring at $L = 4$. is ~ 0.5 second. The longitudinal drift time of a 100 kev electron at 4 R_E is ~ 7000 seconds. So, of the three characteristic times, it appears that violation of the third invariant is most likely.

Northrup and Teller (1959) have commented that violation of the adiobatic invariants could lead to scattering of particles out of the geomagnetic field and Parker (1960) has shown that violation of the third invariant results in a diffusion of particles inward.

Frank et al (1964) found from an examination of Explorer 14 data that the temporal variations of the radial profile of electron ($E > 1.6$ Mev) intensities near the geomagnetic equatorial plane were characterized by an inward radial motion of the inner boundary of the intensity peak, persisting for periods of at least several weeks and an apparent radial velocity of ~ 0.02 RE per day following a magnetic storm. This strongly indicates that inward diffusion of energetic electrons across L shells from $L > 5$ is a source of energetic outer zone electrons. Frank (1965) found that the mechanism causing this diffusion is active even during relatively quiet magnetic periods. Frank also calculated that if the first and second adiabatic invariants

are conserved as an electron moves by radial diffusion from $L \sim 10$ to $L \sim 4$, a 150 kev electron at the magnetopause would have an energy of 1.5 Mev at $L \sim 4$ and the drift time would be ~1 day.

-----ooOoo-----

CHAPTER 2.

THE LOSS OF GEOMAGNETICALLY TRAPPED PARTICLES.

2.1. Introduction:

Since the discovery in 1958 of the natural radiation belts (Van Allen et al, 1959; Vernov et al, 1959), consierable effort has been spent on determining the behaviour of charged particles trapped in the earth's magnetic field. Additional information on the trapping properties of the geomagnetic field was obtained from the Argus nuclear weapon tests (Christofilos, 1959), a series of experiments in which electrons were injected into the earth's field by detonating low-yield atomic bombs above the atmosphere so that the beta particles produced by decaying fission fragments would be trapped. The subsequent behaviour of the electrons was observed by detectors carried in satellites and rockets, (Van Allen et al, 1959).

Various authors (Stormer, 1955; Alfvèn, 1950; Northrup and Teller, 1960) have discussed the theory of charged particle orbits in the dipole field of the earth, and, employing the three adiabatic invariants mentioned previously (Appendix II), have shown that the 'guiding centre' of the electron will generate a shell whose elements lie along the magnetic field lines. In the absence of an atmosphere, this motion would continue indefinitely. In the physical case, however, the trapped

18/.....

particles will be affected both by the atmosphere and by variations in the magnetic field, these effects being responsible for the ultimate removal, or loss, of the particles from the belts. Calculations of the magnitude of these effects have been made by several authors. These will be discussed in what follows, together with the attempts that have been made to derive a mathematical equation describing the behaviour of particles trapped in the belts. This will be done in order to give some idea of the nature of the present approaches to the problem and also to explain the adoption of the treatment used in the following chapter.

2.2. Early Studies:

Christofilos (1958) showed that small-angle coulomb scattering of electrons by the atmosphere is a more important loss mechanism than energy loss by either radiation or ionization. He later (Christofilos, 1959) studied the lifetime of particles produced by the Argus tests. Welch and Whitaker (1959) presented a theoretical formulation for the history of geomagnetically trapped particles in the artificial shell formed by these tests. On the basis of small-angle scattering, they calculated the mean life-time of an electron as a function of its initial mirror-point altitude.

Ray (1960) solved a differential transport equation for trapped protons (neglecting scattering) using the approximation that a proton loses a negligible amount of energy in drifting longitudinally once around the earth. Wentworth et al (1959) were the first to suggest that a Fokker-Planck equation could be used for the study of the loss of trapped particles.

2.3. A Diffusion Equation:

The above authors used a variety of approximations and simplifying assumptions. The results, which included determinations of particle lifetimes and energy spectra, depended upon the assumptions employed and so a more fundamental approach to the problem was needed.

MacDonald and Walt (1961) used a distribution function equal to the number of particles per unit energy in a particular orbit, to describe the particle flux. The time-dependent behaviour of the distribution function was then obtained as a special case of the Fokker-Planck equation for particles experiencing coulomb collisions.

Since the time required for a particle to drift in longitude about the earth is much greater than the period of a north-south osillation, they neglected longitudinal drift and calculated the electron flux along a single magnetic field line. The condition was also imposed that any particle whose mirror point lay beyond a point corres-

ponding to a certain magnetic field strength would no longer return to the trapping region. It was further assumed that collisional diffusion across the magnetic shells does not occur, so that the equation could be applied and solved independently for each separate magnetic shell.

2.4. The Starfish Event:

The diffusion equation derived by MacDonald and Walt, in its steady state representation, has been applied to the natural radiation belts by several authors (Lenchek et al, 1961; Walt and MacDonald 1961; Walt and MacDonald 1962) but with inconclusive results since the source mechanism for the electrons was not known. In fact the calculations indicated that under the influence of atmospheric scattering, high energy electrons in the outer belt mirroring high up near the equatorial plane, would be present for many years. The experimental data contradicted this in many ways, and Argus electrons were observed to decay in a few weeks (Van Allen et al, 1959; Allen et al, 1959; Cladis and Walt, 1962). Also the results do not hold at low altitudes.

On July 9, 1962, a nuclear device was detonated at high altitude over the Pacific Ocean, this being commonly referred to as the Starfish event. Electrons emitted by

21/.....

the radioactive fission fragments of the explosion were injected into the geomagnetic field and trapped, creating an artificial radiation belt (O'Brien et al, 1962).

Walt, Crane and MacDonald (1963) and Walt (1964), calculated the time dependence of the geomagnetically trapped electron flux resulting from this event, using the diffusion equation of MacDonald and Walt (1961). The evaluation of certain terms in the diffusion equation requires a model atmosphere and a model of the geomagnetic field. The model atmosphere used by Walt et al was that of Anderson and Francis (1964) and was characteristic of the first two months following the Starfish event. The magnetic field representation was the 48 term spherical harmonic expansion proposed by Johnson and Cain (1962). Since this field is neither symmetrical about its polar axis nor its equatorial plane, they computed an average atmosphere appropriate to trapped particles by averaging the density of each atmospheric constituent along longitudinal traces of constant B and L.

They then solved the diffusion equation numerically using initial pitch angle distributions obtained with Injun I by Van Allen (1963) a few hours after the Starfish detonation. The spatial distribution obtained with Explorer XV (McIlwain, 1963) was also used and the initial

22/.....

energy spectrum of the electrons was assumed to be a fission beta spectrum as measured by Carter et al (1959).

The theoretical results for the initial decay of the artificial radiation belt on the shells L = 1.185 and 1.25 were compared with the experimental data obtained by satellites Injun I, Injun III and Explorer XV. The agreement between experiment and theory was found to be extremely good. Walt et al concluded that during the latter part of 1962 and the early part of 1963, the major loss mechanism for electrons in regions of L 1.25 was atmospheric scattering but that other processes dominate the behaviour of electrons trapped outside this region.

Welch et al (1963) solved a Fokker-Planck equation (which included scattering and energy loss) by numerical intergration and also used this to predict the time decay of electrons injected into the geomagnetic field by the Starfish event. They used a formulation that on change of variables becomes identical to that of Walt and Mac Donald, but which differed from theirs in that it was valid for population changes deep in the atmosphere and it followed the decay of an initial electron population with no additional source. Only multiple small angle scattering was considered since particles in the artificial radiation belts had energies ranging from 0.5 Mev. to

several Mev and large angle scattering would lead to much longer lifetimes. The calculations were performed for L = 1.18, 1.25 and 1.30 using an atmosphere (characteristic of sunspot minimum) averaged over longitude. Diffusion in L was also neglected so that time histories of the populations of different L shells are calculated independently.

2.5. Longitude Dependence:

Roederer and Welch (1965) set up a general Fokker-Planck equation which describes the distribution of geomagnetically trapped particles as a function of longitude, time energy and mirror point intensity. The reasoning and procedure follows closely that of previous workers (Welch et al, 1963) but as this paper is the most recent on this topic, including a few refinements, it will be described in somewhat more detail as an example of the rather complex nature of this type of approach.

Roederer and Welch have divided this work into three parts, only the first of which is available at present and which deals with the setting up of the equation and discusses its physical meaning. The later parts will present the atmosphere-field configurations to be used on a numerical integration of the equation.

24/.....

In previous approaches, the atmosphere has been averaged longitudinally and the effects of the Anomaly (if considered at all) applied as a pertubation. It is evident that any treatment of the Anomaly must include a longitude term. The equation of Roderer and Welch does include the longitudinal dependence of the electron distribution on a given magnetic shell by the introduction of an additional variable related to longitude. The equation is applied directly to the South American Anomaly by using a model of the field and atmosphere in the Anomaly.

The distribution function of Welch et al (1963) is used to describe the trapped electrons i.e. for a given L-shell

$$\delta N = U (B, E, \chi, t) \delta\phi \, \delta B \, \delta E \qquad (2.1)$$

where δN is the number of electrons at time t in a tube of field lines of magnetic flux $\delta\phi$, with mirror points between B and B + δ B and kinetic energies between E and E + δ E. χ is the magnetic longitude of the tube of field lines and is a variable not included by Welch et al. Since L - scattering is neglected, L is not included explicitly in U.

If δx is the distance between the equatorial points of two neighbouring field lines of a given shell and δy is the distance between two neighbouring shells, then if the tube of field lines has equatorial cross section $\delta x \, \delta y$ and magnetic flux Bo $\delta x \, \delta y$, the number of electrons in this flux tube which mirror between B and B + δ B with kinetic

25/.....

energies between E and E + δ E, is given by

$$\delta N = U \, Bo \, \delta x \, \delta y \, d \, B \, \delta \, E \qquad (2.2.)$$

Since U is a distribution in flux and not in ψ or x, neither of these can be used as the longitudinal variable. Further, not only δx but also δy in (2.2) is a function of longitude.

It is therefore necessary to transorm the flux into an expression $\delta\phi = Bo \, \delta X \, \delta Y$, where δY, which is related to δy, is longitude independent. X would then be the correct longitudinal variable, and its differential X would contain complete information about the longitude dependence of the flux $\delta\phi$ of a tube of particles as they drift around the earth.

For this transormation the longitude dependence of δy must be determined and it is shown that

$$\delta y = \frac{\lambda \delta I}{Ko}$$

where λ is a dimensionless function of the mirror point field intensity B, δI is the increment in the second adiabatic invariant between two neighbouring shells and

$$Ko = \frac{\frac{1}{Bo} \nabla o \, B}{3/RL}$$

which is the curvature of a line of force at the equatorial point in units of the equatorial curvature 3/RL of the corresponding dipole line. (∇oB is the gradient of |B| taken at the equatorial point). Ko is the only longitude dependent quantity in δy.

26/.....

The variables Y and X are therefore written as

$$\delta Y = Ko\ \delta y \text{ and } \delta X = \frac{\delta x}{Ko}$$

Now $\delta\phi = Bo\ \delta x\ \delta y = Bo\ \delta X\ \delta Y$

and $\delta N = U(B,E,X,t)\ \delta B, \delta E, \delta X.\ Bo\ \delta Y \quad (2.3)$

Roederer and Welch then proceed to set up the Fokker-Planck equation for longitude dependence.

The trapped electrons undergo displacements in B, E and longitude :-

(i) a change in the mirror point field B due to multiple Coubomb scattering.

(ii) a change in the kinetic energy E due to ionization.

(iii) a change in longitude due to longitudinal drift.

These three processes are physically independent of each other.

The distribution of electrons in (2.3) is then related to the distribution at a slightly earlier time, $t - \Delta t$, and different longitudinal position.

$$U(B,E,X,t) = \iiint U\ (B-\beta,\ E-\epsilon,\ X-\xi,\ t-\Delta t)$$
$$\times\ \Pi\ (B-\beta,\ E-\epsilon,\ X-\xi, \beta, \epsilon, \xi, \Delta t)\ d\beta\ d\epsilon\ d\xi \quad (2.4)$$
$$+\ Q\ (B,E,x,t)\ \Delta t.$$

i.e. the distribution of electrons which at time t are at position X, is related to the distribution of those electrons which at an earlier time $t - \Delta t$ were at $X - \xi$, and which happened to scatter, slow down and drift the right amount in

27/.....

the interval t in order to become part of the population of the left hand side of (2.4). $\Pi\, d\beta d\epsilon d\xi$ is the a priori probability that these elctrons have undergone the right changes in B, E and X in Δt. $Q\,\Delta t$ is the source term i.e. the contribution of electrons added by injection to the original bunch in Δt.

Equation (2.4) is then expanded in Taylor series in β, ϵ, ξ and Δt to give

$$\frac{\partial U}{\partial t} + \frac{\partial}{\partial x}\left(U\langle \xi \rangle\right) = -\frac{\partial}{\partial E}\left(U\langle \epsilon \rangle\right) - \frac{\partial}{\partial B}\left(U\langle \beta \rangle\right) + \frac{1}{2}\frac{\partial^2}{\partial B^2}\left(U\langle \beta^2 \rangle\right) + Q$$

+ higher order terms in $\xi^2, \epsilon^2, \epsilon\beta$, etc. (2.5)

The $\langle\ \rangle$ brackets represent average per unit time.

After taking the non-stockastic nature of E and X into account (2.6) becomes

$$\frac{\partial U}{\partial t} + \frac{\partial}{\partial x}\left(U\dot{\xi}\right) = \frac{\partial}{\partial E}\left(U\dot{\epsilon}\right) - \frac{\partial}{\partial B}\left(U\langle \beta \rangle\right) + \frac{1}{2}\frac{\partial^2}{\partial B^2}\left(U\langle \beta^2 \rangle\right) + Q \qquad (2.6)$$

where $\dot{\epsilon}$ is the change in energy per unit time and $\dot{\xi}$ is the drift velocity in the X co-ordinate.

This is the most general Fokker-Planck equation describing the longitudinal and time dependence of a trapped particle flux which undergoes scattering and energy loss by ionization in the atmosphere.

28/.....

If eqn (2.6) is integrated over a complete longitudinal cycle of X for a fixed time t, it becomes

$$\frac{\partial}{\partial t}\oint U\,dx = \frac{\partial}{\partial E}\oint U\dot{E}\,dx - \frac{\partial}{\partial B}\oint U\langle\beta\rangle\,dx + \frac{1}{2}\frac{\partial^2}{\partial B^2}\oint U\langle\beta^2\rangle\,dx + \bar{Q} \qquad (2.7)$$

This reduces to the equations used by MacDonald and Walt (1961) and Welch et al (1962) by dividing by $\oint dX$ and writing.

$$U_{AV} = \frac{\oint U\,dx}{\oint dx} = \frac{\oint U\frac{dx}{K_0}}{\oint \frac{dx}{K_0}}$$

$$\dot{E}_{AV} = \frac{\oint \dot{E}\,U\,dx}{\oint U\,dx}$$

$$\langle\beta\rangle_{AV} = \frac{\oint\langle\beta\rangle U\,dx}{\oint U\,dx}$$

$$\langle\beta^2\rangle_{AV} = \frac{\oint\langle\beta^2\rangle U\,dx}{\oint U\,dx}$$

to give

$$\frac{\partial U_{AV}}{\partial t} = \frac{\partial}{\partial E}\left(U_{AV}\,\dot{E}_{AV}\right) - \frac{\partial}{\partial B}\left(U_{AV}\langle\beta\rangle_{AV}\right) + \frac{1}{2}\frac{\partial^2}{\partial B^2}\left(U_{AV}\langle\beta^2\rangle_{AV}\right) + \bar{Q} \qquad (2.8$$

However, the average distribution U_{AV} is computed by integrating over X, which means that U must be weighted at the different longitudes with the inverse of the equatorial curvature of the field lines and the coefficients $\dot{E}_{AV}, \langle\beta\rangle_{AV}$ and $\langle\beta^2\rangle_{AV}$ are weighted with U i.e. they are functions of the unknown distribution. Roederer and Welch therefore conclude that a longitudinally averaged Fokker-Planck equation does not hold for the problem of geomagnetically

29/.....

trapped particles unless the particles mirror at such great altitudes that their distribution function is very nearly longitudinally independent. Such an equation could not be applied to the Anomaly where the mirror points decend to very low altitudes.

They then proceed to consider the steady state case of equation (2.6) i.e. $\frac{\partial \omega}{\partial t} = 0$ and neglect the contribution of the natural source term Q. This approximates very quiet solar wind conditions at times after injection long compared to the longitudinal drift period. They introduce the distribution function

$$\omega = v \dot{\xi}^3$$

and (2.6) eventually becomes

$$\frac{\partial \omega}{\partial x} = -\frac{\partial}{\partial B}\left(\omega \bar{\beta}\right) + \frac{1}{2}\frac{\partial^2}{\partial B^2}\left(\omega \bar{\beta}^2\right) + \frac{\partial}{\partial E}\left(\omega \bar{E}\right) \qquad (2.9)$$

which is the fundamental equation describing the longitude dependence of a stationary, source free electron distribution, used in the rest of their work.

2.6. Conclusions:

It is evident from the above discussion that a treatment of this nature in its present state of development would not be suitable for application to the Southern Radiation Anomaly. Apart from the complex character of the equations, the earlier treatments only hold for particles mirroring at very great altitudes and therefore are of no use in a study of

30/.....

Southern Anomaly.

Furthermore, Roederer and Welch point out that their approach does not hold for $L \gtrsim 1.8$, whereas for the Southern Anomaly treatment is required which is valid for $L \lesssim 4$.

It is for these reasons that the approach described in the next chapter is adopted. This provides a simple method for obtaining a good first approximation description of the manner in which electrons are lost in the Southern Radiation Anomaly.

-----ooOoo-----

CHAPTER 3.

THE LOSS AND REPLENISHMENT OF ELECTRONS IN THE SOUTHERN RADIATION ANOMALY.

3.1. Introduction:

In this chapter a simple model of continuous injection of electrons into the outer radiation belt is developed, by which the average values of the trapped and precipitated electron flux may be predicted for any point on L = 4. The design of the model is based as closely as possible on the experimental data available at present and currently accepted theories of the magnetosphere, while, at the same time, the attempt is made to keep it simple.

The essence of the model is the assumption that there is a continuous injection of electrons, isotropically distributed in pitch angle, into the outer belt at L = 4. The injection rate is assumed to be the same in any two similar longitudinal strips of the L-shell, no matter at what actual longitude they are taken. This involves three assumptions that are supported by present knowledge.

The solar wind blows continuously and it would be reasonable to suppose that there is a continual entry of particles into the outer belt. The intensity of these particles will fluctuate greatly with the fluctuations in the solar wind pressure, but from this model only average

32/.....

values are required. Pitch angle distribution will be dealt with later in this chapter, but for the moment it suffices to say that an isotropic distribution of the injected flux is also a reasonable assumption. The third point, i.e. equal injection rates in all longitudinal strips, involves the assumption that the rate of injection is the same by day as by night. This is also not inconsistent with satellite observations, for, although the satellite Injun 3 observed low energy electron fluxes on the night side only (Fritz and Gurnett, 1965), Sharp et al (1965) have found electron precipitation in both the day and night sides of the auroral zone. Also, an examination by the author of electron flux data observed by the satellite Alovette showed that precipitation of electrons at L = 4.4 occurred as often on the day side as on the night side.

Values of B and L from the curves of constant B and L by Roderer et al (1965) were used for the present calculations. The surface values of B over the Southern Radiation Anomaly were compared with those obtained by the Japanese Antarctic Research Expedition ship, Soya (1961) and the South African ship, the RSA (1965), and found to agree.

3.2. Preliminary Calculations:

By interpolating the curves of Roedereret al (1965),

FIGURE 4.

Mirror heights of electrons mirroring at 100 km at 30°E, L=4, southern hemisphere, (equivalent heights)

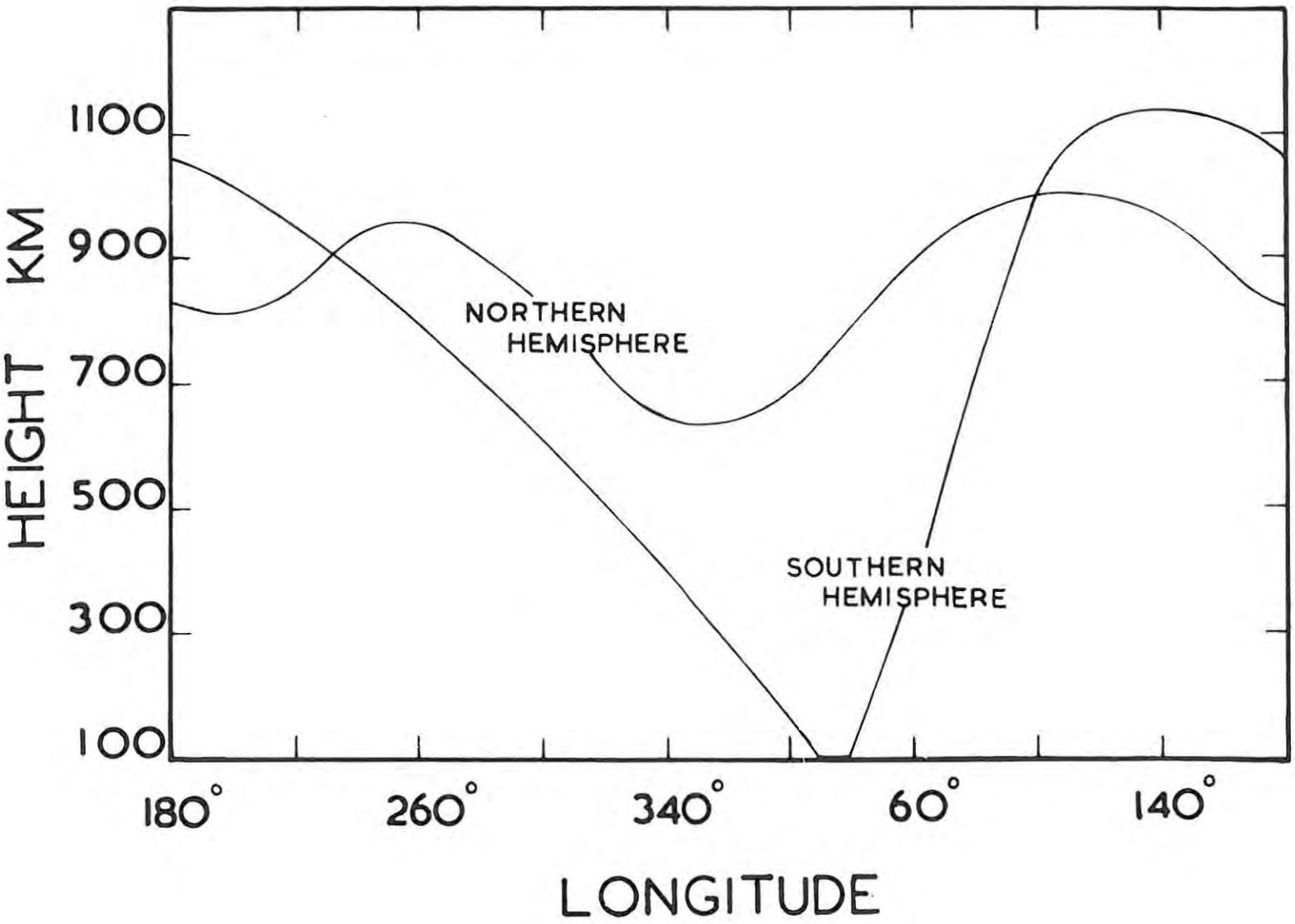
HEIGHT KM
1100
900
700
500
300
100
NORTHERN
HEMISPHERE
SOUTHERN
HEMISPHERE
180°
260°
340°
60°
140°
LONGITUDE

which were calculated for height intervals of 100 km, the heights of points of constant B were calculated for L=4. B was chosen to be the lowest value of the magnetic field on L=4, at an altitude of 100 km. This point (having geographic co-ordinates 30^{o}E and 59.5^{o}S) lay over the centre of the Southern Radiation Anomaly and had the intensity 0.380 gauss.

If scattering is neglected, these heights are the mirror point heights of a particle mirroring at this reference point as it drifts in longitude around the earth, and will be referred to in what follows as 'equivalent heights'. These are shown in Figure 4, in which the steep decent and rise of the equivalent heights over the Southern Anomaly may be clearly seen.

The mirror equation, (Alfvèn, 1950) (see Appendix II, equation (7)), i.e. $\frac{\sin^2 \chi}{B} = \text{constant} = \frac{1}{B_m}$ (where χ is the pitch angle and Bm is the value of the magnetic field at the mirror point i.e. at which $\chi = 90^{o}$), was used to calculate the pitch angle that the electrons would have at each equivalent height if they were to mirror at 100 km. This is the angle of the dumping cone because electrons that decend below 100 km will be regarded as precipitated. These results are shown in Figure 5. Various authors

34/.....

FIGURE 5.

Pitch angle that electrons would have at equivalent heights in order to mirror at 100 km.

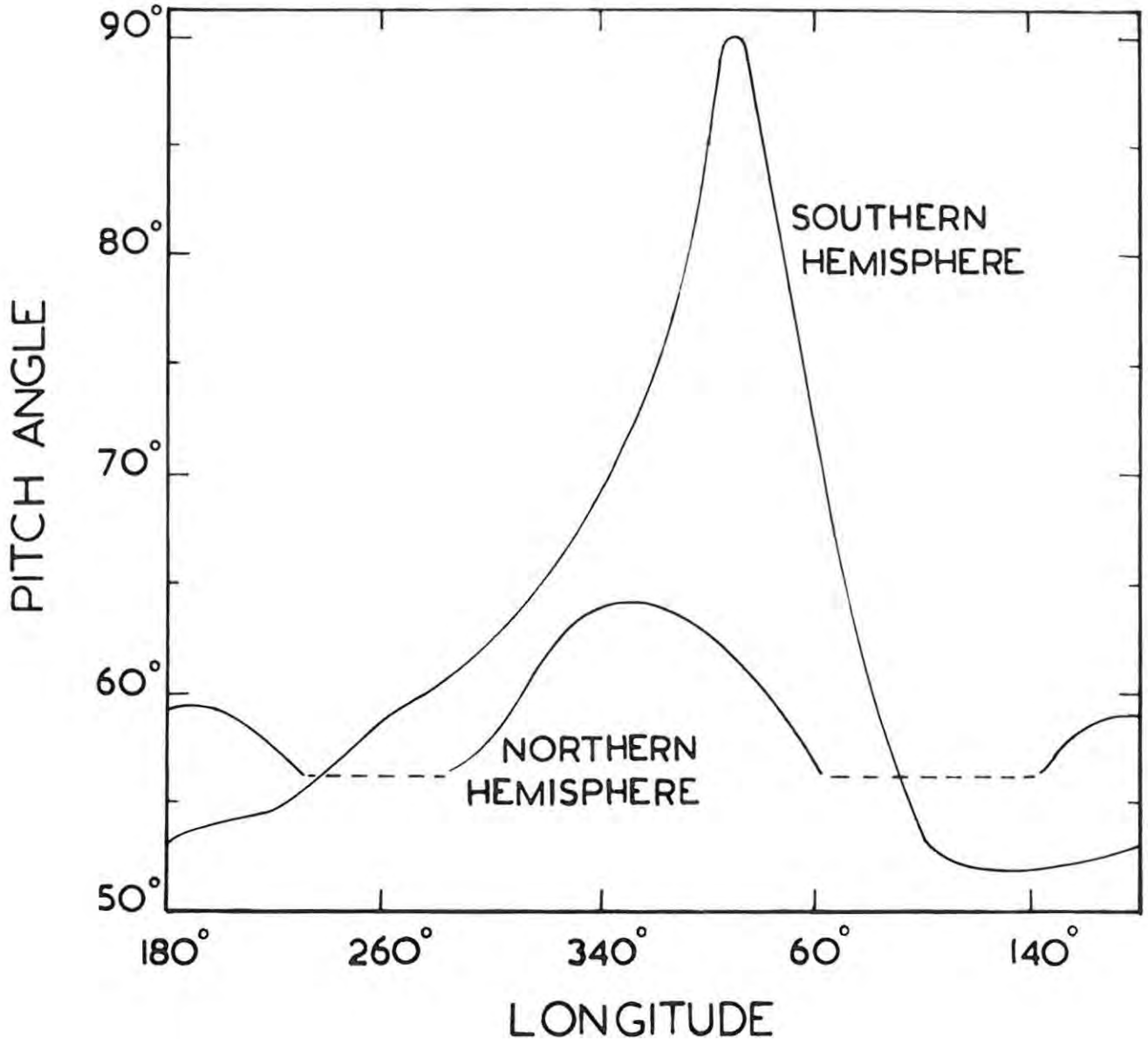
90°
80°
70°
60°
50°
PITCH ANGLE
SOUTHERN
HEMISPHERE
NORTHERN
HEMISPHERE
180°
260°
340°
60°
140°
LONGITUDE

differ as to the altitude below which particles will no longer be trapped, and place this between 100 km to 400 km. However, after examining the height versus energy loss curves for energetic electrons incident on the atmosphere, (Rees, 1963; Gledhill and van Rooyen, 1962), it was decided to use 100 km in these calculations. The dotted portions of the northern hemisphere graph represent areas over which the magnetic field could not be estimated with any accuracy.

Using the list of conjugate intersects to selected geophysical stations (Roederer et al, 1965), a graph was plotted of the (geographic) longitude of stations along L=4 versus the longitude of their conjugate points in the other hemisphere, Figure 6. From this the longitude of the conjugate point of any location along the northern or southern hemisphere equivalent height path could be read.

The L parameter (McIlwain, 1961), for L $\lesssim$ 6, may to a first approximation be regarded as labelling a magnetic shell on which a trapped particle bounces in latitude and drifts in longitude. In this treatment, the L=4 shell will be regarded as coinciding with the corresponding magnetic shell.

The L=4 shell was then divided into sections longitudinally from conjugate point to conjugate point. The width of each section was chosen to be 2^{o} geographic longitude at the southern hemisphere end. This was the

FIGURE 5a.

Curve relating the geographic longitude of points along L = 4 in one hemisphere to the longitude of their conjugate points.

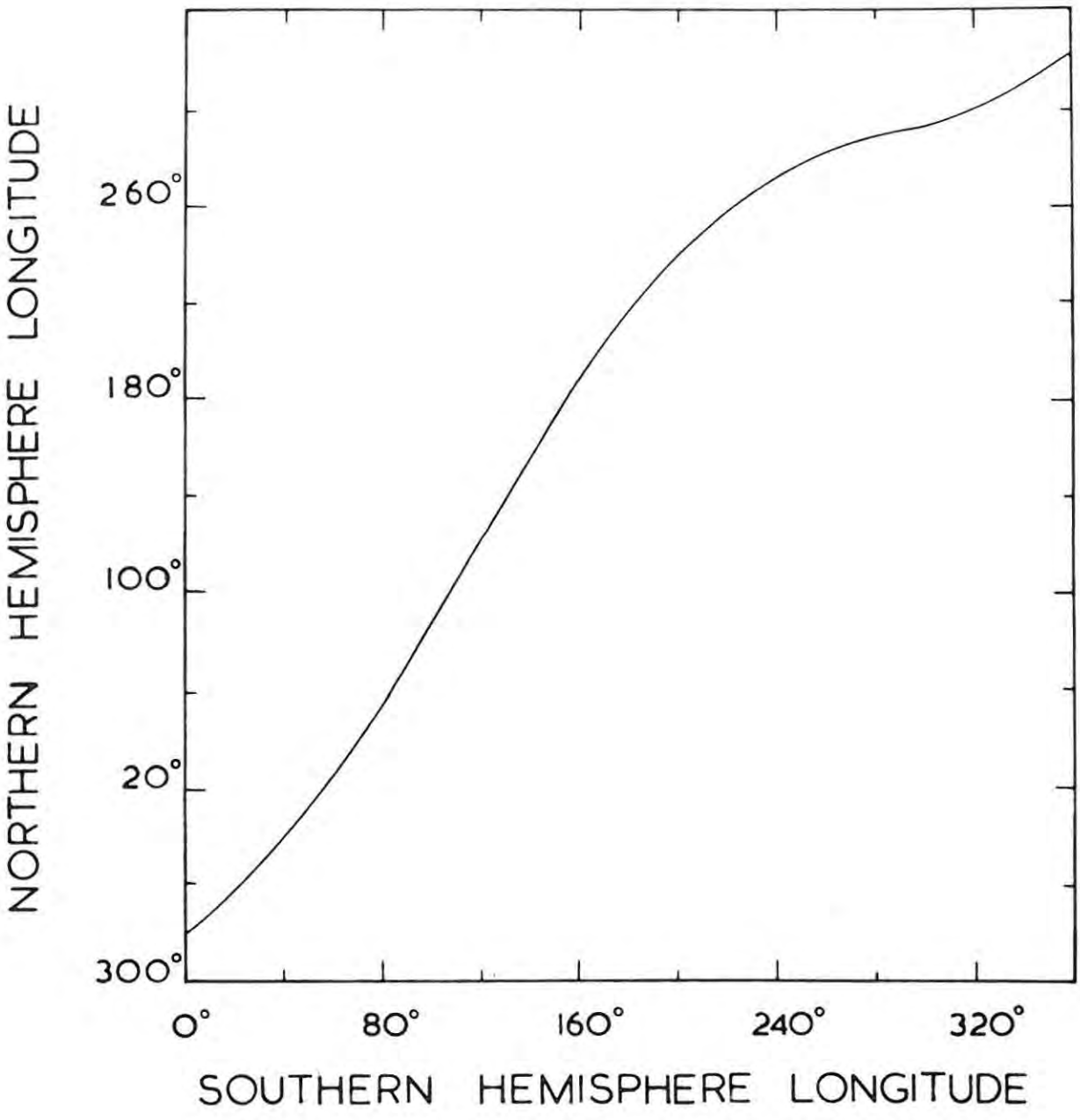
NORTHERN HEMISPHERE LONGITUDE
260°
180°
100°
20°
300°
0°
80°
160°
240°
320°
SOUTHERN HEMISPHERE LONGITUDE

largest longitudinal width over which the equivalent height path was reasonably constant. Also, at L=4, 2^{o} longitude is more than 100 km which is large compared with the longitudinal drift between bounces of electrons with energies less than ~300 km. (this being ~1 km), thus ensuring beyond a doubt that a trapped particle must mirror at least once in each section.

An isotropic electron flux was then assumed to be continuously injected around the equivalent height path (for simplicity) in both hemispheres, and the subsequent history of this flux was followed.

3.3. Precipitated and Trapped Electron Flux:

The isotropic electron flux at the equivalent height points, produced by the injection mechanism, will be denoted by the symbol $\mathcal{X}$ and has the units electrons/cm^2/second. The first step in the procedure is to divide $\mathcal{X}$ into trapped or precipitated fractions in each longitudinal section (at the equivalent height), this being determined by the pitch angles of the particles.

As a starting point in the calculation, a point at 32^{o}E was chosen i.e. the longitudinal lamination immediately to the east of the point of lowest B mentioned above. The reason for the selection of this point will become obvious later.

36/.....

The value of the pitch angle at the equivalent height that will mirror at 100 km can be read from figure 5 for any point around the equivalent height path. Electrons at the equivalent heights with pitch angles $\leq$ this 'critical' pitch angle will be precipitated.

At 32°E (southern hemisphere) the critical pitch angle is 90° (being in the region of very low magnetic field strength at the centre of the Anomaly). Therefore, since the injected flux is isotrpoic, $\frac{90}{90}$ or the whole of χ will be precipitated there. The conjugate point is at 351°E in the northern hemisphere and has a critical pitch angle of 64.2°. Therefore, in the northern hemisphere of this particular longitudinal section, $\frac{64.2}{90}$ or 0.71χ will be precipitated and 0.29χ will mirror and return along the field line to the southern hemisphere, where it will be precipitated because it will consist of electrons with pitch angles between 64.2° and 90° at the equivalent height. The total flux precipitated in the southern hemisphere will therefore be 1.29χ and the trapped flux will be zero for this particular section.

Similarly, for the next 2° section the critical pitch angles are 89.0° and 64.2° for the southern and northern hemispheres respectively. So the precipitated fractions of the injected flux will be 0.99 and 0.71. Therefore 0.01χ will return along the field line from the southern

37/.....

to the northern hemisphere, but it will not be precipitated there because it will consist of electrons with pitch engles between 89.0° and 90° at the equivalent height and the critical pitch angle there is 64.2°. This 0.01x is therefore trapped. Also 0.29x travels along the field line from northern to southern hemisphere and 0.28x i.e. the electrons with pitch angles between 64.2° and 89.0° will be precipitated at the southern end, while the remaining 0.01x will be trapped flux and will drift longitudinally to the next second lamination. The total trapped flux from the second lamination will therefore be 0.02x and will have pitch angles between 89.0° and 90° at the equivalent height. 89.0° will be called the 'minimum pitch angle' of the trapped flux for this section.

For the section at 36°E, the critical pitch angles are 88.2° and 64.1° for southern and northern hemisphere respectively. Of the injected flux, the precipitated fractions are .98 and .71 in these two hemispheres. The fraction precipitated in the southern hemisphere from the northern hemisphere is .27 and none of the flux from the southern hemisphere is precipitated in the northern hemisphere. Thus the total trapped flux in this section is .02x from the northern hemisphere and .02x from the previous sections giving .06x in all.

By the time the 2° section at 40°E is reached, the critical pitch angles have become 85.9° and 64.0° for north

38/.....

LONGITUDE		CRITICAL PITCH ANGLE		FRACTION OF INJECTED FLUX PRECIPITATED IN		FRACTION PRECIPITATED IN	
S.H.	N.H.	S.H.	N.H.	S.H.	N.H.	S.H. FROM N.H.	N.H. FROM S.H.
32	-9	89.7	64.2	1.00	.71	.29	0
34	-7	89.0	64.2	.99	.71	.28	0
36	-4	88.25	64.1	.98	.71	.27	0
38	-2	87.3	64.0	.97	.71	.26	0
40	0	85.90	64.0	.95	.71	.24	0
42	4	85.0	63.8	.95	.71	.24	0
44	7	83.7	63.7	.93	.71	.22	0
46	9	82.3	63.5	.91	.71	.20	0
48	12	80.6	63.3	.90	.70	.20	0
50	14	78.3	63.2	.87	.70	.17	0
52	17	77.6	62.8	.86	.70	.16	0
54	20	76.25	62.6	.85	.70	.15	0
56	22	75.0	62.3	.83	.69	.14	0
58	25	73.5	62.0	.82	.69	.13	0
60	28	72.03	61.7	.80	.69	.11	0
62	31	70.8	61.3	.79	.68	.11	0
64	33	69.5	61.0	.77	.68	.09	0
66	36	68.2	60.6	.76	.67	.09	0
68	39	67.8	60.2	.75	.67	.08	0
70	42	65.77	59.5	.73	.66	.07	0
72	45	64.6	58.6	.72	.65	.07	0
74	47	63.7	57.9	.71	.64	.07	0
76	50	62.8	57.2	.70	.64	.06	0
78	53	62.0	56.8	.69	.63	.06	0
80	56	61.20	56.6	.68	.63	.05	0
82	59	60.6	56.4	.67	.63	.04	0
84	62	59.8	56.3	.66	.63	.03	0
86	65	59.2	56.2	.66	.62	.04	0
88	68	58.5	56.2	.65	.62	.03	0
90	71	57.87	56.2	.64	.62	.02	0
92	74	57.3	56.2	.64	.62	.02	0
94	77	56.5	56.2	.63	.62	.01	0
96	80	55.4	56.2	.62	.62	0	0
98	83	54.2	56.2	.61	.62	0	.01
100	86	53.50	56.2	.60	.62	0	.02
102	90	53.50	56.2	.60	.62	0	.02
104	93	53.50	56.2	.60	.62	0	.02
106	96	53.50	56.2	.60	.62	0	.02
108	99	53.50	56.2	.60	.62	0	.02
110	102	53.50	56.2	.60	.62	0	.02
112	106	53.3	56.2	.59	.62	0	.03
114	109	53.1	56.2	.59	.62	0	.03
116	112	52.7	56.2	.59	.62	0	.03
118	116	52.3	56.2	.58	.62	0	.04
120	119	52.00	56.2	.58	.62	0	.04

TABLE I.

FRACTION PRECIPITATED FROM TRAPPED FLUX IN		TOTAL FRACTION PRECIPITATED IN		TRAPPED FLUX (x $\frac{1}{2}$)	
S.H.	N.H.	S.H.	N.H.	FRACTION OF INJECTED FLUX	TOTAL
0	0	1.29	.71	0	0
0	0	1.27	.71	.01	.01
0	0	1.25	.71	.02	.03
0	0	1.23	.71	.03	.06
0	0	1.19	.71	.05	.11
0	0	1.19	.71	.05	.16
0	0	1.15	.71	.07	.23
0	0	1.11	.71	.09	.32
0	0	1.10	.70	.10	.42
0	0	1.04	.70	.13	.55
0	0	1.02	.70	.14	.69
0	0	1.00	.70	.15	.84
0	0	.97	.69	.17	1.01
0	0	.95	.69	.18	1.19
0	0	.91	.69	.20	1.39
0	0	.90	.68	.21	1.60
0	0	.86	.68	.23	1.83
0	0	.85	.67	.24	2.07
0	0	.83	.67	.25	2.32
0	0	.80	.66	.27	2.59
0	0	.79	.65	.28	2.87
0	0	.78	.64	.29	3.16
0	0	.76	.64	.30	3.46
0	0	.75	.63	.31	3.77
0	0	.73	.63	.32	4.09
0	0	.71	.63	.33	4.42
0	0	.69	.63	.34	4.76
0	0	.70	.62	.34	5.10
0	0	.68	.62	.35	5.45
0	0	.66	.62	.36	5.81
0	0	.66	.62	.36	6.17
0	0	.64	.62	.37	6.54
0	0	.62	.62	.38	6.92
0	0	.61	.63	.38	7.29
0	0	.60	.64	.38	7.65
0	0	.60	.64	.38	8.01
0	0	.60	.64	.38	8.37
0	0	.60	.64	.38	8.73
0	0	.60	.64	.38	9.09
0	0	.60	.64	.38	9.45
0	0	.59	.65	.38	9.80
0	0	.59	.65	.38	10.15
0	0	.59	.65	.38	10.50
0	0	.58	.66	.38	10.84
0	0	.58	.66	.38	11.18

LONGITUDE		CRITICAL PITCH ANGLE		FRACTION OF INJECTED FLUX PRECIPITATED IN		FRACTION PRECIPITATED IN	
S.H.	N.H.	S.H.	N.H.	S.H.	N.H.	S.H. FROM N.H.	N.H. FROM N.H.
122	122	51.9	56.2	.58	.62	0	.04
124	126	51.9	56.2	.58	.62	0	.04
126	129	51.8	56.2	.58	.62	0	.04
128	133	51.8	56.2	.58	.62	0	.04
130	136	51.83	56.2	.58	.62	0	.04
132	140	51.8	56.2	.58	.62	0	.04
134	143	51.7	56.5	.58	.63	0	.05
136	146	51.7	56.7	.58	.63	0	.05
138	150	51.7	57.1	.58	.63	0	.05
140	154	51.70	57.6	.58	.64	0	.06
142	158	51.7	58.3	.58	.65	0	.07
144	161	51.8	58.6	.58	.65	0	.07
146	165	51.8	58.4	.58	.65	0	.07
148	168	51.9	58.2	.58	.65	0	.07
150	172	51.95	58.2	.58	.65	0	.07
152	175	52.0	58.5	.58	.65	0	.07
154	179	52.1	59.0	.58	.65	0	.07
156	-177	52.2	58.9	.58	.65	0	.07
158	-173	52.3	58.8	.58	.65	0	.07
160	-170	52.37	58.8	.58	.65	0	.07
162	-167	52.4	58.9	.58	.65	0	.07
164	-164	52.5	59.1	.58	.65	0	.07
166	-160	52.5	59.1	.58	.65	0	.07
168	-157	52.6	58.9	.58	.65	0	.07
170	-154	52.72	58.7	.59	.65	0	.06
172	-150	52.8	58.4	.59	.65	0	.06
174	-147	52.8	58.1	.59	.65	0	.06
176	-144	52.9	57.8	.59	.64	0	.05
178	-140	52.9	57.3	.59	.64	0	.05
180	-139	53.05	57.2	.59	.64	0	.05
-178	-138	53.2	57.0	.59	.63	0	.04
-176	-136	53.2	56.8	.59	.63	0	.04
-174	-134	53.3	56.5	.59	.63	0	.04
-172	-132	53.3	56.3	.59	.63	0	.04
-170	-129	53.37	56.2	.59	.62	0	.03
-168	-127	53.5	56.2	.59	.62	0	.03
-166	-125	53.6	56.2	.60	.62	0	.02
-164	-123	53.7	56.2	.60	.62	0	.02
-162	-121	53.8	56.2	.60	.62	0	.02
-160	-119	53.97	56.2	.60	.62	0	.02
-158	-117	54.2	56.2	.60	.62	0	.02
-156	-115	54.2	56.2	.60	.62	0	.02
-154	-113	54.3	56.2	.60	.62	0	.02
-152	-111	54.4	56.2	.60	.62	0	.02
-150	-110	54.37	56.2	.60	.62	0	.02

FRACTION PRECIPITATED FROM TRAPPED FLUX IN		TOTAL FRACTION PRECIPITATED IN		TRAPPED FLUX ($\times \frac{1}{2}$)	
S.H.	N.H.	S.H.	N.H.	FRACTION OF INJECTED FLUX	TOTAL
0	0	.58	.66	..38	11.56
0	0	.58	.66	.38	11.94
0	0	.58	.66	.38	12.32
0	0	.58	.66	.38	12.70
0	0	.58	.66	.38	13.08
0	0	.58	.66	.38	13.46
0	.06	.58	.74	.37	13.77
0	.05	.58	.73	.37	14.09
0	.05	.58	.73	.37	14.41
0	.14	.58	.84	.36	14.63
0	.20	.58	.92	.35	14.78
0	.09	.58	.81	.35	15.04
0	0	.58	.72	.35	15.39
0	0	.58	.72	.35	15.74
0	0	.58	.72	.35	16.09
0	.01	.58	.73	.35	16.43
0	.15	.58	.87	.35	16.63
0	0	.58	.72	.35	16.98
0	0	.58	.72	.35	17.33
0	0	.58	.72	.35	17.68
0	0	.58	.72	.35	18.03
0	.05	.58	.77	.35	18.33
0	0	.58	.72	.35	18.68
0	0	.58	.72	.35	19.03
0	0	.59	.71	.35	19.38
0	0	.59	.71	.35	19.73
0	0	.59	.71	.35	20.08
0	0	.59	.69	.36	20.44
0	0	.59	.69	.36	20.80
0	0	.59	.69	.36	21.16
0	0	.59	.67	.37	21.53
0	0	.59	.67	.37	21.90
0	0	.59	.67	.37	22.27
0	0	.59	.67	.37	22.64
0	0	.59	.65	.38	23.02
0	0	.59	.65	.38	23.40
0	0	.60	.64	.38	23.78
0	0	.60	.64	.38	24.16
0	0	.60	.64	.38	24.54
0	0	.60	.64	.38	24.92
0	0	.60	.64	.38	25.30
0	0	.60	.64	.38	25.68
0	0	.60	.64	.38	26.06
0	0	.60	.64	.38	26.44
0	0	.60	.64	.38	26.82

LONGITUDE		CRITICAL PITCH ANGLE		FRACTION OF INJECTED FLUX PRECIPITATED IN		FRACTION PRECIPITATED IN	
S.H.	N.H.	S.H.	N.H.	S.H.	N.H.	S.H. FROM N.H.	N.H. FROM S.H.
-148	-108	54.5	56.2	.61	.62	0	.01
-146	-106	54.5	56.2	.61	.62	0	.01
-144	-104	54.5	56.2	.61	.62	0	.01
-142	-103	54.5	56.2	.61	.62	0	.01
-140	-101	54.5	56.2	.61	.62	0	.01
-138	-100	54.5	56.2	.61	.62	0	.01
-136	- 98	54.6	56.2	.61	.62	0	.01
-134	- 97	54.7	56.2	.61	.62	0	.01
-132	- 95	54.8	56.2	.61	.62	0	.01
-130	- 94	54.95	56.2	.61	.62	0	.01
-128	- 93	55.1	56.2	.61	.62	0	.01
-126	- 91	55.3	56.2	.61	.62	0	.01
-124	- 90	55.6	56.2	.62	.62	0	0
-122	- 89	55.9	56.2	.62	.62	0	0
-120	- 88	56.23	56.2	.62	.62	0	0
-118	- 86	56.4	56.2	.63	.62	.01	0
-116	- 85	56.5	56.2	.63	.62	.01	0
-114	- 84	56.7	56.2	.63	.62	.01	0
-112	- 83	56.7	56.2	.63	.62	.01	0
-110	- 82	56.60	56.2	.63	.62	.01	0
-108	- 81	56.8	56.2	.63	.62	.01	0
-106	- 80	57.1	56.2	.63	.62	.01	0
-104	- 79	57.6	56.2	.64	.62	.02	0
-102	- 78.5	58.2	56.2	.65	.62	.03	0
-100	- 78	58.57	56.2	.65	.62	.03	0
- 98	- 77	58.7	56.2	.65	.62	.03	0
- 96	- 76	58.9	56.2	.65	.62	.03	0
- 94	- 75.5	59.0	56.3	.66	.63	.03	0
- 92	- 75	59.2	56.3	.66	.63	.03	0
- 90	- 74	59.38	56.3	.66	.63	.03	0
- 88	- 73.5	59.5	56.4	.66	.63	.03	0
- 86	- 73	59.7	56.4	.66	.63	.03	0
- 84	- 72	59.8	56.5	.66	.63	.03	0
- 82	- 71.5	60.0	56.5	.67	.63	.04	0
- 80	- 71	60.08	56.5	.67	.63	.04	0
- 78	- 70	60.3	56.6	.67	.63	.04	0
- 76	- 69.5	60.5	56.7	.67	.63	.04	0
- 74	- 69	60.7	56.7	.67	.63	.04	0
- 72	- 68	60.8	56.8	.68	.63	.05	0
- 70	- 68	60.90	56.8	.68	.63	.05	0
- 68	- 67.75	61.2	56.9	.68	.63	.05	0
- 66	- 67.5	61.5	56.9	.68	.63	.05	0
- 64	- 67	61.7	57.0	.69	.63	.06	0
- 62	- 66.5	62.0	57.0	.69	.63	.06	0
- 60	- 66	62.38	57.0	.69	.63	.06	0

FRACTION PRECIPITATED FROM TRAPPED FLUX IN		TOTAL FRACTION PRECIPITATED IN		TRAPPED FLUX ($\times \frac{1}{2}$)	
S.H.	N.H.	S.H.	N.H.	FRACTION OF INJECTED FLUX.	TOTAL
0	0	.61	.63	.38	27.20
0	0	.61	.63	.38	27.58
0	0	.61	.63	.38	27.96
0	0	.61	.63	.38	28.34
0	0	.61	.63	.38	28.72
0	0	.61	.63	.38	29.10
0	0	.61	.63	.38	29.48
0	0	.61	.63	.38	29.86
0	0	.61	.63	.38	30.24
0	0	.61	.63	.38	30.62
0	0	.61	.63	.38	31.00
0	0	.61	.63	.38	31.38
0	0	.62	.62	.38	31.76
0	0	.62	.62	.38	32.14
0	0	.62	.62	.38	32.52
.12	0	.76	.62	.37	32.77
.03	0	.67	.62	.37	33.11
.07	0	.71	.62	.37	33.41
0	0	.64	.62	.37	33.78
0	0	.64	.62	.37	34.15
.04	0	.68	.62	.37	34.48
.12	0	.76	.62	.37	34.73
.21	0	.87	.62	.36	34.88
.27	0	.95	.62	.35	34.96
.19	0	.87	.62	.35	35.12
.05	0	.73	.62	.35	35.42
.10	0	.78	.62	.35	35.67
.05	0	.74	.63	.34	35.96
.16	0	.85	.63	.34	36.14
.20	0	.89	.63	.34	36.28
.10	0	.79	.63	.34	36.52
.21	0	.90	.63	.34	36.65
.11	0	.80	.63	.34	36.88
.22	0	.93	.63	.33	36.99
.11	0	.82	.63	.33	37.21
.22	0	.93	.63	.33	37.32
.22	0	.93	.63	.33	37.43
.23	0	.94	.63	.33	37.53
.11	0	.84	.63	.32	37.74
.12	0	.85	.63	.32	37.94
.35	0	1.08	.63	.32	37.91
.36	0	1.09	.63	.32	37.87
.24	0	.99	.63	.31	37.94
.37	0	1.12	.63	.31	37.88
.49	0	1.24	.63	.31	37.70

LONGITUDE		CRITICAL PITCH ANGLE		FRACTION OF INJECTED FLUX PRECIPITATED IN		FRACTION PRECIPITATED IN	
S.H.	N.H.	S.H.	N.H.	S.H.	N.H.	S.H. FROM N.H.	N.H. FROM S.H.
-58	-66	62.7	57.0	.70	.63	.07	0
-56	-65.75	62.9	57.1	.70	.63	.07	0
-54	-65	63.1	57.2	.70	.64	.06	0
-52	-64.25	63.3	57.3	.70	.64	.06	0
-50	-64	63.8	57.3	.71	.64	.07	0
-48	-63.5	63.8	57.4	.71	.64	.07	0
-46	-63	64.0	57.4	.71	.64	.07	0
-44	-62	64.3	57.5	.71	.64	.07	0
-42	-61.5	64.5	57.6	.72	.64	.08	0
-40	-61	64.83	57.7	.72	.64	.08	0
-38	-60	65.1	57.9	.72	.64	.08	0
-36	-59.5	65.5	58.0	.73	.64	.09	0
-34	-59	65.8	58.0	.73	.64	.09	0
-32	-58	66.1	58.2	.73	.65	.08	0
-30	-57	66.32	58.3	.74	.65	.09	0
-28	-56	66.8	58.5	.74	.65	.09	0
-26	-55	67.2	58.7	.75	.65	.10	0
-24	-54	67.5	58.9	.75	.65	.10	0
-22	-53	68.0	59.0	.75	.65	.10	0
-20	-52	68.33	59.3	.76	.65	.11	0
-18	-51	68.7	59.4	.76	.65	.11	0
-16	-50	69.1	59.6	.77	.66	.11	0
-14	-48	69.5	60.0	.77	.67	.10	0
-12	-47	70.0	60.2	.78	.67	.11	0
-10	-46	70.22	60.5	.78	.67	.11	0
- 8	-45	71.0	60.6	.79	.67	.12	0
- 6	-43	71.6	61.0	.80	.68	.12	0
- 4	-42	72.3	61.2	.80	.68	.12	0
- 2	-40	73.0	61.5	.81	.68	.13	0
0	-39	74.03	61.7	.82	.69	.13	0
2	-37	74.5	62.0	.83	.69	.14	0
4	-36	75.3	62.2	.84	.69	.15	0
6	-34	76.3	62.5	.85	.69	.16	0
8	-32	77.2	62.7	.86	.70	.16	0
10	-31	77.40	62.8	.86	.70	.16	0
12	-29	79.4	63.0	.88	.70	.18	0
14	-27	80.5	63.3	.90	.70	.20	0
16	-25	81.9	63.5	.91	.71	.20	0
18	-23	83.4	63.7	.93	.71	.22	0
20	-21	85.00	63.8	.95	.71	.24	0
22	-19	86.5	63.9	.96	.71	.25	0
24	-17	87.9	64.0	.98	.71	.27	0
26	-15	89.0	64.1	.99	.71	.28	0
28	-13	89.8	64.2	1.00	.71	.29	0
30	-11	90.00	64.2	1.00	.71	.29	0

FRACTION PRECIPITATED FROM TRAPPED FLUX IN		TOTAL FRACTION PRECIPITATED IN		TRAPPED FLUX ($\times \frac{1}{2}$)	
S.H.	N.H.	S.H.	N.H.	FRACTION OF INJECTED FLUX	TOTAL
.37	0	1.14	.63	.30	37.63
.25	0	1.02	.63	.30	37.68
.26	0	1.02	.64	.30	37.72
.26	0	1.02	.64	.30	37.76
.65	0	1.43	.64	.29	37.40
0	0	.77	.64	.29	37.69
.27	0	1.04	.64	.29	37.71
.40	0	1.17	.64	.29	37.60
.27	0	1.07	.64	.28	37.61
.41	0	1.21	.64	.28	37.48
.42	0	1.22	.64	.28	37.34
.56	0	1.38	.64	.27	37.05
.42	0	1.24	.64	.27	36.90
.43	0	1.24	.65	.27	36.74
.29	0	1.12	.65	.26	36.71
.73	0	1.56	.65	.26	36.24
.59	0	1.44	.65	.25	35.90
.38	0	1.23	.65	.25	35.77
.75	0	1.60	.65	.25	35.27
.45	0	1.32	.65	.24	35.06
.61	0	1.48	.65	.24	34.69
.62	0	1.50	.66	.23	34.30
.62	0	1.49	.67	.23	33.91
.79	0	1.68	.67	.22	33.34
.32	0	1.21	.67	.22	33.24
1.28	0	2.19	.67	.21	32.17
.98	0	1.90	.68	.20	31.39
1.15	0	2.07	.68	.20	30.44
1.16	0	2.10	.68	.19	29.47
1.67	0	2.62	.69	.18	27.98
.85	0	1.82	.69	.17	27.30
1.36	0	2.31	.69	.16	26.10
1.70	0	2.71	.69	.15	24.55
1.58	0	2.60	.70	.14	23.11
.35	0	1.37	.70	.14	22.87
3.91	0	4.97	.70	.12	19.08
1.98	0	3.08	.70	.10	17.20
2.56	0	3.67	.71	.09	14.73
2.77	0	3.92	.71	.07	12.03
2.99	0	4.18	.71	.05	9.09
2.86	0	4.07	.71	.04	6.27
2.70	0	3.95	.71	.02	3.59
2.14	0	3.41	.71	.01	1.46
1.57	0	2.86	.71	0	.11
.40	0	1.69	.71	0	0 0

and south equivalent heights respectively, with corresponding precipitated fractions of 0.97 and 0.71. The fraction precipitated in the southern hemisphere from the northern hemisphere is 0.24. The trapped flux consists of all those electrons with pitch angles greater than 85.9°. This is 0.10% for this particular section and to this must be added the trapped flux that has accumulated from the former sections i.e. 0.12%. The total trapped flux at this point is therefore 0.22%.

Similarly, the fractions were determined for the next 2° section and so on. The fractions (or multiples) were tabulated as shown in Table 1.

It is therefore evident from the above that the trapped flux accumulates to the east of the Anomaly as the electrons drift in that direction. However, should the minimum pitch angle of the trapped flux in any section increase above that of the previous section, a portion of the trapped flux with pitch angles between these two values of minimum pitch angle will be precipitated. So it is necessary to keep account of the trapped electron flux and its pitch angle distribution. This may be done graphically as follows.

Figure 6 shows a plot of the minimum pitch angle of the trapped flux versus southern hemisphere longitude.

39/.....

FIGURE 6.

'Minimum pitch angle' of the trapped electron flux in each longitudinal section versus southern hemisphere longitude. At 134°E, the shaded portion of the total trapped flux will be precipitated.

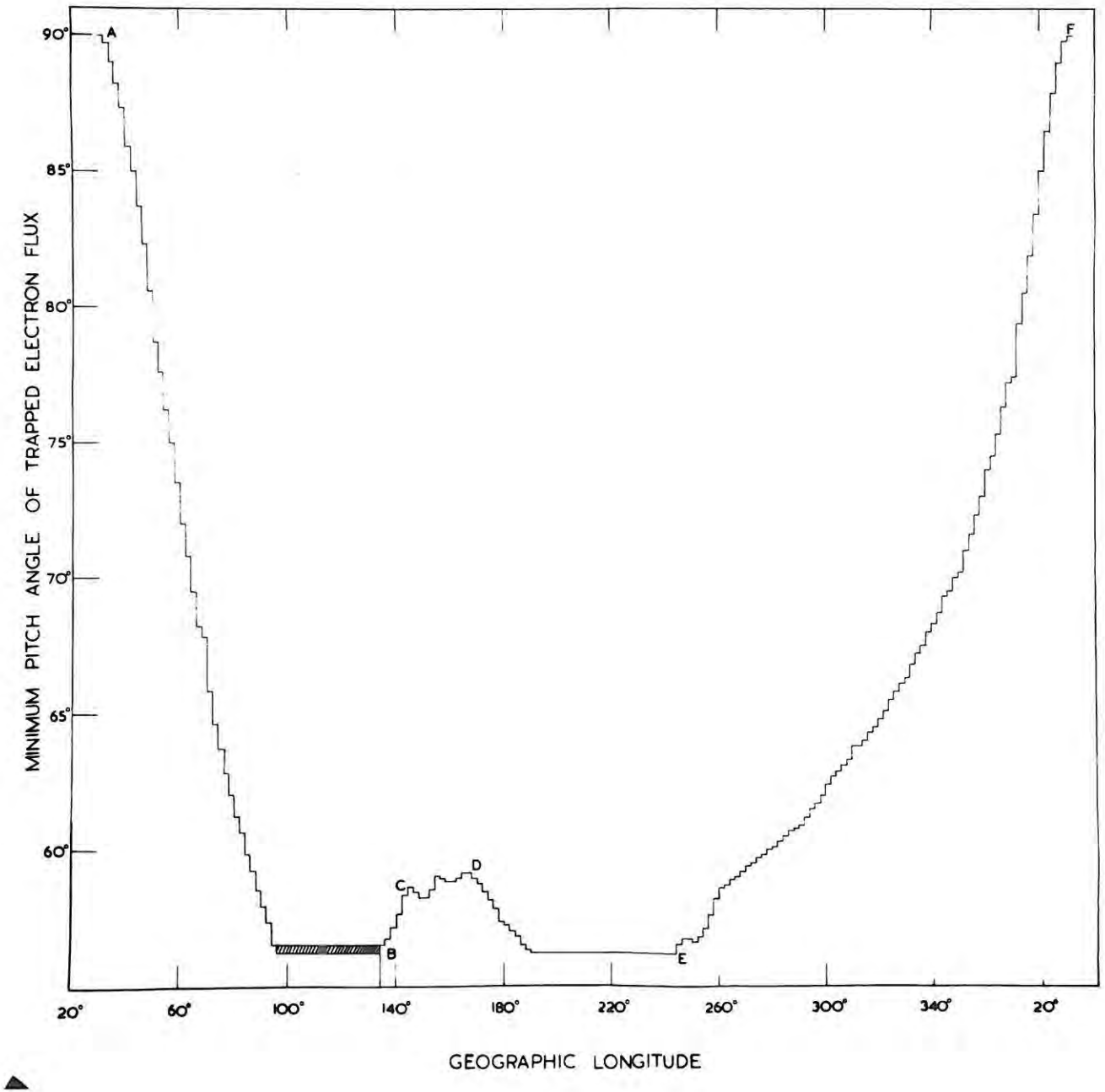
90°
85°
80°
75°
70°
65°
60°
A
B
C
D
E
F
20°
60°
100°
140°
180°
220°
260°
300°
340°
20°
MINIMUM PITCH ANGLE OF TRAPPED ELECTRON FLUX
GEOGRAPHIC LONGITUDE

Starting at 32°E and moving eastward (points A to B in Figure 6) it can be seen that none of the total trapped flux is precipitated in this region, as the minimum pitch angle is decreasing. At point B, however, the minimum pitch angle begins to increase and each successive section will 'chop off' a fraction of the total trapped flux, e.g. the section at 134°E will chop off the shaded area in Figure 6. The trapped flux from B to D is precipitated in the northern hemisphere because in this region the minimum pitch angle of the trapped flux is the northern hemisphere critical pitch angle. Between points D and E there is again no trapped flux precipitated but from E to F successive fractions of the total trapped flux are precipitated this time into the southern hemisphere) until at E, all the electron flux has been wiped out. (Note that in order to obtain the fraction of the trapped flux that is lost, the fractions obtained from Figure 6 must be multiplied by 2 in order to take into account the two hemispheres).

Account is kept of the total trapped flux in Table 1, by adding the trapped fractions of the injected flux for each section progressively and subtracting from this the precipitated fraction of the total trapped flux.

Figure 7 is a plot of the precipitated flux (in multiples of $\varkappa$) versus the longitude, while Figure 8 shows

40/.....

FIGURE 7.

The precipitated flux in multiples of the injected electron flux, x electrons/cm^2/sec. Curves A and B are for the southern and northern hemispheres respectively, in the case of an isotropic injected flux. CurveB is an example (southern hemisphere) of an anisotropic injected electron flux being used in the calculation.

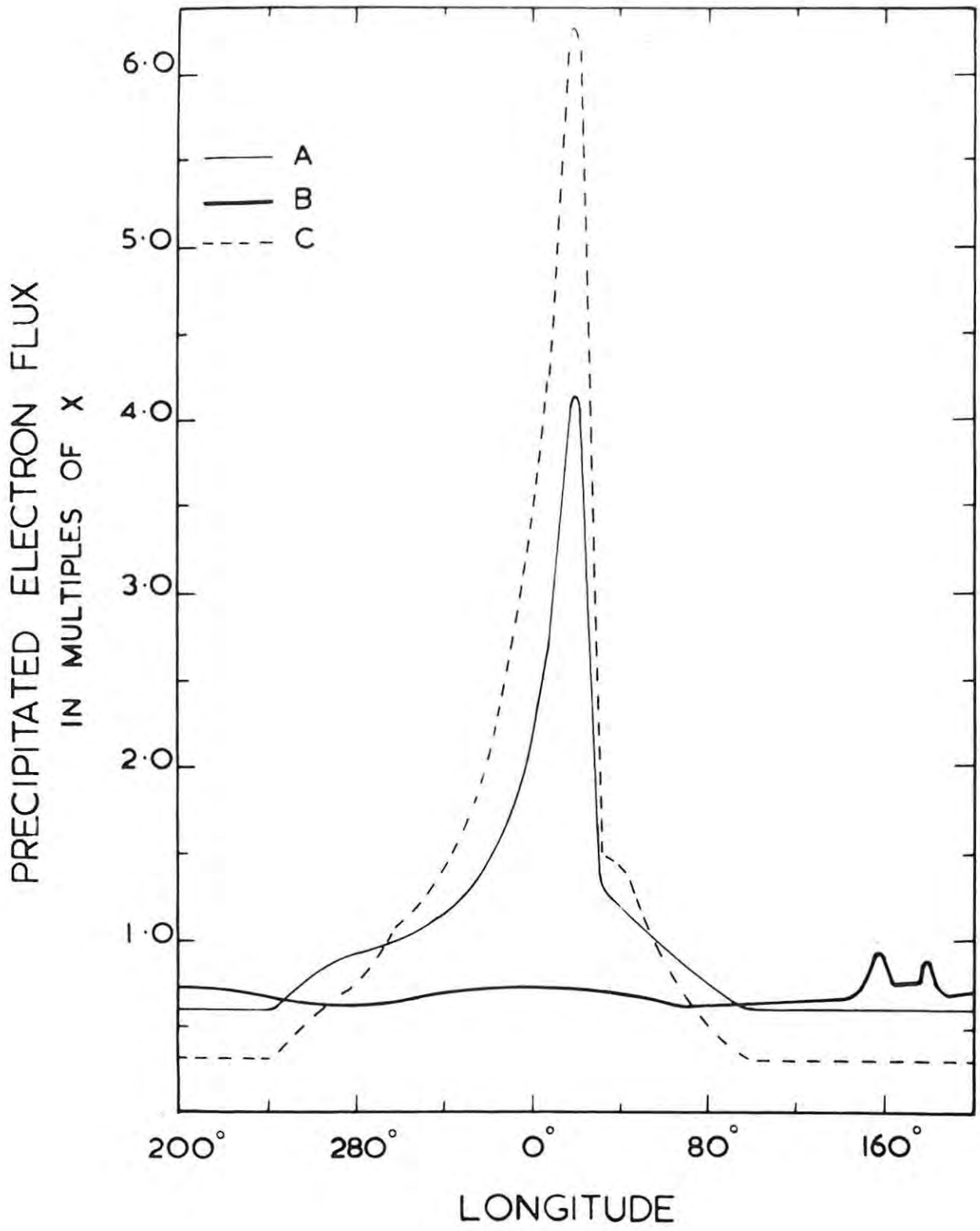
PRECIPITATED ELECTRON FLUX
IN MULTIPLES OF X
6·0
5·0
4·0
3·0
2·0
1·0
A
B
C
200°
280°
0°
80°
160°
LONGITUDE

FIGURE 8.

Trapped electron flux in multiples of x electrons/cm^2/sec. as a function of the longitude of the southern hemisphere equivalent heights.

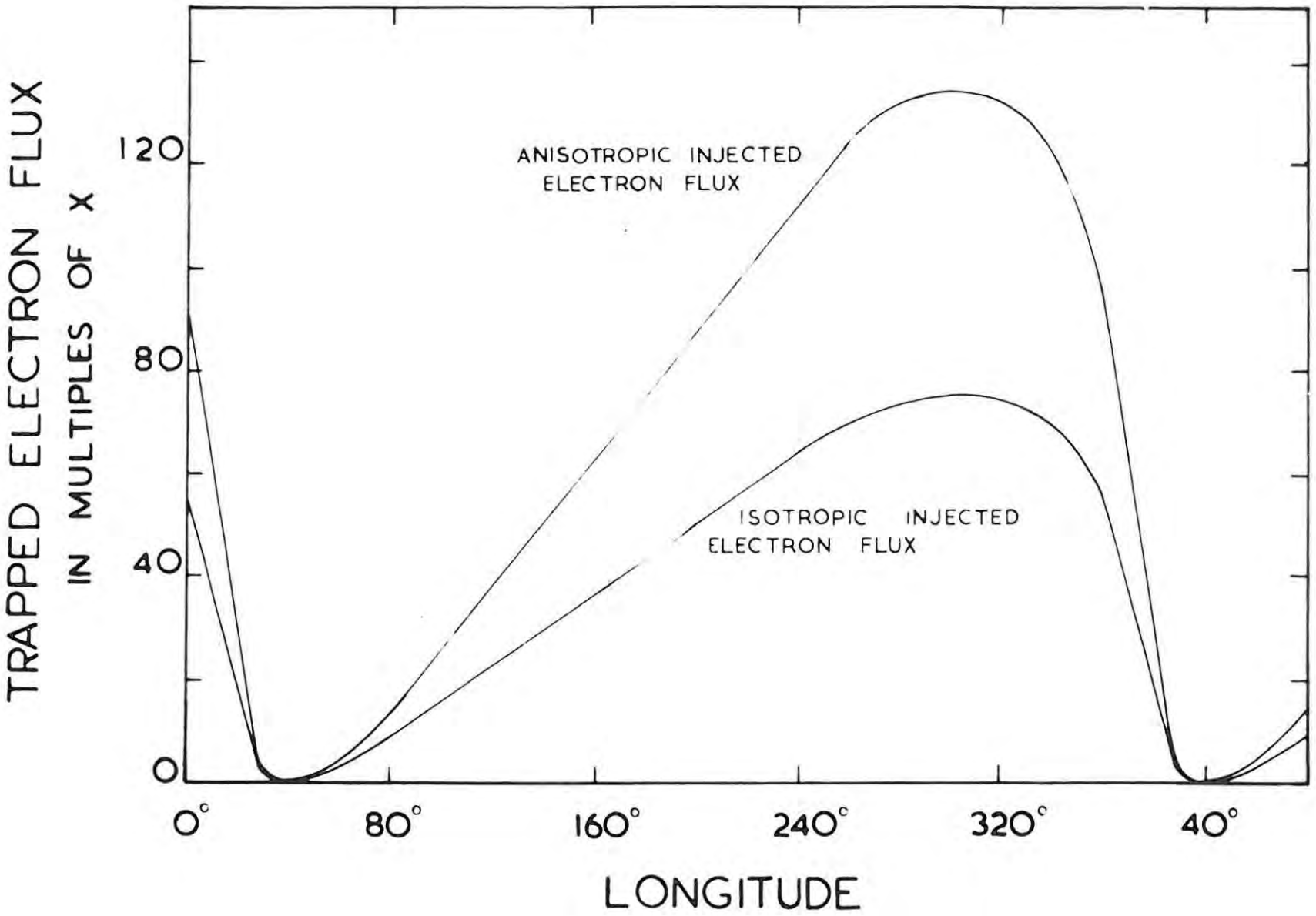
TRAPPED ELECTRON FLUX
IN MULTIPLES OF X
120
80
40
0
ANISOTROPIC INJECTED
ELECTRON FLUX
ISOTROPIC INJECTED
ELECTRON FLUX
0°
80°
160°
240°
320°
40°
LONGITUDE

the total trapped flux (also in multiples of $\varkappa$) as a function of the longitude of the southern hemisphere equivalent heights. There is a great increase in the precipitated flux over the Southern Anomaly where it forms a sharp peak with a maximum at 20°E. However, outside the Anomaly and in the northern hemisphere the curve is almost flat. From figure 8 it is seen that the total trapped flux is wiped out by 30°E and then builds up fairly linearly until it reaches a maximum, roughly centred on 300°E. This is the reason for chosing the 32°E section as the first one, as there is no trapped flux drifting in from the previous (30°E) section.

3.4. Anisotropic Pitch Angle Distribution:

It has been assumed in the above calculations of the trapped and precipitated electron flux, that the injected electron flux has isotropic pitch angle distribution. The rocket observations of Davis et al (1960) and McDiarmid et al (1961) established that the fluxes of electrons tended towards isotropy at the relatively low altitudes of 150 km. Chamberlain (1961) has advanced arguments in favour of the incoming flux being isotropic. He stated that an isotropic distribution is 'to be expected for particles propelled toward the atmosphere from an injection

41/....

FIGURE 9.

Pitch angle distributions for 'old' and 'fresh' particles, (O'Brien, 1964).

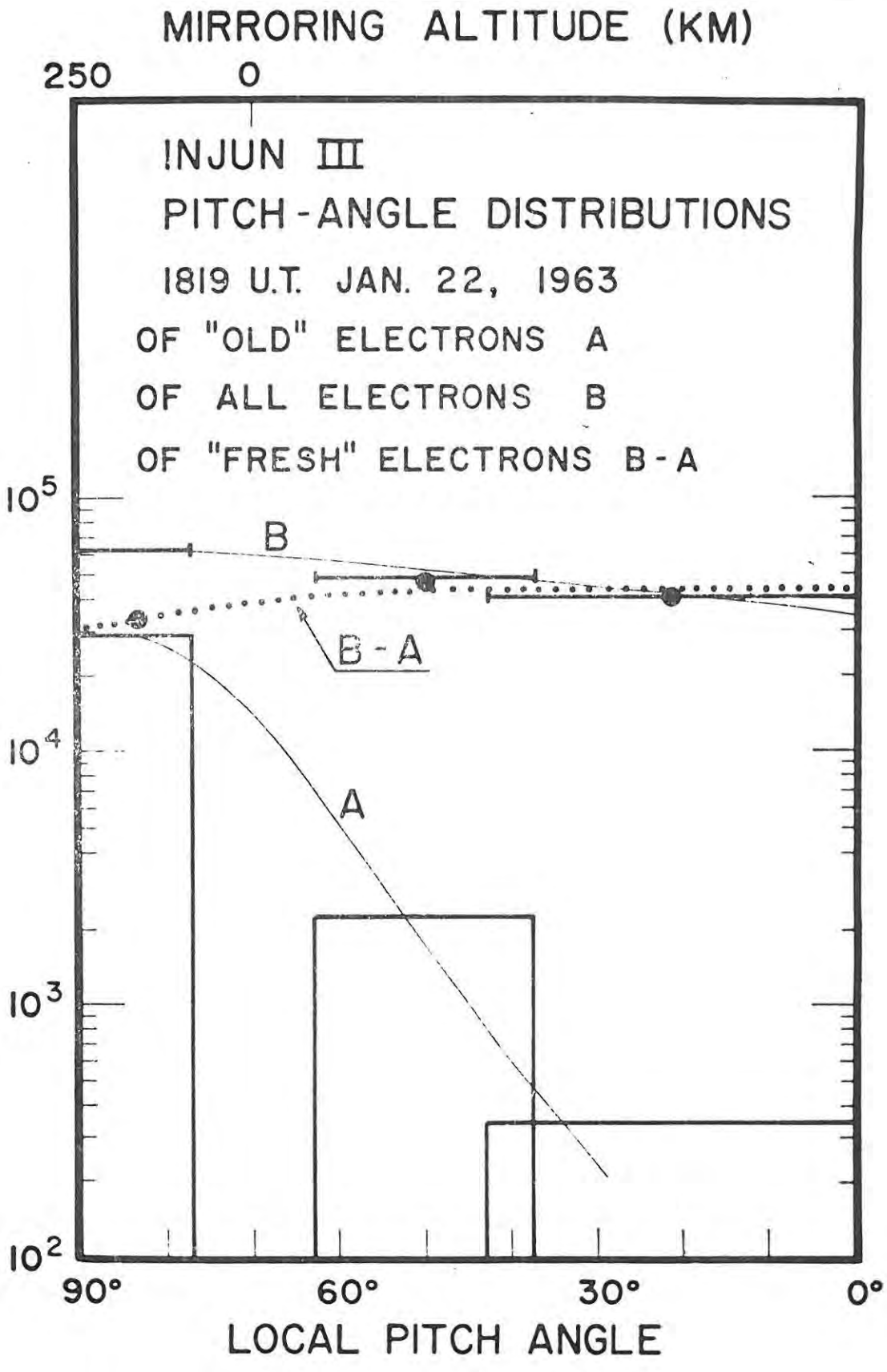

FLUX
PARTICLES
CM^{-2} SEC^{-1}
$STERAD^{-1}$

source or centre of acceleration located far above the atmosphere'. O'Brien (1964) found the incoming or 'fresh' particles to have the angular distribution indicated by the dotted line in Figure 9, and this is very nearly isotropic.

McDiarmid and Budzinski (1964) using Black Brant II rockets fired from Fort Churchill, investigated the pitch angle distributions of auroral electrons with energies greater than 40 kev. They observed varying degrees of isotropy but in no case found a distribution in which the intensity increased towards small angles. This is as would be expected from the model because of the build up of the higher pitch angles in the trapped flux.

It would appear then that to assume isotropic angular distribution for the injected flux is most reasonable and that observed distributions showing increased intensity towards the higher pitch angles is a result of the longitudinal drift of trapped particles and the immediate precipitation of those particles having small pitch angles at low altitudes, rather than as a result of the angular distribution of the incoming particles.

However, the effects of the injected flux being anisotropic were also examined. Using the worst case of anisotropy reported by McDiarmid and Budzinski (1964) (see Figure 10) for the pitch angle distribution of the continuously injected flux, the calculations were repeated. In this

FIGURE 10.

Pitch angle distribution of electrons with energies $\geq$ 40 kev. (McDiarmid and Budzinski, 1964).

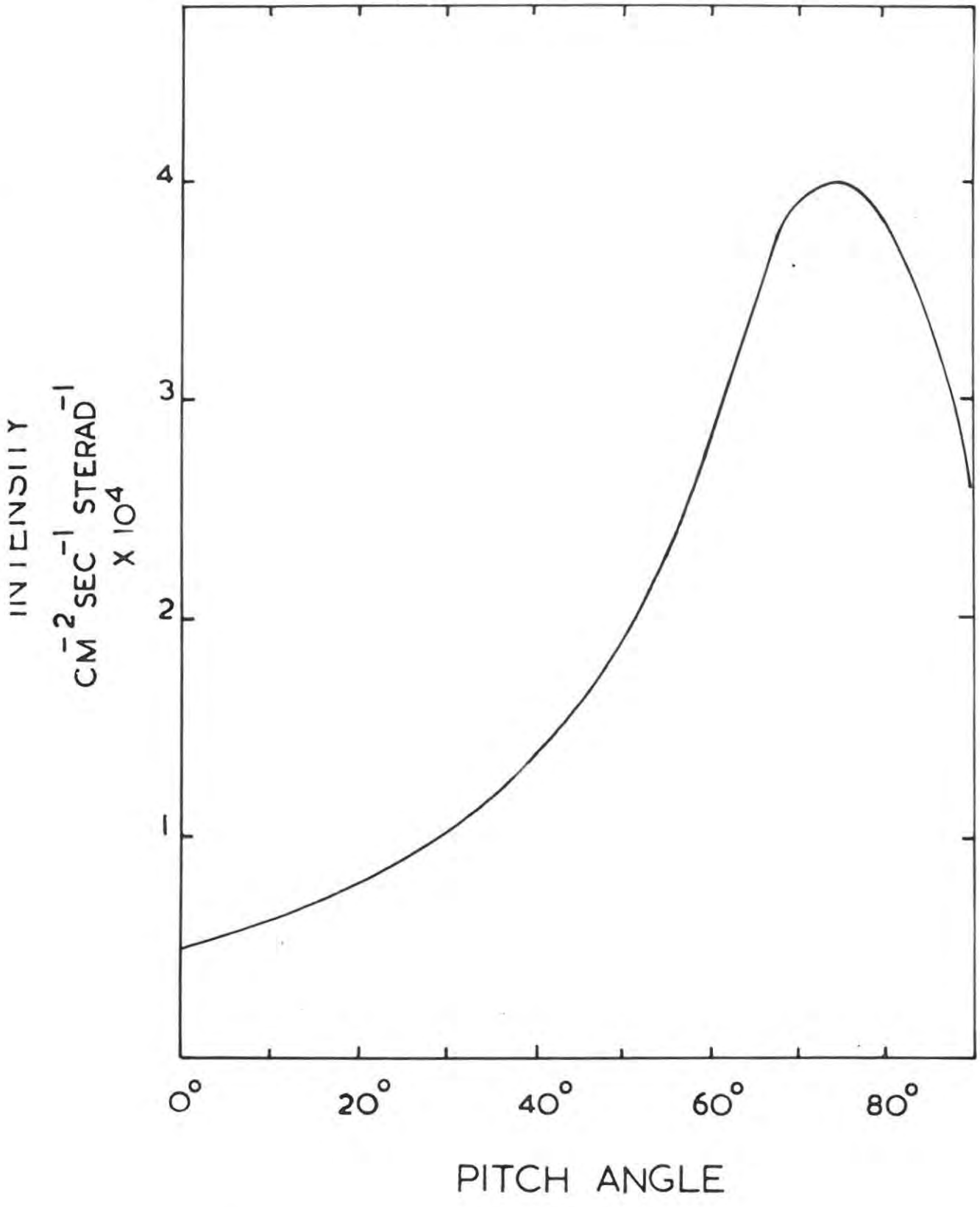
INTENSITY
CM^{-2} SEC^{-1} STERAD^{-1}
X 10^4
4
3
2
1
0°
20°
40°
60°
80°
PITCH ANGLE

case, the precipitated and trapped fractions were not calculated on the basis of the ratio of pitch angle to 90^{o}, but rather as the ratio of the area contained under the particular pitch angle on the McDiarmid - Budzinsky distribution, to the total area under the curve. The shape of the precipitated and trapped fraction curves then obtained are also shown in Figures 7 and 8. These however, are likely to be for more exaggerated than the actual case.

An interesting point to notice on the pitch angle distribution curves observed by McDiarmid and Budginsky is that there is a peak in intensity at $\sim 75^{o}$ and a fall off in intensity from 75^{o} to 90^{o}. This type of distribution is not predicted by the above model with injection at the equivalent height points. However, such a mode of injection is obviously highly artificial and was adopted only for the sake of simplicity. In fact it would be expected that injection would take place over a diffuse band of altitude along the field lines. The effects of this will be briefly considered.

If injection takes place only at the equivalent height points, the pitch angle distribution there will be altitude of 100 km above the equivalent height points as well, the angular distribution at these points will no longer be

isotropic. Of the particles injected 100 km above, all those with pitch angles between 76° and 90° will mirror above the equivalent height. By the time that the remaining particles (with pitch angles between 0° and 76°) have reached the equivalent height they will have been re-distributed in pitch angle between 0° and 90° i.e. they will 'fan out'. However, the new distribution is not isotropic there being fewer particles with higher pitch angles. If these particles are added to those introduced at the equivalent height to give the total intensity versus pitch angle at the equivalent height, the new total distribution is as shown by the curve labelled '100 km' in Figure 11. Similarly, this may be repeated assuming that injection takes place over a band of 200 km above the equivalent heights and so on. (Note that if the injection takes place over a band of n x 100 km in height and the flux injected over each 100 km band is y electrons /cm^2/sec, then ny = x).

It may be seen from Figure 11, that the angular distribution at the equivalent height points becomes less and less isotropic with increasing height of the injection band, resulting in a fall off in intensity towards the higher pitch angles that becomes more pronounced with increased height of the band.

This then explains the pitch angle distribution observed by McDiarmid and Budzinski. The lower pitch angles will

44/.....

FIGURE 11.

Diagram of increasing anisotropy with increasing height of injection band.

PRECIPITATED ELECTRON FLUX
IN MULTIPLES OF Y

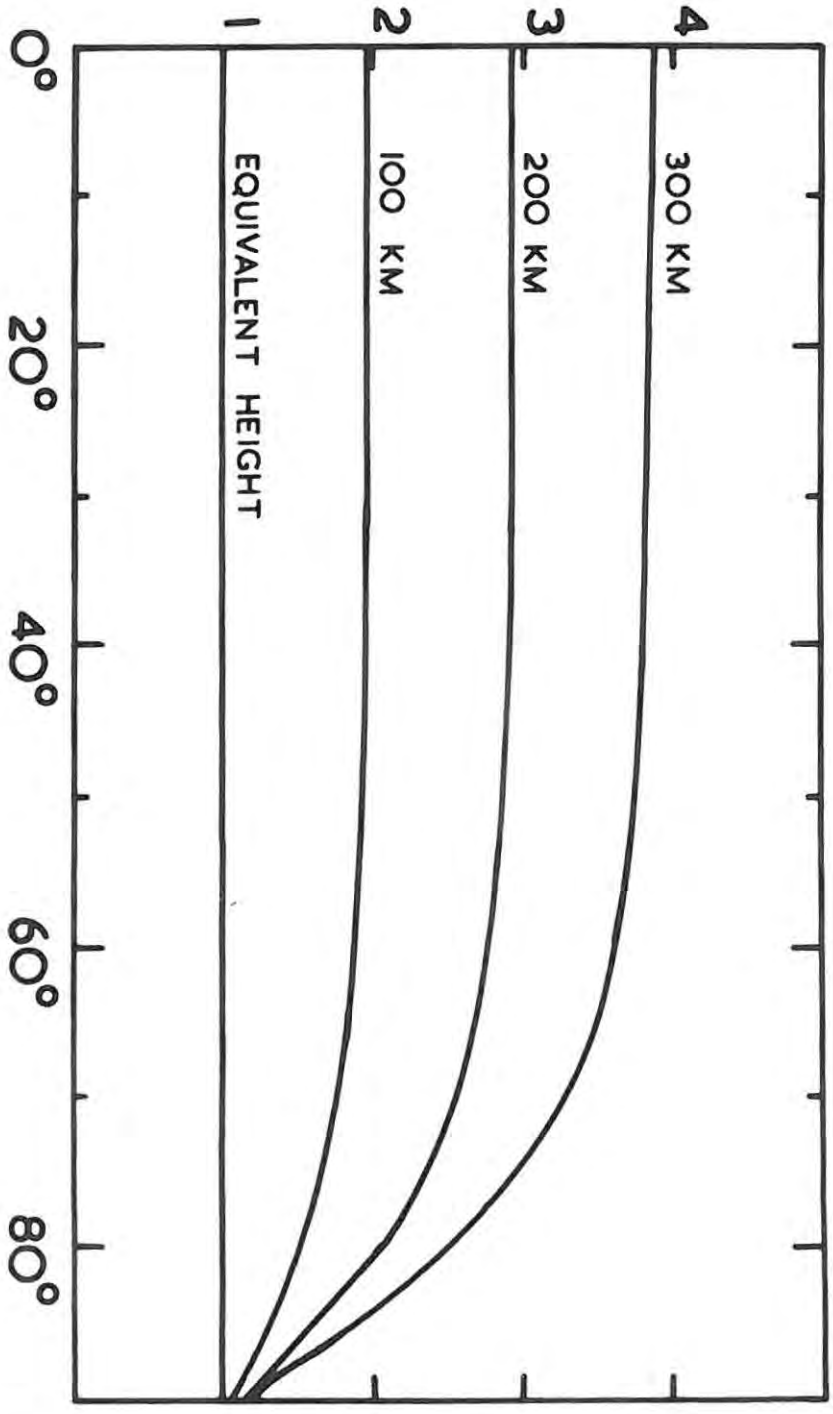

be precipitated while the higher pitch angles accumulate, but there is a fall-off in the intensity of the accumulated flux after ~70°.

From a more detailed investigation of this type, an estimate could be made of the size of the height interval of injection.

3.5. Comparison with Experimental Observations:

(a) Electron flux data observed by the satellite Alouette at 1000 km over L = 4.4 between ~170°E to 330°E in the northern hemisphere for the period 1st October, 1962, to 31st March, 1963, were used to check the validity of this model.

According to McDiarmid (private communication) the minimum value of the elctron flux that could reliably be detected by the satellite was 1.4×10^4 electrons /cm^2/second. The medians of the measured precipitated and trapped electron flux values (≯ this minimum of 1.4×10^4 electrons /cm^2/second) were calculated for each 10° longitudinal lamination over which the satellite operated. The northern hemisphere longitudinal range 210°E to 280°E suited the purpose of this comparison rather well as in this longitudinal interval, the northern hemisphere equivalent height is approximately 1000km, i.e. the satellite altitude.

Over the range 210°E to 230°E the median values of the precipitated and trapped electron fluxes were constant for the three laminations involved, and were found to be 2.5×10^4 electrons /cm^2/sec and 151.5×10^4 electrons /cm^2/sec respectively. From the model, the critical pitch angle, the precipitated fraction and the trapped multiple of x are 57°, 0.68 and 42.3 respectively.

Therefore, equating the median value of the observed precipitated flux to the theoretical value in multiples of x,

$$2.5 \times 10^4 \text{ electrons /cm}^2\text{/sec} = 0.68x$$

giving $x = 3.69 \times 10^4$ electrons/cm^2/sec

and for the trapped electron flux

$$151.5 \times 10^4 \text{ electrons /cm}^2\text{/sec} = 42.3x$$

giving $x = 3.59 \times 10^4$ electrons /cm^2/second.

Similarly for the ranges 230°E to 250°E and 250°E to 280°E, (using the correct values for precipitated and trapped fluxes, fractions and critical pitch angle in each case), the two pairs of values obtained for x were 3.80×10^4 elec/cm^2/sec ; 3.88×10^4 elec/cm^2/sec and 3.49×10^4 elec/cm^2/sec ; 3.14×10^4 elec/cm^2/sec.

These values show extremely good agreement considering the vast difference between the precipitated fractions in this region and the large variations which occur with time and the simplicity of the model.

46/.....

(b) The position of the Southern Radiation Anomaly emerging from this model agrees rather well with the regions of maximum charged particle intensity observed by satellites Discover 31 (Seward and Kornblum, 1963) and Sputnik 5 and 6 (Ginsburg et al, 1961). The plot of the precipitated fraction for the northern hemisphere show the smaller 'Russian' anomaly, although the position of this anomaly is to the east of the positions in which it was observed by satellites Sputnik 5 and 6.

(c) Paulikas and Freden (1964) and Imhof and Smith (1965) found an assymetry in trapped electrons for ranges of L corresponding to the Brazilian Anomaly. Imhof and Smith found that in the energy range 0.28 to 0.71 Mev, the electron fluxes observed just to the west of the Brazilian Anomaly (for particles mirroring below 100 km) were about an order of magnitude greater than those measured just to the east of the Anomaly.

The Russian Cosmos satellites (Vernov et al, 1965) observed a similar loss of trapped electrons with longitudinal drift from west to east across the Brazilian Anomaly and a longitudinal assymetry was also found in trapped protons drifting in the opposite direction.

Williams and Kohl (1965), have examined the spatial characteristics of electrons trapped at high B values in the region $1.4 \leq L \leq 3.4$, using data from the satellite 1963

47/....

38c. They present a plot of the longitudinal dependence of electron intensity through the Brazilian Anomaly for L = 2.2, and this is very similar in appearance to Figure 8. The total trapped fraction curve (Figure 8) was normalized to the relative intensity of electrons versus longitude observed by the satellite 1963 38c. The results, Figure 12, show extremely good agreement considering the difference in L values.

-----oooOooo-----

FIGURE 12.

Comparison of the total trapped electron flux with the relative intensity curve observed by satellite 1963 38C (Williams and Kohl, 1965).

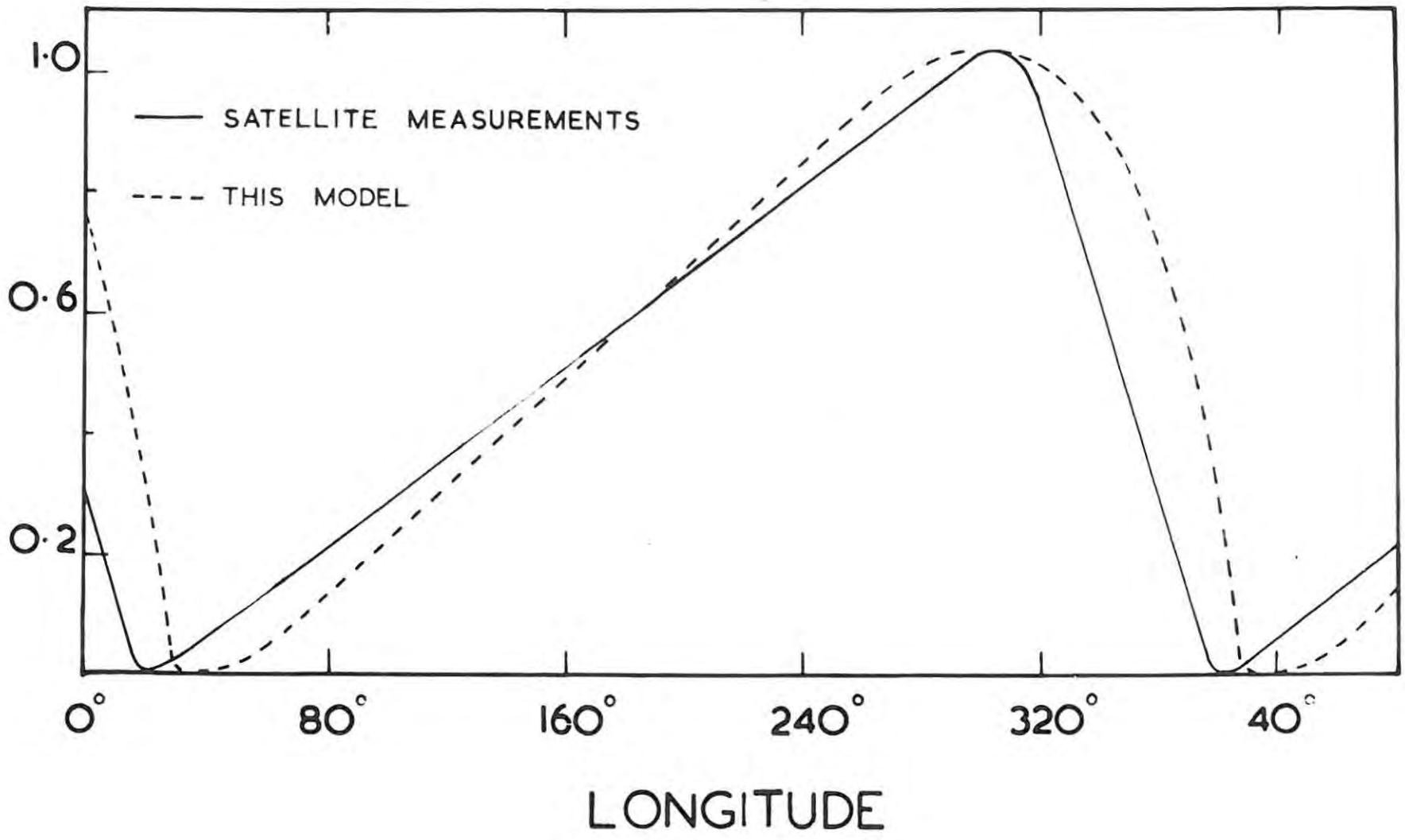
1·0
0·6
0·2
SATELLITE MEASUREMENTS
THIS MODEL
0°
80°
160°
240°
320°
40°
LONGITUDE

PART II.

CHAPTER 4.

ELECTRON PRECIPITATION AND IONOSPHERIC DISTURBANCE.

4.1. Introduction:

Since the pioneer work of Birkeland (1908) and Störmer (1955), it has generally been accepted that aurorae are produced by fast electric particles entering the atmosphere, guided by the magnetic lines of force. Meinel (1951) measured Doppler-shifted Balmer emissions in aurorae and detected protons bombarding the upper atmosphere. As a result of this, much of the emphasis in auroral studies centred on proton excitation for several years until it was realized that protons could not be responsible for all aurorae. In fact Vegard had suggested in 1921 that the lateral dimensions of auroral rays were too small ($\lesssim$ 1 km) to be caused by proton bombardment since the cyclotron radius of a proton of the required energy is much larger. He suggested that electrons might be responsible.

The rockoon flights of the Iowa group from 1952 onwards (Van Allen, 1957) detected electrons with energies of $\sim$100kw in fluxes of 10^6 to 10^8 particles /cm^2/sec at altitudes of $\sim$100km in the auroral zone (magnetic latitude $\sim 67^\circ$) but not at higher or lower latitudes. During the I.G.Y. rockets were launched into visible aurorae. McIlwain (1960) and

49/.....

Davis et al (1960) found aurorae caused by electrons with energy spectra usually most intense round 5 to 10 kev. The results verified the conclusions of Omholt (1957, 1959) based on spectroscopic observations of aurorae, that protons play a very minor role in the excitation of most aurorae. Injun 3 (O'Brien, 1964) found precipitation all the time in the auroral zone. Figure 13 is an example of simultaneous Injun 3 observations of trapped and precipitated electrons and auroral luminosity, showing clearly that the aurora is brightest where the precipitation of electrons is the greatest.

Gledhill and Van Rooyen (1963) predicted, because of the large precipitation in the Southern Anomaly, that there should be enhancement of other geophysical phenomena such as X-ray fluxes and ionization and heating of the atmosphere.

On the basis of energy considerations, O'Brien (1962b) has shown that it is highly unlikely that precipitated electrons are able to sustain midlatitude 5577Å airglow. However, the excitation energy of 3914 Å in night airglow is as high as 18.8 ev so that no mechanism other than particle bombardment seems to be effective enough to excite these bands (Hiao et al, 1964), and their emission is taken to be a definite proof of particle precipitation.

Auroral absorption is generally defined on riometer records as all the absorption except that associated with

FIGURE 13.

Observations of trapped and precipitated electrons and auroral luminosity by Injun 3 (O'Brien, 1964).

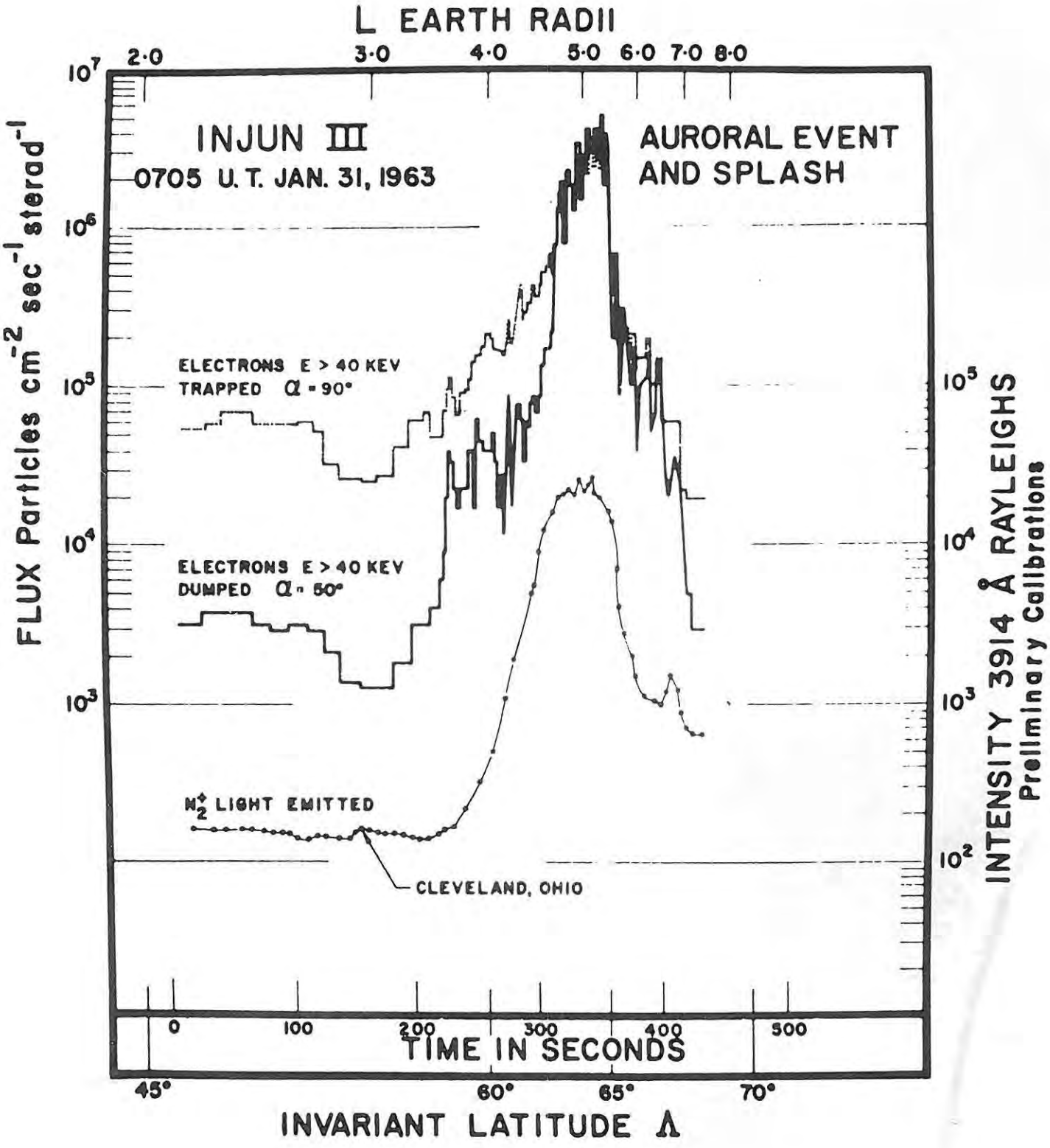
L EARTH RADII
2·0
3·0
4·0
5·0
6·0
7·0
8·0
INJUN III
0705 U.T. JAN. 31, 1963
AURORAL EVENT
AND SPLASH
ELECTRONS E > 40 KEV
TRAPPED α = 90°
ELECTRONS E > 40 KEV
DUMPED α = 50°
N2+ LIGHT EMITTED
CLEVELAND, OHIO
FLUX Particles cm-2 sec-1 sterad-1
INTENSITY 3914 Å RAYLEIGHS
Preliminary Calibrations
TIME IN SECONDS
INVARIANT LATITUDE Λ

either polar cap absorption or sudden cosmic noise absorption these being due to high energy solar protons and solar ultraviolet light respectively.

These geophysical effects have been definitely correlated with electron precipitation. Although it is known that the precipitation of electrons is able to cause ionization of the upper atmosphere (Rees, 1963), no relationship had been established between precipitated electrons and any ionospheric phenomena until Gledhill and Torr (1965) found a high correlation between precipitated electron flux (P.E.F.) and ionospheric disturbances (I.D.) at Sane (70.3^{o}S, 2.4^{o}W) which lies in the Southern Radiation Anomaly.

In this chapter the criterion used by Gledhill and Torr for determining whether or not the ionosphere is disturbed is applied to other stations along L=4. The definite relationship between P.E.F. observations and ionospheric disturbances is proved beyond doubt. In fact it is shown that the precipitation of electrons accounts for ionospheric disturbances at all stations along L=4.

As various ionopheric parometers are used in this analysis, an outline of the structure of the ionosphere will first be given.

51/.....

4.2. The Ionosphere:

4.2.1. The Structure of the Ionosphere:

The ionosphere owes its existence to the ionisation of the neutral gas molecules of the upper atmosphere by ultra violet light from the sun. The normal ionosphere in temperate climates consists of several ionised regions or layers. The lowest of these, the D region, lies between 50 to 90 km. It is followed by the E region at about 100 to 140 km, and then the F region at heights of 150 to about 400 kms. The latter is a single layer during the night, but often splits into two layers during the day. The lower of these is called the F1, and the upper the F2 layer. Figure 14 shows a typical distribution of electron density with height. The peaks of ionisation which demarcate the different layers usually correspond to quite small 'ledges' in the N(h) profile. The E and F regions may be separated by a minimum of electron density at sunrise and during solar exlipses.

On the basis of experimental evidence it is believed that the electron density in the E and F layers is controlled by the sun. The electron density shows diurnal, seasonal, solar cyclic and latitudinal variations. Analysis of data obtained during solar exlipses has shown that it is electromagnetic radiation that is the control-

52/.....

FIGURE 14.

Typical distribution of electron density with height.

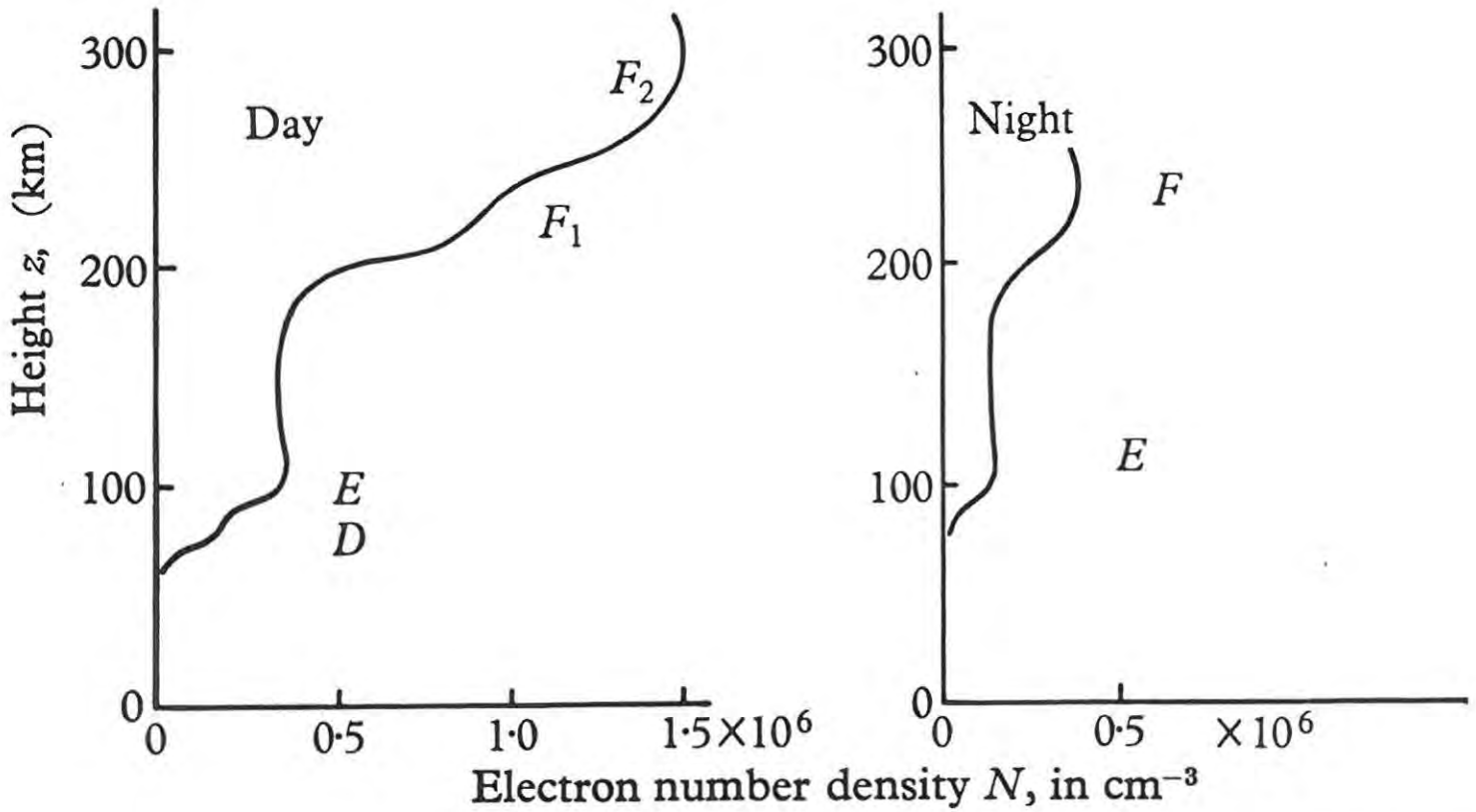
300
200
100
0
Height z, (km)
Day
F_2
F_1
E
D
0
0·5
1·0
1·5×10⁶
Night
F
E
×10⁶
Electron number density N, in cm⁻³

ling factor rather than corpuscular streams. Although it is most likely that the F2 layer is also formed by solar radiation, there are a number of irregularities in the behaviour of this layer that cannot be explained by simple theory. For example, the maximum density occurs well after noon at most stations.

4.2.2. Layer Formation:

Solar ultraviolet and X-radiation ionize and dissociate the atmospheric gasses as they are absorbed. The idealized process of layer formation has been studied in detail by Chapman (1931). Briefly, this can be summorized as follows. If a beam of U.V. radiation, of a single wavelength capable of producing photoionization of an atmospheric constituent, enters the atmosphere, it is absorbed in producing ionization. Because the rate of absorption is controlled by the intensity of the incident radiation and the density of the gas, this will result in a maximum in the rate of ion production at a certain level. With decreasing altitude, the intensity of the radiation will decrease, but the density of the atmosphere increases. These two factors will combine to produce a maximum.

The rate of production of ions is also dependent on the solar zenith angle χ, as this determines the thickness of atmosphere through which the radiation must pass before reaching a given level.

The expression derived by Chapman for q, the rate of ion production, is

$$q = qm \exp (1 - z - e^{-z} \operatorname{Sec} \chi)$$

where $qm = B I_\infty \frac{\operatorname{Cos} \chi}{H \exp (1)}$

and z = height normalized by the scale-height

$$H = \frac{h - h_m}{H} \quad , \quad H = \frac{RT}{Mg}$$

B= number of electrons produced when unit energy is absorbed.

I_∞ = power flux/unit area, incident from above at an angle χ to the zenith.

h = height.

h_m = height of layer maximum.

R = gas constant

T = absolute temperature

M = molecular weight of gas

g = accelration due to gravity.

The E and F, layers result from 2 different combinations of radiation and ionizable gas in the above.

All the atmospheric sonstituents capable of photo-ionization would become completely ionized, were it not for the processes of ionization decay. The chief loss mechanisms are recombination of electrons and positive ions and the attachment of electrons to neural molecules.

The rate of recombination is proportional to the electron density and to the positive ion density and is given by

$$\frac{dN}{dt} \text{ (recombination)} = -\alpha N^2$$

54/....

where N is the electron density in electrons/$_{cm}3$ and is equal to the number of positive ions/$_{cm}3$, α is known as the recombination coefficient.

The rate of attachment is proportional only to the electron density and is expressed by

$$\frac{dN}{dt} \text{ (attachment)} = -\beta N$$

where β is the attachment coefficient.

The actual electron density present at any given time will represent a balance between the rates of production and loss, so that the rate of change of electron density at a given height may be written

$$\frac{dN}{dt} = q - \alpha N^2 - \beta N$$

In the E and F1 layers, recombination is the dominant loss mechanism

$$\text{i.e. } \frac{dN}{dt} = q - \alpha N^2$$

and it is thought that the dominant loss mechanism in the F2 region is attachment,

$$\text{i.e. } \frac{dN}{dt} = q - \beta N$$

The morphology of the D, E and F, layers may be explicable to a good approcimation by processes of electron production and loss alone. But in the F2 layer, the long mean free paths allow transport of charge to play a role. Transport of plasma due to gravity is called diffusion and

55/.....

that due to electric fields, drift. With transport included, the complete continuity equation for electrons in the F_2 layer is

$$dN = P - L - \text{div}\,(n\vec{V})$$

where P is the total production, L is total loss and div $(N\vec{V})$ where V is the mean velocity, is the change resulting from transport, (Ferraro, 1945, Norton and Van Zandt, 1961, 1963 and Martyn, 1947).

4.2.3. Exploration of the Ionosphere:

Most of the present knowledge of the ionosphere has been and is obtained by radio pulse sending. The lower region of the atmosphere is not appreciably ionised and is in fact almost an insulator. However, the changing electric field of the radio wave generates a displacement current. Once the ionised regions are reached, the electric field sets the free electrons into motion, thus generating a convection current which is in antiphase with the displacement current. The resulting phase of the wave is changed, having the effect of speeding up the phase velocity v of the wave. As the radio wave passes through increasing ionisation, the convection current plays an increasingly important part with the result that the phase velocity of wave becomes greater.

However, from elementary wave theory

$$vv^{-1} = c^2$$

56/.....

where v^1 is the group velocity, or velocity of energy transfer of the wave, and C is the velocity of light in vacuo. Therefore in the ionised regions the group velocity decreases with increasing phase velocity. When the group velocity becomes zero, the wave is 'reflected' and travels downward again with increasing group velocity until it reaches the non ionised region in which it travels with velocity C. The electron density which will reflect the wave is dependent on the wave frequency, which is then called the plasma frequency fo. The following standard relation has been derived from ionospheric theory

$$N = 1.24 \times 10^4 \ fo^2.$$

The basis of the method of investigating the ionosphere therefore consists of sweeping through a range of different frequencies. Different electron density maximum will reflect different frequencies and the times of travel of the reflected pulses are noted.

Because of the small electron density and high collisional frequency at altitudes corresponding to the D region, the excessive absorption results in it being almost impossible to obtain reflections at vertical incidence from the layer. Therefore, in the past, information regarding the D-region has been obtained from observations of absorption of radio waves reflected from other layers as

57/.....

these must pass through the D region. However, considerable progress has been made recently with rocket experiments and also the cross-modulation technique.

The lowest frequency at which echoes or reflections from any layer are observed is defined as fmin.

It was mentioned above that a radio pulse does not travel at constant speed through the ionosphere. However, by assuming constant speed (C), it is possible to calculate the height to which the pulse would have travelled, the virtual height, h'. Methods have been developed for calculating the real heights (Titheridge, 1959).

The main aim of this chapter will now be considered, namely to investigate the possible existence of a relationship between ionospheric disturbances and precipitated electron fluxes.

4.3. Satellite Data:

As mentioned in Chapter 4, the satellite Alouette measured P.E.F. values at 1000 kms in the northern hemisphere between ~170°E and 330°E. Satellite observations for the period 1st October, 1962 to 31st March, 1963 were used.

Because telemetary was not received from the satellite over the southern hemisphere, it was necessary to compare ionospheric disturbance occuring at stations in that

hemisphere with P.E.F. values measured over their conjugate points. Since the altitude of the equivalent height path (see Chapter 4) between 210°E and 280°E was ~1000km, i.e. the satellite altitude, the values of P.E.F. may be regarded as having been measured along the mirror height path. Therefore, over this longitudinal range, these observations may be compared, or used in conjunction with the theoretical values of P.E.F. at the equivalent heights.

In order to have enough electron flux data with which to investigate a possible relationship with I.D.'s, all the electron flux values observed within a certain longitudinal and latitudinal range on either side of any particular ionosphere station were used, i.e. it was necessary to define an 'area' around the station (or conjugate point) and to use the observational data taken in this area rather than over an exact geographic point. The maximum extent in latitude of these areas was determined by a characteristic of the satellite, viz. it measured over certain bands of 2° inveriant latitude. In this analysis, the band centred on L=4.4 was used. 2° invariant latitude corresponds to $\triangle L = 0.5$ and L=4.4 was the closest of those available to L = 4.

After careful examination, it was found that a 20° range of longitude centred on the geographic co-ordinates

of any particular station was usually large enough an area to provide sufficient observational data for the analysis. For some stations (or their conjugate areas) over which the satellite made a large number of observations, it was possible to reduce the longitudinal dimension. In the case of Winnipeg, however, this had to be extended to as much as 28^{o} because of fewer satellite observations over that region. The effect of varying the longitudinal range is discussed later in this chapter.

4.4. Ionospheric Disturbances:

The criterion for an I.D. introduced by Gledhill and Torr (1965) was used in this analysis. They found that the type of I.D. most frequently occompanying the precipitation of electrons, involved large deviations from the median of the minimum virtual height of the F2 layer, h'F2, and increases in the minimum reflected frequency, fmin, often amounting to a total blackout. These two parameters were therefore used in defining a disturbance criterion.

Hourly values of h' F2 and Bmin for the 10 internationally quiet days (Lincoln, 1963) were used to determine the undisturbed ranges at each station for each month. Then if either h' F2 or fmin lay outside these ranges, the ionosphere was classified as disturbed. The disturbance had to occur within one hour of the time of the satellite P.E.F.

60/.....

FIGURE 15.

h'F2 and fmin at Sanae over a 12 hour period during which a typical ionospheric disturbance occurred.

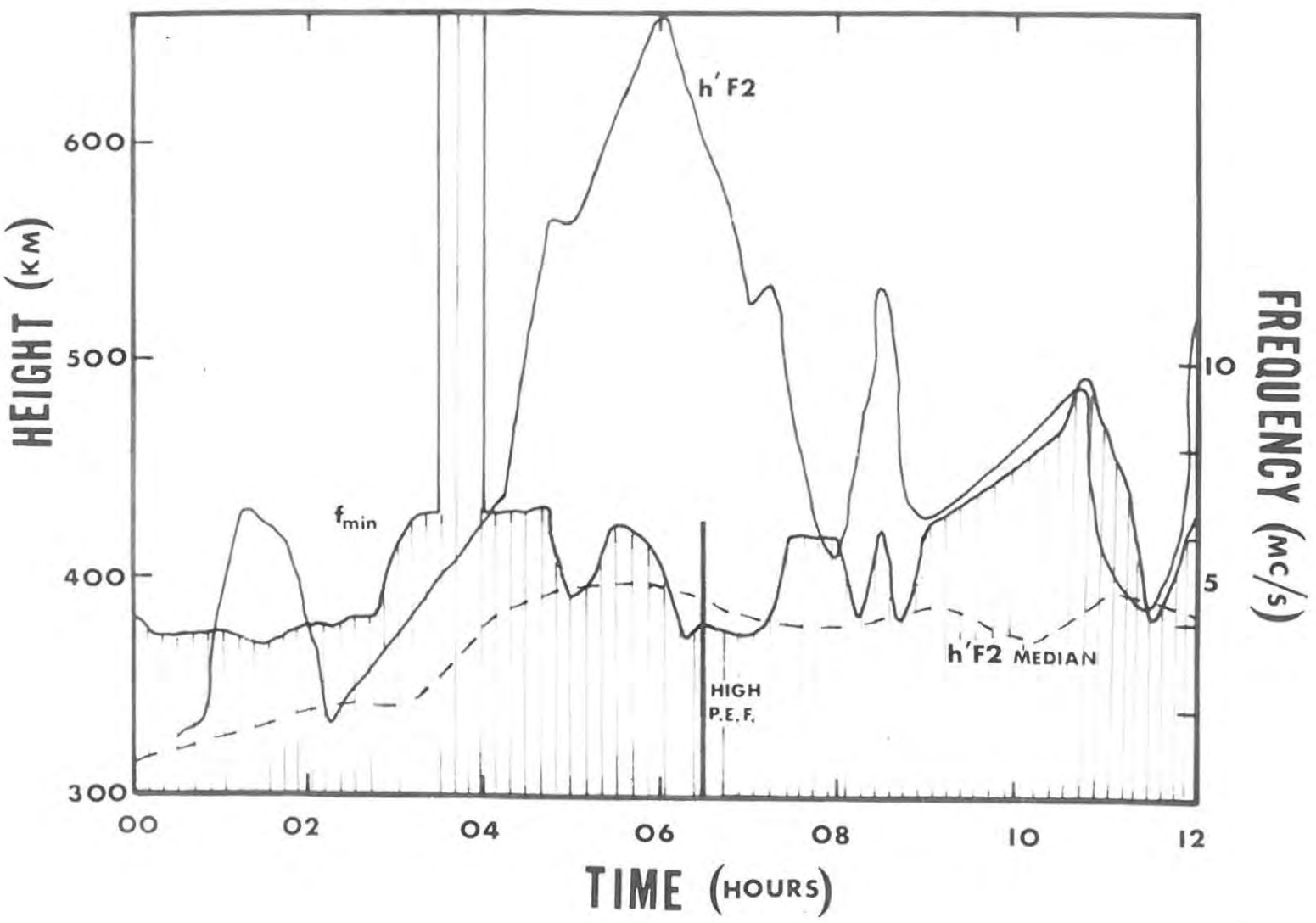
HEIGHT (KM)
600
500
400
300
h' F2
f_{min}
h'F2 MEDIAN
HIGH
P.E.F.
FREQUENCY (MC/S)
10
5
00
02
04
06
08
10
12
TIME (HOURS)

measurement in order for these to be regarded as correlated. Gledhill and Torr did not define the maximum undisturbed range in this way for October, 1962, but used instead the quartile range as determined from the values for all the days of the month. The reason for this is that the F - region is unstable in its behaviour at Antarctic stations near the Weddell Sea during this period while it changes from typical winter to typical summer behaviour. However, this was not necessary for the other stations used in the analysis.

Figure 15 shows a plot of h' F2 and fmin for a 12 hour period during which a typical ionospheric disturbance occurred at Sanae . In this case the fmin disturbance is a blackout, but in other instances it is seen as a sharp peak.

4.5. Comparison of Data:

Gledhill and Torr found that on every occasion on which a P.E.F. of a magnitude greater than the lowest value that could reliably be detected by the satellite (viz. 1.4×10^4 electrons /cm^2/second) was measured over an area magnetically conjugate to Sanae, there was a disturbance in progress in the ionosphere over Sanae. They displayed their results as shown in Table A, where H = high flux $\equiv$ P.E.F. $\geq$ 1.4×10^4 electrons /cm^2/sec.
L = low flux $\equiv$ P.E.F. $<$ 1.4×10^4 electrons /cm^2/sec.

61/.....

and D and Q represent ionosphere disturbed and ionosphere quiet respectively, according to the above criterion.

TABLE A.

	H	L
D	28	30
Q	0	19

In no instance was the ionosphere over Sanae quiet when a high value of P.E.F. was measured in the conjugate area.

A similar analysis was performed for Campbell Island which is also an L=4 but which lies outside the Southern Radiation Anomaly. It was found that the Satellite measured P.E.F. values above 1.4×10^4 electrons /cm^2/second in a conjugate area of 5^o longitude and 1^o invariant latitude on either side of the conjugate point on 25 occasions. These are shown in Table B, where again high flux is $\geq 1.4 \times 10^4$ electrons/cm^2/second. Also the low flux values have been represented in the table by the symbols a and b, as these were not counted for this particular station, and only the high P.E.F. values are of interest here.

TABLE B.

	H	L
D	14	a
Q	11	b

62/.....

It can be seen from this, that of the 25 high flux observations, 14 correlated with an ionospheric disturbance and 11 did not.

When a P.E.F. of 1.4×10^4 electrons /cm^2/second is found in the conjugate area, then from Figure 7, a flux of 1.2×10^4 electrons /cm^2/second is precipitated over Campbell Island. This may be seen as follows. The conjugate point of Campbell Island (169°E) lies at 203°E in the northern hemisphere and the precipitated fluxes at this station and conjugate point from Figure 7 are 0.62x and 0.72x respectively, i.e. the flux over the conjugate area.

$$1.4 \times 10^4 \text{ electrons/cm}^2\text{/sec} = 0.72x$$

$$\therefore \quad x = 1.95 \times 10^4 \text{ elec/cm}^2\text{/sec.}$$

$$\therefore 0.62x = 1.2 \times 10^4 \text{ elec/cm}^2\text{/sec} = \text{flux}$$

precipitated over Campbell Island.

It is evident that the 11 cases that do not correlate with an I.D. might be attributed to the fact that a P.E.F. of 1.2×10^4 elec/cm^2/sec over Campbell Island is too low to cause an ionospheric disturbance.

By successively increasing the high/low flux boundary from 1.4×10^4 electrons/cm^2/sec, some of the HD and HQ cases in Table B moved into the LD and LQ squares. On doing this, a value of the minimum high flux was reached which gave a Table similar to that of Gledhill and Torr, i.e. no high flux with a quiet ionosphere. In this case the minimum

value of the P.E.F. over the conjugate area was 2.5×10^4 electrons/cm^2/sec. Using this new criterion for high flux, Table B was redistributed to give Table C.

TABLE C.

	H	L
D	8	6+a
Q	0	11+b

Again applying fractions obtained from Figure 7, the minimum disturbing flux (M.D.F.) over Campbell Island, when a M.F.C. of 2.5×10^4 electrons/cm^2/sec. is measured in the conjugate area, is 2.2×10^4 electrons/cm^2/sec.

Returning then to the Sanae case, in the light of the above, it was necessary to investigate whether some of the 30 LD cases were due to the fact that a value of 1.4×10^4 electrons/cm^2/second was too high to be regarded as the boundary value of P.E.F. able to cause an I.D. at Sanae. The high/low P.E.F. boundary was therefore incrementally decreased from 1.4 elec/cm^2/sec to successively lower values. On doing this, some of the 30 LD cases moved into the HD square. The process was stopped when some of the 19 LQ cases began to move into the HQ square i.e. when the exact correlation between P.E.F. and I.D. began to collapse. The high/low P.E.F. boundary was found to be 8.2×10^3 electrons/cm^2/sec. by this method. This may then be

regarded as the M.F.C. corresponding to the M.D.F. over Sanae. Table A then becomes Table D.

TABLE D.

	H	L
D	38	20
Q	0	19

The actual flux that should be precipitated over Sanae when a P.E.F. of 8.2×10^3 elec/cm^2/sec is measured in the conjugate area is 2.63×10^4 electrons/cm^2/sec.

From the Alouette P.E.F. data for L= 4.4 it was found that fluxes $\geq$ the M.F.C. (and hence the M.D.F.) for Sanae were measured for 67% of the time. This can be seen from Figure 16 which is a plot of the integrated percentage occurrence of P.E.F. versus P.E.F. This value (67%) is strikingly close to the value obtained for the percentage of disturbance of the ionosphere over Sanae calculated from a random sample i.e. $65 \pm 5\%$.

Similar analysis were carried out for other stations along L=4 for which both satellite and ionospheric data were available. In the case of northern hemisphere stations it was not necessary to determine the M.D.F. from the M.F.C. since the satellite measured the actual P.E.F. there and thus the M.D.F. could be directly obtained. The tables obtained

65/.....

FIGURE 16.

Integrated percentage occurrence
of P.E.F. versus P.E.F.

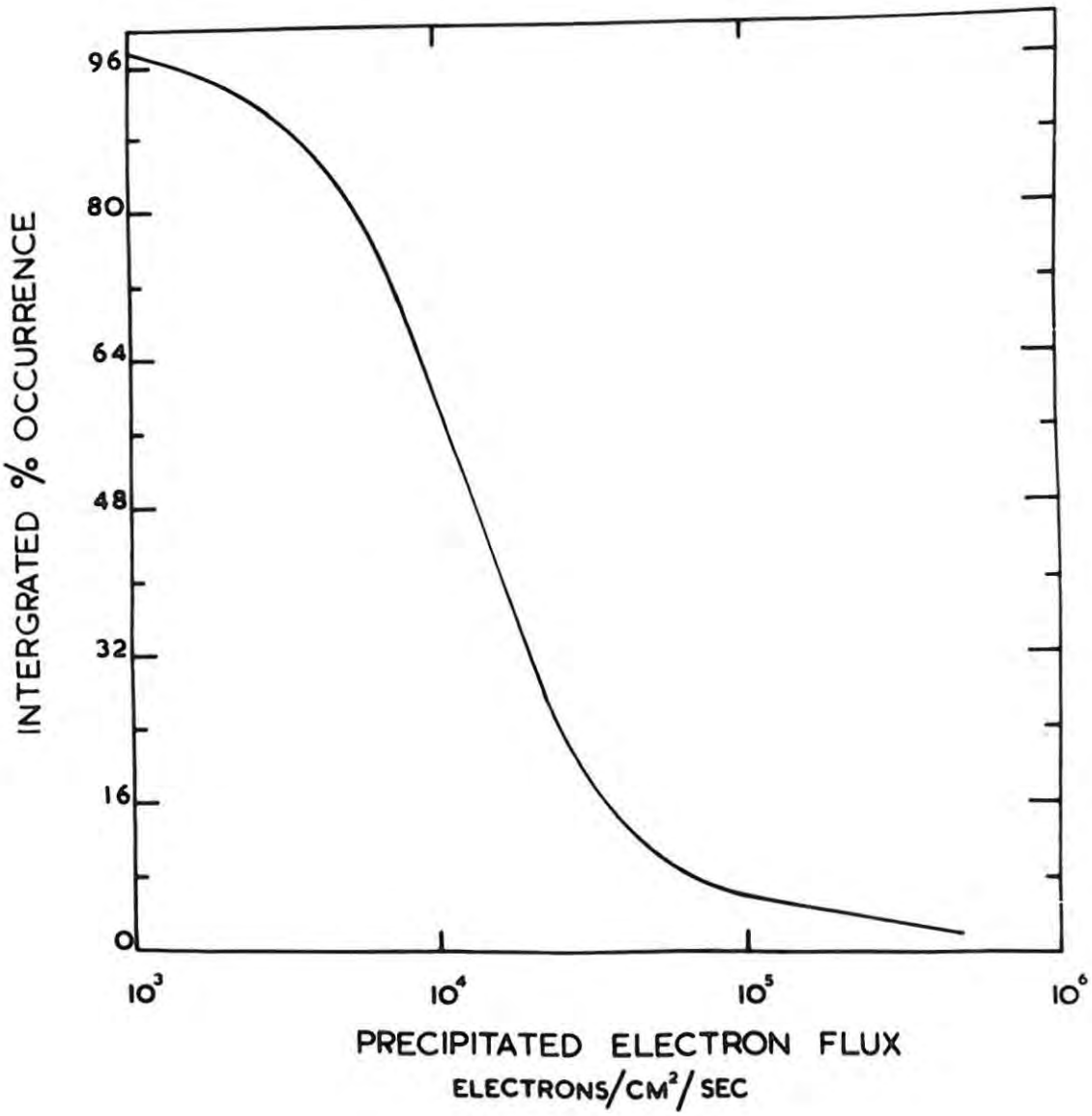
INTERGRATED % OCCURRENCE
96
80
64
48
32
16
0
10^3
10^4
10^5
10^6
PRECIPITATED ELECTRON FLUX
ELECTRONS/CM²/SEC

TABLE 2.

STATION	GEOGRAPHICAL CO-ORDINATES	L VALUE	P.E.F. IN UNITS OF x OVER STATION	P.E.F. IN UNITS OF x OVER AREA CONJUGATE.
SANAE	70.3°S 2.4°W	3.99	2.15	0.67
CAMPBELL ISLAND	52.55°S 169.15°E	4.02	0.62	0.72
HALLEY BAY	75.52°S 26.60°W	4.17	1.30	0.65
ST. JOHNS	47.52°N 52.78°W	3.47		
WINNIPEG	49.90°N 97.40°W	4.22		
OTTAWA	75.75°W 45.40°N	3.64		

STATION	M.D.F. IN ELECTRONS/ cm^2/SEC.	M.F.C. IN ELECTRONS/ cm^2/SEC.	INTEGRATED PERCENTAGE OCCURRENCE P.E.F.$\geq$ M.F.C. AND M.D.F.	PERCENTAGE DISTURBANCE OF IONOSPHERE.
SANE	2.6×10^4	8.2×10^3	67%	65%
CAMPBELL ISLAND	2.2×10^4	2.5×10^4	29%	31%
HALLEY BAY	2.5×10^4	1.2×10^4	53%	58%
ST. JOHNS	2.5×10^4		24%	23%
WINNIPEG	2.1×10^4		30%	31%
OTTAWA	2.2×10^4		28%	26%

percentage occurrence of flux $\geq$ the M.F.C. for the southern hemisphere stations; while the last three rows show integrated percentage occurrence of flux $\geq$ the M.P.F. for the M.P.F. for the northern hemisphere stations. Column 9 gives the percentage disturbance of the ionosphere at these stations.

It can be seen from Table 2 that the values shown in columns 8 and 9 agree very well. The average value of the M.D.F. for all stations is 2.25×10^4 electrons/cm^2/sec. Note that of the 6 stations used, only the analysis for Sanae and Halley Bay required utilization of P.E.F. measurements classified by McDiarmid as 'unreliable'. However, the fact that this did not destroy the correlation and the good agreement with the other stations tends to indicate that the accuracy of P.E.F. measurements as low as 8.2×10^3 electrons/cm^2/sec. was sufficient for this type of analysis.

4.6. Frequency of Ionospheric Disturbance Along L=4.

Assuming 2.25×10^4 electrons/cm^2/sec. to be the real M.D.F. value for all stations along L=4, a curve was drawn (using the inverse of the above method) of the predicted integrated percentage occurrence of flux $\geq$ the M.D.F. for the southern hemisphere. This is shown as the full line curve in Figure 17. A similar curve for

FIGURE 17.

Predicted frequency of occurrence
of P.E.F's able to cause I.D's.

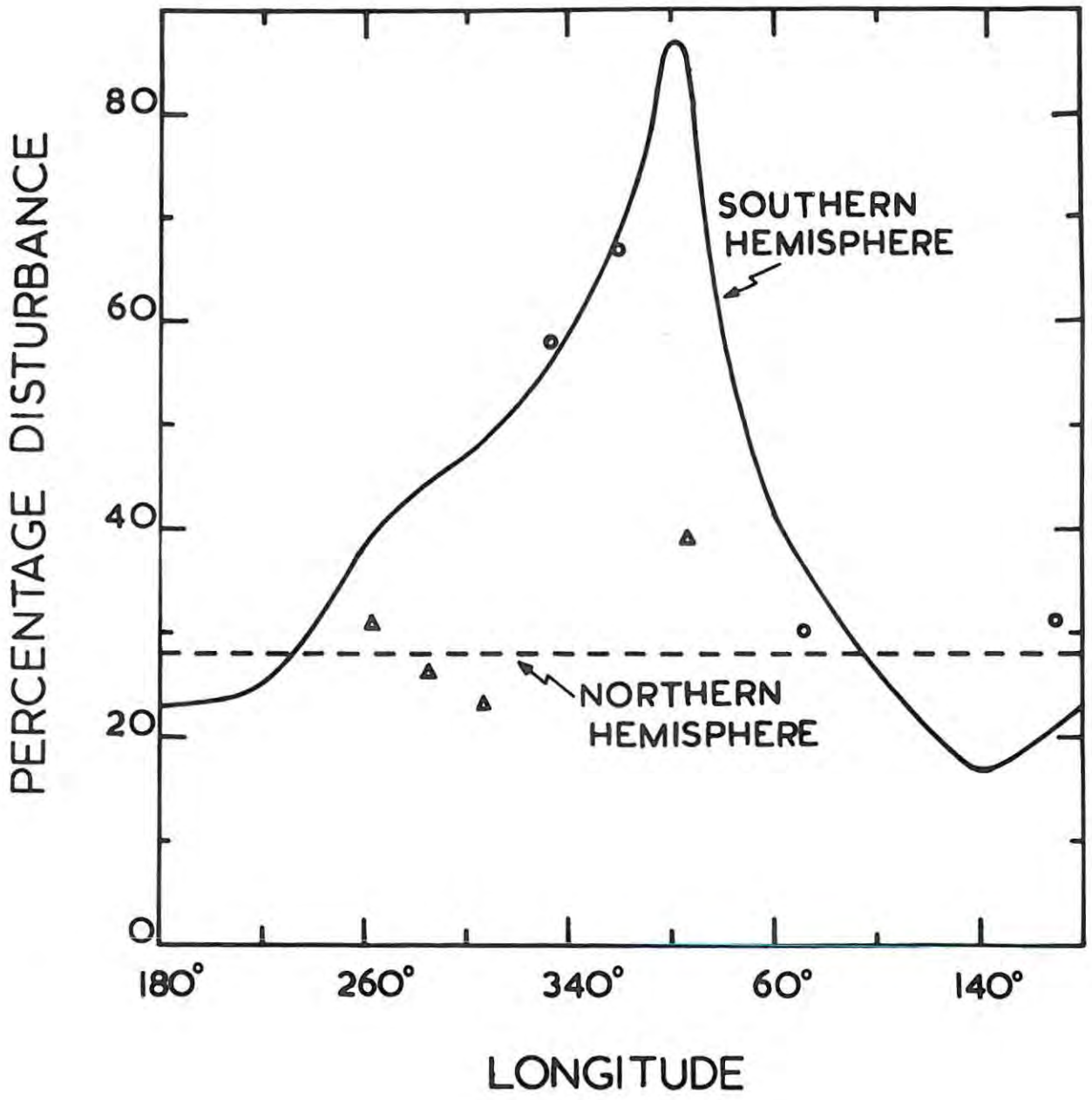
PERCENTAGE DISTURBANCE
80
60
40
20
0
SOUTHERN HEMISPHERE
NORTHERN HEMISPHERE
180°
260°
340°
60°
140°
LONGITUDE

the northern hemisphere is shown as the dotted line. The shape of these curves can be understood by considering Figure 7 in conjunction with Figure 16.

It can be seen from Figure 7, that the theoretical values of P.E.F. in units of x lie on almost a straight line for the northern hemisphere, i.e. to a first approximation the precipitation of electrons is independent of longitude there. Therefore it would be expected that any one value of P.E.F. would be observed with approximately the same frequency of occurrence at all locations along L=4 in the northern hemisphere. This means that the integrated percentage occurrence of flux $\geq$ the M.D.F. will be constant for the northern hemisphere and that it is valid to determine this from the observations made by the satellite in this particular range of L. These are the data represented in Figure 16 and so a straight line is obtained in Figure 17.

In the southern hemisphere, the theoretical values of P.E.F. in Figure 7 show a marked longitude dependence. However, since Figure 16 represents the integrated percentage occurrence of flux for all longitudes in the northern hemisphere, the integrated percentage occurrence of flux $\geq$ the M.F.C. and hence the M.D.F. for all locations in the southern hemisphere are immediately available. The latter is the full curve shown in Figure 17.

68/.....

Also shown on Figure 17 are the experimental points of the percentage disturbance of the ionosphere for all stations along L=4 for which data could be obtained, including some over which no telemetry was received from the satellite. (See Table 2). The experimental points tend to follow the curves of predicted I.P.O. of flux $\geq$ M.D.F. for both hemispheres, also indicating that the precipitation of electrons around L=4 can explain the ionospheric disturbances observed there.

4.7. Discussion:

Co-ordinated measurements have been made with a polar orbiting satellite (Sharp et al, 1965) of trapped and precipitated electron fluxes together with the ionization of the F region. These also show a definite correlation between high electron flux peaks and increase in ionization. The correlation was not 100% but was very high. In 13 out of 15 cases, large particle fluxes were obtained at or near the peak in ion density.

In this analysis, all the measurements of high P.E.F. taken over 6 stations and over a period of 6 months, were accompanied by an ionospheric disturbance.

It is of interest here to consider the implications of this concerning the longitudinal extent of precipitation. Except for the station Winnipeg, the areas (or

69/.....

conjugate areas) were taken to be 10^{o} longitude on either side of the actual conjugate point. The fact that all the high P.E.F. measurements, made over a range extending from directly over the station or conjugate point to 10^{o} longitude away from it, correlated with ionospheric disturbances, seems to indicate that precipitation is usually about 10^{o} in longitudinal extent. For areas wider than $\sim 13^{o}$, however, the one to one relationship between electron precipitation and ionospheric disturbance begins to break down. For example, two high P.E.F. values were observed 15^{o} from the geographic longitudinal co-ordinate of Winnipeg and neither of these correlated with an I.D. It is probable that this lack of correlation is due to precipitation limited in longitudinal extent, (O'Brien, 1964).

4.8. Comparison of P.E.F. with Magnetic Data:

Of the 6 month period 1st October, 1962 to 31st March, 1963, over which this analysis was performed, results of magnetic observations made at Sanae were only available for 1st October, 1962 to 31st December, 1962. The horizontal intensity data were compared with the P.E.F. observations in the same way as the ionospheric data was used in the above.

70/.....

The maximum undisturbed range was determined for the data using the 10 internationally quiet days for each month and again, if the magnetic intensity lay outside this range over a period of one hour on either side of the P.E.F. observation, then the period was taken to be magnetically disturbed.

The results of this analysis are shown in Table F, where the high/low flux criterion is the value of M.F.C. determined for Sanae in Section 5.4 viz. 8.2×10^4 electrons/cm^2/sec.

TABLE F.

	H	L
D	12	0
Q	7	8

Here it is interesting to note that on no occasion was the magnetic intensity disturbed when a low electron flux was precipitated into Sanae's conjugate area.

Of the 19 high P.E.F. values observed in the conjugate area during this period, 12 were accompanied by disturbed magnetic conditions and 7 were not. (By the same method used for determining the percentage disturbance of the ionosphere, the percentage magnetic disturbance at Sanae was found to be 30%).

71/.....

4.9. Absorption:

Riometer as well as ionosphere data were available for the Kerguelen station. Using the data on the 10 internationally quiet days to determine the maximum undisturbed range for each month, the percentage disturbance was calculated using the riomiter data, and found to be 30% as compared with the 31% obtained using the ionospheric data.

It would appear from this that the disturbance criterion may be applied to geophysical data other than ionospheric, such as riometer and in all probability airglow, but unfortunately no airglow data could be obtained.

-----ooOoo-----

CHAPTER 5.

ENERGY RANGE OF ELECTRONS CAUSING IONOSPHERIC DISTURBANCES.

5.1. Introduction:

It was shown in Chapter 4 that a precipitated electron flux of magnitude 2.25×10^4 electrons /cm^2/second is the minimum able to cause an ionospheric disturbance. This implies that there must be an upper limit on the energy of these particles. Considering, for example, Sanae and its conjugate area; when a flux of 2.6×10^4 electrons/cm^2/sec is precipitated over Sanae, a flux of 8.2×10^3 electrons /cm^2/sec is precipitated in the conjugate area. The former produces geophysical effects whereas the latter does not. If there were no upper energy limit on the precipitated particles, some value of energy must exist above which a flux of 8.2×10^3 electrons/cm^2/sec would be energetic enough to cause ionospheric disturbances.

The energy range could be estimated by comparing theoretically deduced ionization profiles (for a precipitated electron flux of 2.25×10^4 electrons/cm^2/sec) for various energy spectra, with the electron density profies obtained while this flux was precipitated. However, apart from individual N(L) profiles appearing in articles, the profiles were not available for L = 4 stations. Because of this the above method was modified by defining a D-region

73/.....

disturbance criterion. In this form the approach serves to illustrate a method that may easily be applied when the necessary data became available.

5.2. Loss of Energy to the Atmosphere by Precipitated Electrons.

Various methods for obtaining height versus energy loss profies for energetic electrons incident on the atmosphere will be discussed as such a profile will be used in the analysis to follow.

Rees (1963) made semi-empirical calculations on the luminosity distribution of aurorae, based on laboratory data by Grün (1957). He computed the ionization of the atmosphere produced by energetic primary auroral electrons in the energy range 0.4 to 300 kev. considering three types of angular distributions, a monodirectional beam, a distribution varying with the cosine of the pitch angle and an isotropic distribution.

Electrons, upon penetrating the atmosphere lose their energy almost entirely by excitation and ionization of the atmospheric constituents, (Rees, 1964; Maeda, 1965). The mean energy lost per ion pair formed, $\Delta\mathcal{E}$, is very nearly constant and for electrons in air is generally taken to be 35 ev, (Dalgarno, 1962). Rees used the following ionization rate/unit volume, q_z, per incident unit electron Flux F, (Spencer, 1955; Chamberlain, 1961),

$$\frac{q_z}{F} = \frac{E_o}{r_o \Delta\mathcal{E}} \lambda \left[\frac{z}{R}\right] \frac{n\,(M)_z}{n\,(M)_R}$$

74/.....

where Eo is the initial electron energy, $n(M)_z$ and $n(M)_R$ are the number densities of ionizable atoms or molecules at atmospheric depth z and R respectively. The range at the top of the atmosphere is $ro = \frac{R}{\rho}$ where ρ is the mass density at the maximum penetration depth R and $\lambda\left[\frac{z}{R}\right]$ is the normalized energy dissipation distribution function.

Grüns' theory did not consider the possible effects of a magnetic field on the motion of the electrons. However, Rees suggested that since the geomagnetic lines of force in the auroral zone are nearly perpendicular to the horizontally stratified atmosphere, the component of motion of an electron parallel to the lines is unaffected by the magnetic field while the perpendicular component is merely changed in direction within a given layer of atmosphere and does not lose or gain energy because the field is nearly uniform in the height interval considered. This, he said, is equivalent to 'unwinding' the spiral of the electron's motion, leaving the total range unaffected.

Gledhill and van Rooyen (1962) proposed a method for calculating height versus energy loss profiles, which takes into account the spiralling of the electron around the field line. In their treatment the geomagnetic field appears in the expression for the path which the spiralling electrons would follow. The range-energy relation was that determined experimentally by Katz and Penfold (1952) for soft β

75/...

-rays in Aluminium.

Probably the last attempt to date is that by Maeda (1965) who used a Monte Carlo method to take into account the dominating effect of Coulomb scattering and its statistical nature in collision processes. In his computations he calculated the mean energy loss according to the Bethe theory (Rohrlich and Carlson, 1954) and included scattering (using the multiple scattering theory of Goudsmit and Saunderson (1940) with Mott's (1929) cross-section for a single scattering and Landau (1944) fluctuation in energy loss (straggling).

His results are based on the analysis of 2,000 Monte Carlo histories with two cases of incident distribution (vertical and isotropic) and in order to examine the effects of straggling, all calculations were done with and without straggling. Maeda also regarded the electrons as travelling in an oblique path with the pitch angle equal to the incident angle by unwinding the spiral.

The height versus energy loss profiles obtained by the above authors for electrons incident on the atmosphere with initial energies of 20 kev were compared after converting to the same units (viz. km versus Joules/$_{km}$). These are shown in Figure 18.

Despite the differences in approach it is of interest to note that the peaks of the curves are of very much the

76/.....

FIGURE 18.

Comparison of height versus energy loss profiles obtained by various authors.

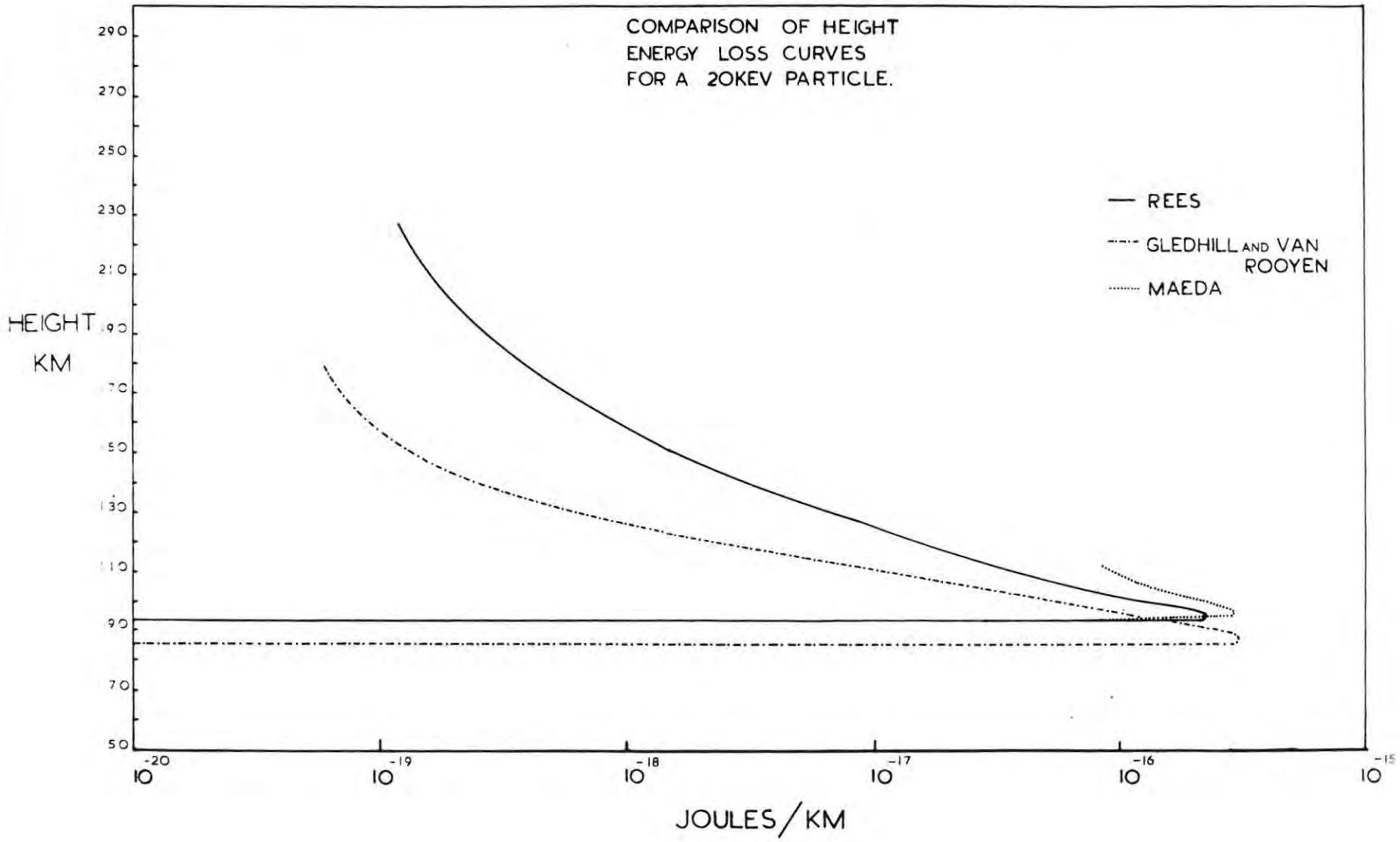
COMPARISON OF HEIGHT
ENERGY LOSS CURVES
FOR A 20KEV PARTICLE.
REES
GLEDHILL AND VAN ROOYEN
MAEDA
HEIGHT
KM
290
270
250
230
210
190
170
150
130
110
90
70
50
10^{-20}
10^{-19}
10^{-18}
10^{-17}
10^{-16}
10^{-15}
JOULES/KM

same magnitude, although the Gledhill-van Rooyen curve has its peak at about 8 km lower in altitude than the other two. In the region 80 to 90 km, and 8 km difference may be significant, being about equal to a scale height there. It would in fact appear that these should be the other way round, since if a horizontally stratified atmosphere is considered, then from Alfvéns'mirror equation, the pitch angle of an electron decending into the atmosphere along a field line will increase with decreasing altitude. As a result of this the particles considered in the Gledhill-van Rooyen method will travel a longer distance through each height interval than do the Rees or Maeda particles and so would be expected to lose their energy sooner.

There are three possible reasons as to why this is not the case :-

(i) Different range-energy treatments are used; Gledhill and van Rooyen use a relation (derived for β particle in Al) which only holds well for particles with energies 100 kev$> E >$2.5 Mev, whereas Rees and Maeda use relations derived for electrons in air with initial energies less than 54 and 25 kev respectively.

(ii) The initial heights differ i.e. 300, 200 and 112 km.

(iii) Different model atmospheres are used.

Therefore, there are three methods, two taking no specific account of the geomagnetic field and one including

77/.....

Therefore, there are three methods, two taking no specific account of the geomagnetic field and one including its variations explicitly, all giving practically the same results. The question then arises as to what effect the magnetic field does in fact have.

Gledhill and van Rooyen use a monopole approximation for the geomagnetic field over the height range for which their calculations are performed, where the position of the monopole in an analysis of this nature, for any specific location, is determined by the surfact value of the magnetic field at that location. In the former comparison (i.e. Maeda ; Rees ; Gledhill - van Rooyen), the Gledhill-van Rooyen curve for a location with a surface magnetic field value of 0.3 gauss was used. Using the same method, a curve was calculated for a location with a surface magnetic field value of 0.57 gauss and this was compared with that for 0.3 gauss. It was found that these curves are insensitive to the magnetic field, being practically identical in shape. This may be explained as follows.

A particle will mirror when its pitch angle is 90^{o}. From Alfvén's mirror equation the altitude at which this occurs depends only on the initial pitch angle and the ratio of geomagnetic field values $\frac{Bm}{Bo}$, where Bm is the magnetic field at the mirror point and Bo at some reference height.

78/....

It was found that the ratio $\frac{B100km}{B200km}$ was practically constant along L = 3, 4 and 5. This is because the geomagnetic field is approximately and inverse cube field over these L values and the height interval considered is small compared with the radius of the earth. Hence one would expect that for any two places with the same field ratio and the same atmosphere, the curves would be the same.

This has important consequences for application purposes i.e. any one of these curves could be applied at any location around L = 4.

5.3. Energy Spectra Observed by Satellites:

From analysis of Injun 3 data (O'Brien, 1964) it was found that the integral fluxes above 40 kev were composed mostly of electrons with energy $40 \leq Ee \leq 110$ kev. In this energy range no significant variation could be detected with pitch angle and the spectrum before, during and after a precipitation event was found to be very much the same. It was also concluded that the spectrum in the range $Ee \leq 100$ kev may be greatly variable but was generally softer towards higher latitudes. In many precipitation events there was a predominance of electrons with energies between 10 to 40 kev.

The integral spectrum of particles greater than some energy E, as observed by a number of satellites may be represented by the power law spectrum $J(>E) = CE^{-\gamma}$, where $J(>E)$ is the number of electrons with kinetic energy $> E$

79/....

FIGURE 19.

Normal midday D-region, and minimum disturbance criterion with theoretical layer.

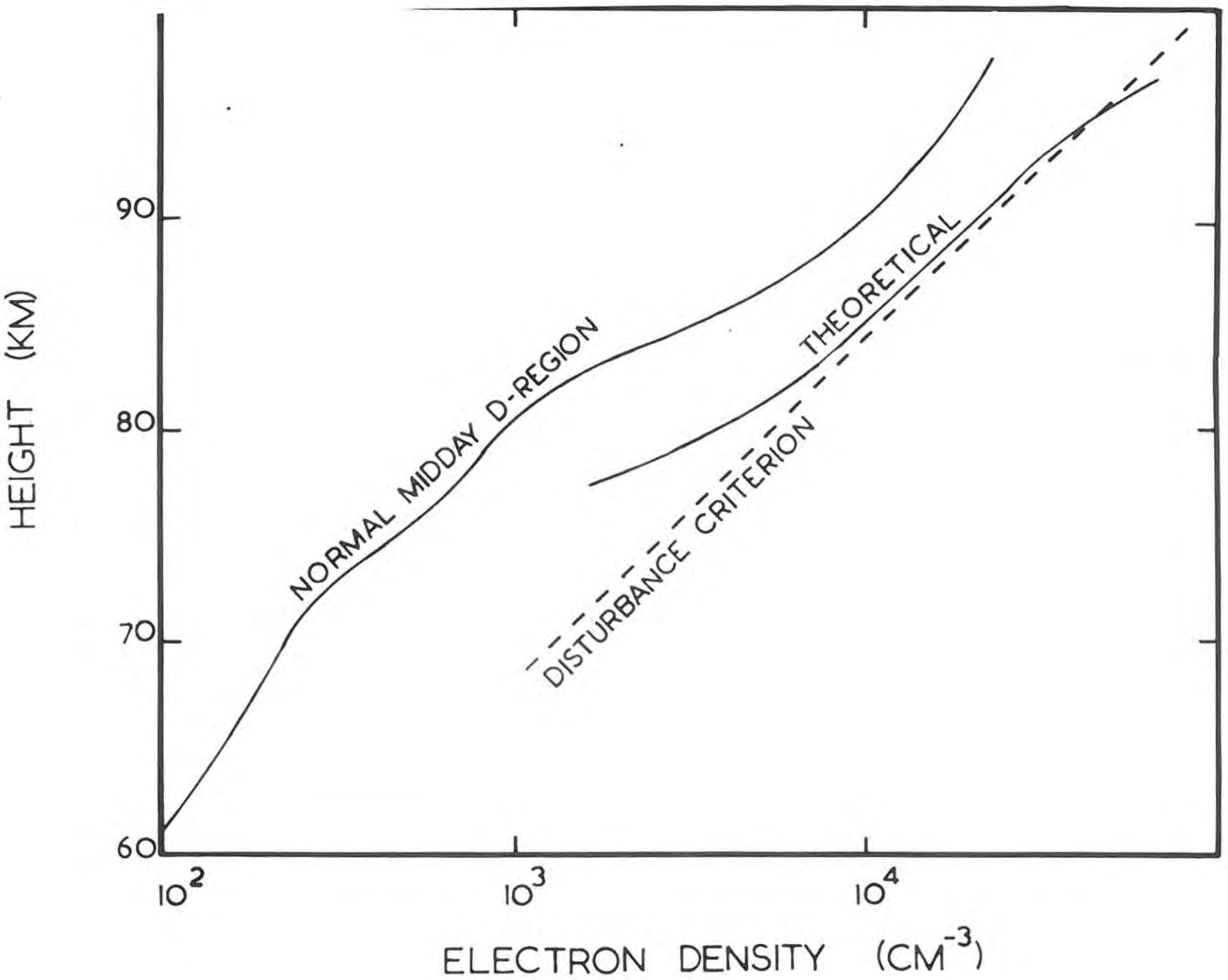
HEIGHT (KM)
90
80
70
60
10^2
10^3
10^4
ELECTRON DENSITY (CM^{-3})
NORMAL MIDDAY D-REGION
THEORETICAL
DISTURBANCE CRITERION

and C and γ are constants. Satellites Injun 1 and 3 found that for most events in this energy range, $\gamma = 5$.

5.4. D-layer Disturbance Criterion:

A curve of electron density (N) versus height is generally known as an N(h) profile. Because of the solar control of the D-region, such profiles show duirnal and seasonal variations. An attempt was therefore made to obtain a mean midday profile dor the normal D-region, at an intermediate level in the 11-year solar activity cycle. Typical midday profiles obtained by a number of authors, using various methods examined. These included curves by Barrington et al (1963) using the cross-modulation technique; Ichimija et al (1961), Adey and Heikkila (1961) Smith (1963) and Hall (1963) from rocket experiments; and Belrose (1962) using partial reflection techniques. The mean curve determined from these is shown in Figure 19, and will be used in what follows as the standard for an undisturbed D-region. (It must be noted that this curve applies only to the intermediate periods in the solar activity cycle, as Tithridge (1962) has estimated a fourfold increase in D-layer electron densities from sunspot minimum to sunspot maximum.

Various disturbances occur from time to time that cause the electron density in the D-region to increase con-

80/.....

siderably. These disturbances are classified into four groups and are summarized briefly below:-

(i) Sudden ionospheric disturbances (S.I.D's) appear as large simultaneous increases in the electron density over the entire sunlit side of the earth. These are caused by large increases in solar X-ray flux and have duration from a few minutes to several hours.

(ii) Polar cap absorption events (P.C.A.) occur only over the polar caps. PCA's are caused by solar protons emitted during solar flares and can last for several days.

(iii) Auroral absorption events are caused by electron bombardment of the atmosphere.

(iv) The 'winter anomaly' events appear as moderate increases in D-region electron densities in the winter at midlatitudes, and last for several days. Their cause is unknown.

In order to define a disturbed D-region N(h) profile, profiles obtained during such events as the above were examined. Among those examined were those observed during SID's by Belrose and Cetiner (1962), Swift (1962) and a theoretical curve by Nicolet and Aikin (1960); during PCA's by Jackson and Kane (1959) and Parthasarathy et al (1963); during auroral absorption events by Jespersen et al and Holt et al (1962), and finally during winter anomaly effects by Belrose and Cetiner (1963) (See also Fejer (1962) and Landmark and Lied (1962)).

A number of these curves were determined for Ottawa, one of the northern hemisphere L = 4 stations.

From these, a minimum disturbance profile was determined and this is also shown in Figure 19.

5.5. Calculation of Ionization Profiles:

Rourke (1965) using Rees' method has calculated an integrated electron production rate /unit isotropic electron flux in the energy range of 40 to 160 kev, and has used a power low spectrum of the form CE^{-5}, Figure 20, (see Section 5.3). As this fills the power low requirements of the satellite Injun 3 and covers approximately the same energy range, it is most convenient for this analysis.

The D-region profile that should be obtained when the minimum electron flux able to cause an ionospheric disturbance (i.e. 2.25×10^4 electrons/cm^2/second) and with the above energy spectrum, is precipitated, was calculated as follows.

The value of $q_{\overline{f}}$ (the production rate/unit flux) was read from Rourke's curve for various heights and multiplied by the M.D.F. 2.25×10^4 electrons/cm^2/sec. to give q. Assuming equilibrium, $q = \alpha N^2$ for the D-region. Using this and a value of α of 10^{-7} (Rourke, 1965; Ivanov-Kholodnyy 1964), values of q were calculated for the undisturbed D-region profile. These values of q were added to the values of q obtained using Rourke's curve and the sum was reconverted to N.

82/.....

FIGURE 20.

Integrated electron production rate/unit isotropic electron flux, (Rourke, 1965).

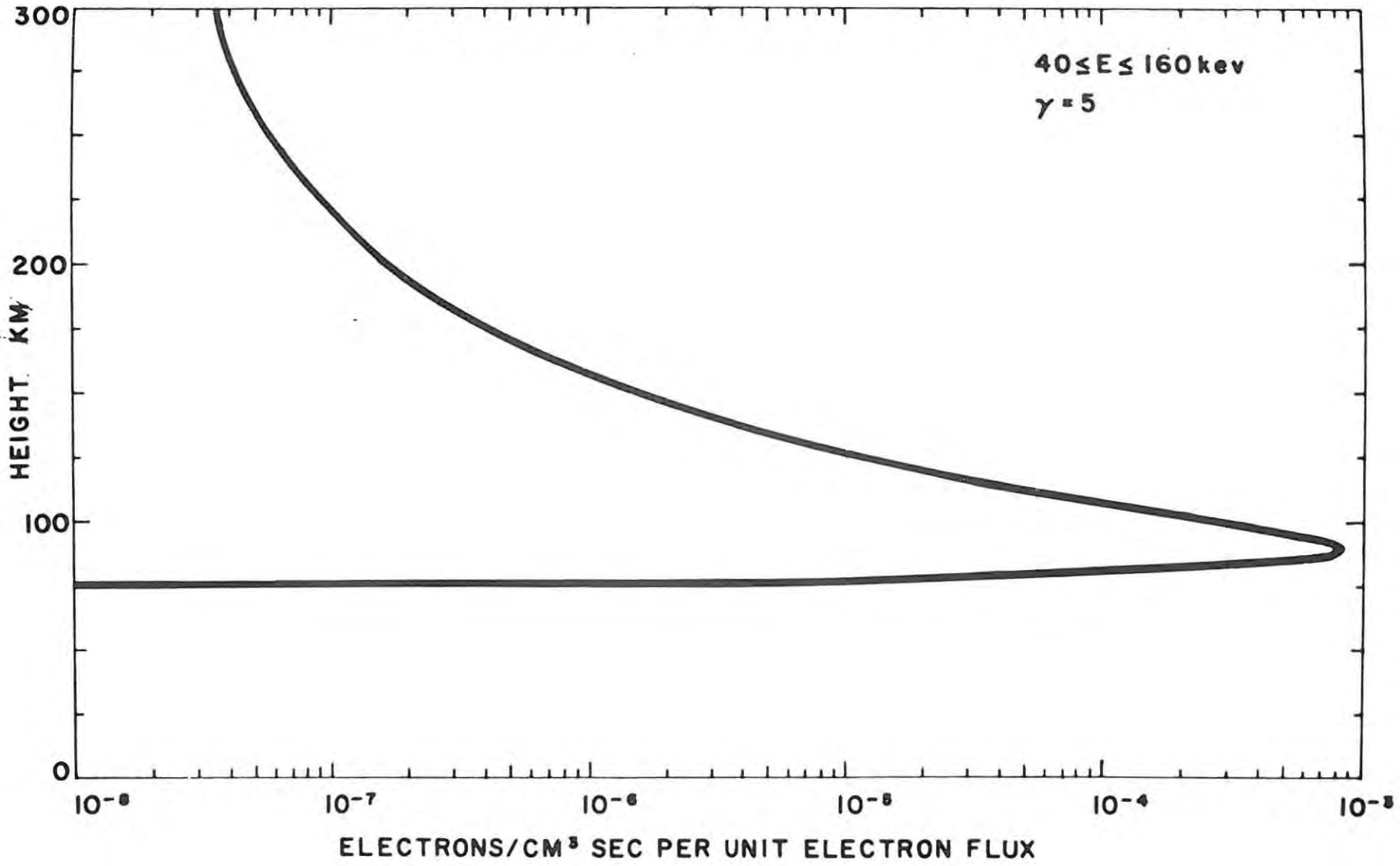
300
200
100
0
HEIGHT KM
40≤E≤160kev
γ=5
10⁻⁸
10⁻⁷
10⁻⁶
10⁻⁵
10⁻⁴
10⁻³
ELECTRONS/CM³ SEC PER UNIT ELECTRON FLUX

The resulting N(h) curve was plotted on Figure 19, and from this it can be seen that the N(h) curve calculated in this way lies very close to the minimum D-region disturbance criterion.

As a number of satellites have measured energy spectra of this order, it will be assumed that such a spectrum would generally be observed at L~4. This then offers further support to the previous result that a P.E.F. of 2.25×10^4 electrons/cm^2/second is the smallest able to cause an ionospheric disturbance of the type mentioned.

Alternately, since an analysis of the data for 6 stations indicated very closely that the minimum disturbing flux is~2.25×10^4 electrons/cm^2 second, the N(h) curve results appear to support an energy spectrum of this type.

From the above then, although an analysis of this sort could by no means be offered as proof on its own, the results are consistent with satellite observations and the conclusions of the former chapter.

-----ooOoo-----

CHAPTER 6.

SUMMARY AND CONCLUSIONS.

6.1. The Model.

The model developed in Chapter 3 has been shown by comparison with satellite data to be extremely successful. Not only does it predict the correct ratio of precipitated to trapped flux, but also the Southern Radiation Anomaly appears in the position in which it was observed by a number of satellites. The northern hemisphere 'Russion' anomaly is some 20^{o} east of the positions in which it was observed by the satellites Sputnik 5 and 6. However, there is a difference of 30^{o} longitude between the positions in which these two satellites observed this anomaly.

The calculations are easily performed, requiring no electronic computer for excessively time consuming labour. Also, detailed knowledge of the energy spectrum, bounce times and collisional and magnetic scattering are not required in order to perform this preliminary analysis.

6.2. Pitch Angle Distribution:

The pitch angle distribution of the incoming particles has been discussed in some detail in Section 4.4. The results emerging from the injection model and satellite pitch angle distribution observations are consistent with an isotropic angular distribution of the incoming electron

84/.....

flux. In this section it was shown that the observed pitch angle distributions, with increased intensity towards higher pitch angles, may be explained in terms of a build-up of the particles with higher pitch angles (i.e. 'trapped' particles) through longitudinal drift. A reason for the fall-off in intensity between 75° and 90°, observed by McDiarmid and Budzinski (1964), was suggested. It is evident from the model that the pitch angle distribution should be longitudinally dependent.

6.3. Precipitation by the Anomaly.

It has been shown in Chapter 3 that the entire electron flux entering the L=4 shell along the mirror height path of an electron mirroring at 100 km over the centre of the Southern Radiation Anomaly, will be wiped out by the Anomaly. The whole calculation outlined in this Chapter was then repeated for particles mirroring at 200 km over the Anomaly.

The resulting trapped electron flux curve is shown in Figure 20. From this it can be seen that after one complete longitudinal drift around the earth, there is an overlap of magnitude 50x on returning to the reference point, i.e. of the total injected electron flux (2 x 180x electrons/cm^2/sec), 50x passes through the Anomaly without being precipitated. In other words, of those particles

FIGURE 21.

Total trapped electron flux versus southern hemisphere longitude for particles mirroring at 200 km over the centre of the Southern Radiation Anomaly.

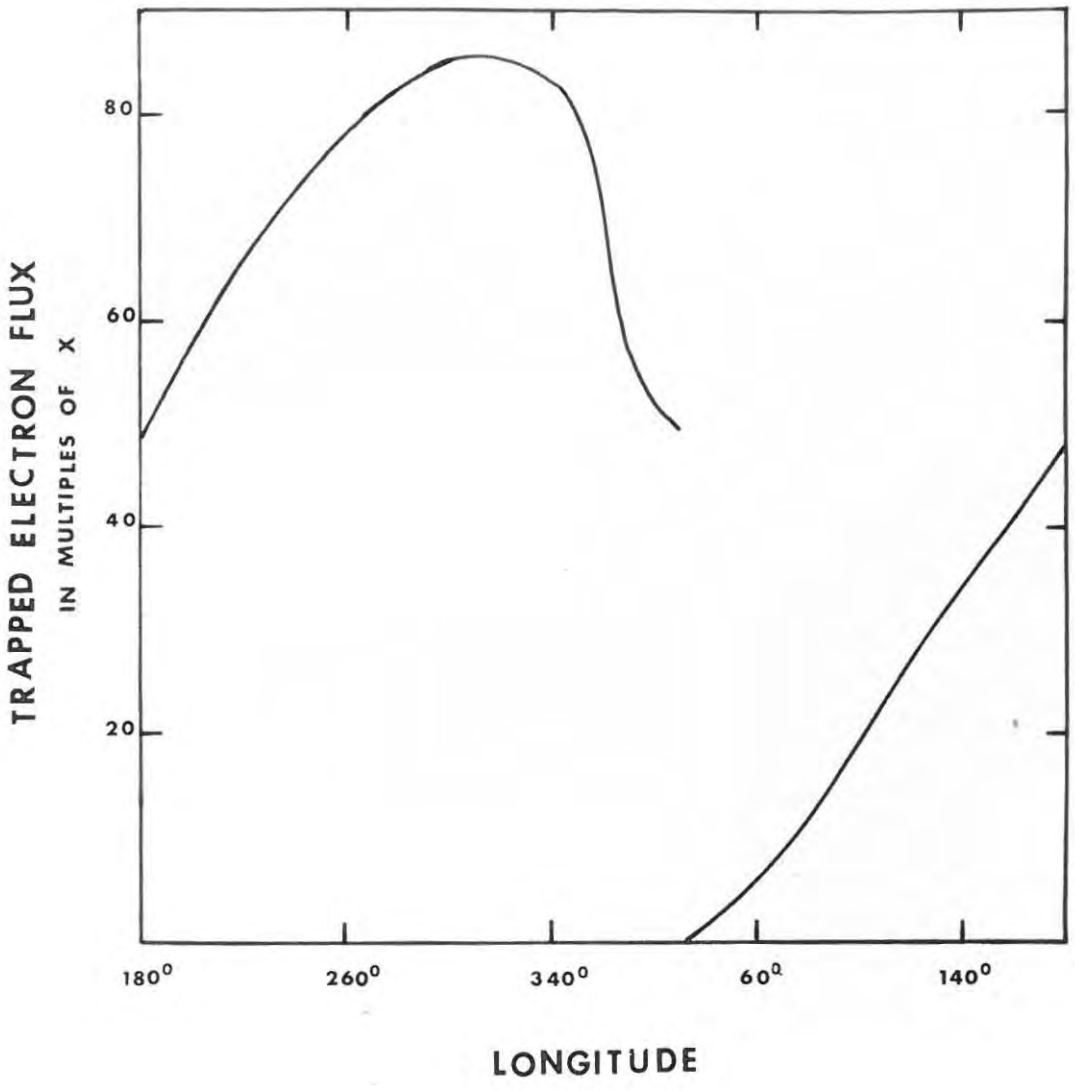
TRAPPED ELECTRON FLUX
IN MULTIPLES OF X
80
60
40
20
180°
260°
340°
60°
140°
LONGITUDE

mirroring at 200 km over the centre of the Southern Radiation Anomaly, 14% will not be wiped out by the Anomaly. It must be remembered here that this figure would probably be somewhat different were scattering considered.

The percentage of injected particles able to pass through the Anomaly will increase with increasing height of the mirror points over the centre of the Anomaly, where the magnetic field value is the lowest. Eventually some height will be reached (probably about 400 to 500 km) above which all particles will be able to drift across the Anomaly without appreciable loss.

6.4. Scattering:

In the whole of this treatment, scattering of the electrons due to collisions with the atmosphere above 100 km has been neglected. Welch and Whitaker (1959) plotted a curve of the relative air density encountered by a particle mirroring at 45° magnetic latitude versus time (on which depend the pitch angle and longitudinal position of the particle). From this they concluded that the air density throughout the entire bounce period is only appreciable when χ, the pitch angle, is very nearly 90°. This means that practically all scatterings will occur when the particle is mirroring, with the result that a scattering will only

lead to the lowering of a mirror point. This, however, needs further investigation.

Should this be the case, the effect will be to increase the precipitated electron flux predicted by the injection model. The increase in the precipitated flux at any longitude will be proportional to the atmospheric density at the mirror point i.e. to the altitude of the equivalent height point. The increase in precipitation due to scattering will only become significant for mirror points below a certain altitude and so will probably only become appreciable over the Anomaly.

Scattering due to collisions with the atmosphere will be included in future research.

6.5. The Position of the Anomaly:

The theorectical positions of electron dumping due to longitudinal drift of trapped electrons have also been investigated by Gassman and Pike (1965), but their results are rather puzzling. The areas of intense precipitation in the South Atlantic and over Russia have been mapped out by a number of satellites, as has been mentioned previously. Also, a reasonable estimate of the positions of these regionsmay be made from maps of constant B curves.

However, Gassman and Pike find that the region of most intense precipitation in the southern hemisphere is centred on the tip of the South American continent i.e. some 100^{o} west of the centre of the position in which it is

predicted to lie in this thesis and in which it has been found to lie by satellites. The Russion anomaly emerging from their calculations is in approximately the observed longitudinal position.

In their article Gassman and Pike give no account or details of their calculations apart from stating that their approximation of an injection mechanism is to assume that 'in every volume element of the B, L, ϕ_o space of the magnetosphere with $\Delta B = 0.01; \Delta L = 0.01; \Delta \phi_o = 1^o$, one additional electron per second is assumed to mirror.

They use curves of constant B and L calculated for an altitude of 100km by Dudziak et al (1963) and these are very similar to those of Roderer et al (1965). Therefore, until further details of their calculations are published, it is difficult to explain their results.

This is probably the only other work of this nature that has been published to date.

6.6. Ionospheric Disturbances:

The main significance of the work in this thesis lies in the results of Chapter 4 in which it was shown that there is a one to one correspondence between precipitated electron fluxes and ionospheric disturbances (of a type defined by the disturbance criterion) at the stations examined along L = 4. Although it has been suspected for

88/.....

some time that such a relationship exists, this is the first definite evidence that has been presented. The positions of the stations are so widely spread and the disturbance criterion is of such a broad nature that it seems valid to conclude that all ionospheric disturbances of the type defined previously around L = 4 are caused by precipitated electrons. Other L values are to be examined in future research.

Another striking result emerging from this analysis is that there is a minimum value of the precipitated electron flux able to cause an ionospheric disturbance conforming to the criterion on L = 4. This value was $\sim 2.25 \times 10^4$ electrons/cm^2/sec. at least for the period 1st October, 1962 to 31st March, 1963.

Fluxes below this magnitude will not cause ionospheric effects detectable by such an examination of ionospheric records (although smaller disturbances may well be observable by other techniques). This implies that there is an upper limit to the energy of the incoming particles. As was mentioned in the discussion of the magnetosphere (Chapter 1), particles at the magnetopause have been observed by satellites to have in general energies of 1 kev or less. In fact there has been a very definite absence

89/.....

of particles with energies of 40 kev. If these solar wind particles (with an upper energy limit at the magnetopause) become trapped at some L-value > 5 and drift in L-space to reach L=4 (being accelerated in the process), it is to be expected that the limit will still exist at L=4 but, of course, its value will be increased. This will also be examined in greater detail in research to be carried out shortly.

6.7. Conjugacy:

In 1964 as an Honours degree project, a relation was sought between ionospheric events occuring at Sanae and those occuring at three stations (viz. St.Johns, Reykjarvik and Narssuasauk) in the vicinity of its conjugate point. This was done by correlating the hourly deviations from the medians of foF2 at Sanae for various monthly periods with those at each of the above stations. A significant but very small positive correlation was obtained.

The reason for this (besides precipitation limited in extent) is now clear from Figure 7 and the results of Chapter 4. Even if fluxes of equal magnitude are injected at the equivalent heights of Sanae and its conjugate point, the magnitudes of the precipitated fluxes will be very different and although the flux precipitated over Sanae may

90/.....

be large enough to cause an observable ionospheric disturbance, this will not necessarily be true for that precipitated over the conjugate point.

However, the fact that on every occasion on which a flux of greater than a certain value was measured at the conjugate point, a disturbance was found to be in progress over Sanae, is very substantial evidence in favour of conjugacy.

6.8. Magnetic Disturbances:

It would appear from the very brief analysis described in Section 4.8, that only about 50% of the high precipitated electron fluxes are accompanied by periods of magnetic disturbance. It is most interesting to note however, that on no occasion was a low value of precipitated electron flux accompanied by a magnetic disturbance. This also requires further investigation.

6.9. Summary:

The value of the injection model is therefore, that it provides highly informative preliminary results at an early stage in the development of this research.

It has been shown conclusively that PEF's can account for ID's at all stations around L=4 for which data was available. The disturbance criterion method may be applied

to other geophysical data such as riometer and airglow.

Using an energy spectrum of the type mentioned in Section 5 and the average flux values obtained using the Alouette data and Figure 7, it will be a relatively simple matter to calculate the average energy input versus longitude. It should then be possible to predict the average airglow around L=4 and to check this against airglow data when it becomes available.

-----ooOoo-----

APPENDIX I.

1. Magnetohydrodynamic Waves:

Fluctuationsof the magnetopause due to compressions by the solar wind give rise to magnetohydrodynamic waves which travel inward through the magnetosphere. It was found (Nishida and Cahill, 1964) that when sudden impusles were observed inside the magnetosphere between 5 to 10 R_E by Explorer 12, corresponding impulses occurred about one minute later in the ground records, indicating that sudden impulses originate near the magnetopause.

A second type of long period magnetohydrodynamic wave was found by Explorer 6 and 12 (Judge and Coleman, 1962). It is possible that these waves have a considerable effect on the particles trapped in the belts e.g. by accelerating them. The particle populations of the belts exhibit large fluctuations, particularly during times of magnetic disturbance.

2. Ring Currents:

During the initial phase of a typical large magnetic storm, the value of the magnetic field at the surface of the earth increases by $\sim 50\gamma$ above prestorm level and then drops abruptly by $\sim 500\gamma$ during the main phase. Schmidt-(1917) ascribed this to the influence of a westward electric

93/.....

current that encircles the earth and which he suggested is a permanent companion of the earth. This is now generally called the ring current and is due to the motion of particles trapped in the belts.

According to the model of Chapman and Ferraro (1931 - 1940) when the number or energy of the trapped particles is increased there is a resulting decrease in the strength of the magnetic field between the current path and the earth and an increase above the current path. Satellite observations indicate that the ring currents lie between 2 to 4 R_E. (Heppner et al, 1963).

The model ring current of Chapman and Ferraro was toroidal. Singer (1957) proposed a model for the ring current in which the particles have the now familiar latitudinal motion and simultaneous longitudinal drift - protons to the west on electrons to the east. It is the longitudinal drift that gives rise to the current round the earth.

-----ooOoo-----

APPENDIX II.

The following is a brief summary of the 3 adiabatic invariants connected with the motion of particles trapped in the geomagnetic field. For a detailed presentation see Alfvén, (1950) and Spitzer, (1956.)

a. 1st Adiabatic Invariant:

A particle with charge q and rest mass m, moving with a velocity $\vec{v}$ in a magnetic field $\vec{B}$ is affected by a Lorentz force $\vec{F}$.

$$F = \frac{d}{dt}(m\delta\vec{v}) = q\vec{v} \times \vec{B} \qquad \ldots\ldots (1)$$

where $\delta = (1-\beta^2)^{-\frac{1}{2}}$; $\beta = \frac{v}{c}$

The radius of gyration, $a = \frac{V\perp}{Wc}$ where Wc is the cyclotron frequency and $V\perp$ is the velocity component $\perp$ to $\vec{B}$.

$$\therefore a = \frac{V\perp}{Wc} = \frac{m\delta\, V\perp}{q\,B} = \frac{m\delta\, v}{q\,B}\,\mathrm{Sin}\,\chi \qquad \ldots (2)$$

where χ is the pitch angle, i.e. the angle between $\vec{B}$ and $\vec{v}$. For slow variations in $\vec{B}$, the magnetic moment μ of a charged particle is nearly constant.

$$\mu = I\,A \qquad \ldots\ldots\ldots\ldots\ldots\ldots (3)$$

where I is the current that circles an area A and $A = \pi a^2$

$$\therefore \text{from (2)}, \mu = \pi a^2 \frac{q\,v\perp}{2\pi a} = \frac{1}{2}\frac{m\delta v^2}{B}\mathrm{Sin}^2\chi. \quad (4)$$

For μ to be constant, the changes in B must be small over one radius of gyration. In a static field no work is done on

95/.....

the particle and hence the energy $\frac{1}{2} m \delta v^2$ is constant.

$$\therefore \text{Sin}^2 \frac{\alpha}{B} = \text{constant} \quad \ldots\ldots\ldots\ldots (5)$$

b. 2nd Adiabatic Invariant:

This is called the longitudinal invariant and is defined by

$$I = \oint v_{11} \, dl \quad \ldots\ldots\ldots\ldots\ldots\ldots (6)$$

where dl is an element of length along the line of force, and the integration is over an entire north-south cycle. Combining the first and second invariants it can be shown that a particle drifts in longitude in such a manner that after one complete revolution in the magnetosphere, it is again on the same line of force as that which it started from.

c. 3rd Adiabatic Invariant:

This is the flux invariant, defined by

$$\bar{\phi} = \int \vec{B} \cdot d\vec{A} \quad \ldots\ldots\ldots\ldots\ldots (7)$$

where integration is over a surface bounded by the line traced out by one of the mirror points in its azimuthal drift. In a dipole field, this surface would be evolved by rotating about the axis a line of force on which a particle is trapped. Since the flux invariant is a constant, an expansion or contraction of the field must take place in such a way that $\bar{\phi}$ will remain constant inside the magnetic shell.

-----ooOoo-----

REFERENCES.

1. Adey, A.W. and W.S. Heikkila, Rocket electron density measurements at Fort Churchill, Canada, Can. J. Phys., 39, 219, 1961.

2. Akasofu, S.I., Deformation of Magnetic shells during magnetic storms, J. Geophys. Res., 68, 4437, 1963.

3. Alfvén, H., Cosmical electrodynamics, Oxford University Press, London, 1950.

4. Anderson, K.A., Balloon observations of X-rays in the auroral zone 1, J. Geophys. Res., 65, 551, 1960.

5. Anderson, A.D., and W.E. Francis, A semi-theoretical model for atmospheric properties from 90 to 10,000 km., Lockheed Missiles Space Co., Rept. 6-74-64-19, 1964.

6. Arnoldy, R.L., R.A. Hoffman, J.R. Winckler, and S. - I. Akasofu, Observations of the Van Allen radiation regions during August and September 1959. 5. Visual auroras, high-altitude X-ray bursts and simultaneous satellite observations, J. Geophys. Res., 67, 3673, 1962.

7. Axford, W.I., and C.O. Hines, A unifying theory of high-latitude geophysical phenomena and geomagnetic storms, Can. J. Phys. 39, 1433, 1961.

8. Axford, W.I., The interaction between the solar wind and the earth's magnetosphere, J. Geophys. Res., 67, 3791, 1962.

9. Barrington, R.E., E.V. Thrane, and B. Bjelland, Can. J. Phys., 41, 271, 1963.

10. Beard, D.B., The interaction of the terrestrial magnetic field with the solar corpuscular radiation, J. Geophys. Res. 65, 3559, 1960.

11. Belrose, J.S., Proc. AGARD Conf., Munich, Germany 1962.

12. Belrose, J.S., and E. Cetiner, Measurement of electron densities in the ionospheric D-region at the time of a 2^+ solar flare, Nature, 195, 688, 1962.

13. Belrose, J.S. Proc. NATO Advances Study Institute, Norwy, 1963.

97/.....

14. Biermann, L., Solar corpuscular radiation and the interplanetary gas, Observatory 77, 109, 1957.

15. Birkeland, K., The Norwegian Aurora Polaris Expedition 1902 - 1903, Aschenhoug and Co., Christiania, 1908.

16. Brown, R.R., Balloon observations of auroral-zone X-rays, J. Geophys. Res., 66, 1379, 1961.

17. Cahill, L.J., The geomagnetic field, Space Physics, Wiley and Sons, New York, London, Sydney, 1964.

18. Carter, R.E., F. Reines, J.J. Wagner, and M.E.Wyman, Free antineutrino absorption cross section, 2, Expected cross section from measurements of fission fragment electron spectrum, Phys. Rev., 113, 280, 1959.

19. Chamberlain, J.W., Physics of the aurora and airglow, Academic Press, New York and London, 1961.

20. Chapman, S., and V.C.A. Ferraro, A new theory of magnetic storms, Terr. Mag. and Atmos. Elect., Part I 36, 77 - 97, 171 - 186, 1931. Part II, 38, 79-96, 1933.

21. Chapman, S., and V.C.A. Ferraro, The theory of the first phase of a geomagnetic storm, Terr. Mag. and Atmos. Elect., 45, 245, 1940.

22. Chapman, S., and C.G. Little, J. Atm. Terr. Phys., 10, 20, 1957.

23. Christofilos, N.C., Trapping and lifetime of charged particles in the geomagnetic field, Univ, Calif. Radiation Lab. Rept., U.C.R.L. 5407, 1958.

24. Christofilos, N.C., The Argus experiment, J. Geophys. Res., 64, 869, 1959.

25. Coleman, P.J., L. Davis, and C.P. Sonett, steady component of the interplanetary magnetic field, Pioneer 5, Phys. Rev. Letters, 5, 43, 1960.

26. Davis, L.R., O.E. Berg, and L.H. Meredith, Direct measurements of particle fluxes in and near auroras, Space Research 1, 721, 1960.

27. Dessler, A.J., and R. Karplus, Some effects of diamagnetic ring currents on Van Allen radiation, J. Geophys. Res., 66, 2289, 1961.

98/....

28. Dessler, A.J., and R.D. Juday, Configuration of auroral radiation in space, Planetary Space Sci., 13, 63, 1965.

29. Dudziak, W.F., D.D. Kleinecke, and T.J. Kostigen, Graphic displays of geomagnetic geometry, General Electric Company, Santa Barbara, California, 1963.

30. Dungey, J.W. Cosmic electroclynamics, Cambridge University Press, 1958.

31. Fejer, J.A., The absorption of short radio waves in the ionospheric D and E regions, Radiowave Absorption in the Ionosphere (AGARD ograph 53) Permagen Press, 260, 1962.

32. Frank, L.A., J.A. Van Allen, W.A. Whelpley, and J.D. Craven, Absolute intensities of geomagnetically trapped particles with Explorer 14, J. Geophys. Res. 68, 1573, 1963.

33. Frank, L.A., J.A. Van Allen, and H.K. Hills, A study of charged particles in the earth's outer radiation zone with Explorer 14, J. Geophys. Res. 69, 2171, 1964.

34. Frank, L.A. Inward radial diffusion of electrons of greater than 1.6 million electron volts in the outer radiation zone, J. Geophys. Res., 70, 3533, 1965.

35. Freden, S.C., and R.S. White, Phys. Rev.Letters, 3, 9, 1959.

36. Freeman, J.W., J.A. Van Allen, and L.J. Cahill, Explorer 12 observations of the magnetospheric boundary and the associated solar plasma on September 13, 1961, J. Geophys. Res., 68, 2121, 1963.

37. Fritz, T.A., and D.A. Gurnett, Duirnal and latitudinal effects observed for 10 -kev electrons at low satellite Altitudes, J. Geophys. Res. 70, 2485, 1965.

38. Gassman, G.J. and C.P. Pike, Jr., On the observation of ionospheric effects due to dumping of trapped particles, Advances Study Institute, Bergen Norway, 1965.

99/.....

39. Ginsberg, V.L., L.V. Kurnosova, V.I. Logachev, L.A. Razorenov, I.A. Sirotkin, and M.I. Fradkin, Investigation of charged particle intensity during the flights of the second and third spaceships, Planetary Space Sci, 9, 845, 1962.

40. Gledhill, J.A., and H.O. van Rooyen, Cape Town anomaly and auroral emission, Nature, 196, 973,1962.

41. Gledhill, J.A., and H.O. van Rooyen, The South Atlantic geomagnetic anomaly and the radiation belts, 5th International Conference on Space Technology and Science, Tokyo, 1963.

42. Gledhill, J.A., and D.G. Torr, Ionospheric effects of precipitated electrons in the south radiation anomaly Space Research VI, 1965.

43. Gold, T., Motions in the magnetosphere of the earth, J. Geophys. Res., 64, 1219, 1959.

44. Goudsmit, S., and J.L. Saunderson, Phys. Rev., 57, 24, 1940.

45. Grün, A.E., Z. Naturf, 12a, 89, 1957.

46. Hall, S.E. Proc. NATO Advances Study Institute, Norway, 1963.

47. Heppner, J.P. N.F. Ness, C.S. Scearce, and T.L. Skillman, Explorer 10 magnetic field measurements, J. Geophys. Res., 68, 1, 1963.

48. Hirao, K., N. Wakai, K. Sawada, T. Hikosaka, K. Yano, and K. Maeda, Some evidence of the particle effects on the ionosphere at the middle latitude, (no date).

49. Holly, F.E., and R.G. Johnson, J. Geophys. Res., 56, 771, 1960.

50. Holt, O., B. Landmark, and F. Lied, Electron density profiles in the ionosphere and exosphere, B.Maehlum ed., Permagon, Oxford, 37, 1962.

51. Ichimiya, T.E. K. Takayama, T. Dote, Y. Aono, K. Hirao, S. Miyazake, T. Sugiyama and T. Muraoka, Nature, 190, 156, 1961.

100/.....

52. Jackson, J.E. and J.A. Kane, J. Geophys. Res., 64, 1074, 1959.

53. Jensen, D.C., and J.C. Cain, An interim magnetic field, J. Geophys. Res., 67, 3368, 1962.

54. Jespersen, M., O. Petersen, J. Rybner, B. Bjelland, O. Holt, and B. Landmark, Royal Norwegian Council for Scientific and Industrial Research, N.S.R.C., Report No. 3.

55. Johnson, F.S. The gross characteristic of the geomagnetic field in the solar wind, J. Geophys. Res., 65, 3049, 1960.

56. Judge, D.L., and P.J. Coleman, Observations of low-frequency hydromagnetic waves in the distant geomagnetic field: Explorer 6, J. Geophys. Res., 67, 5071, 1962.

57. Katz, L., and A.S. Penfold, Range-energy relations for electrons and the determination of beta-ray end-point energies by absorption, Rev. Mod. Phys., 24, 28, 1952.

58. Kellogg, P.J., Flow of plasma around the earth, J. Geophys. Res., 67, 3805, 1962.

59. Landau, L., J. Phys. (Acad. Sci. U.S.S.R.) 8, 201, 1944.

60. Landmark, B., and F. Lied, Observations of the D-region from a study of ionospheric cross modulation, Radiowave Absorption in the Ionosphere, (AGARDograph 53), Permagon Press, 92, 1962.

61. Lenchek, A.M., S.F. Singer, and R.C. Wentworth, Geomagnetically trapped electrons from cosmic ray albedo neutrons, J. Geophys. Res., 66, 4027, 1961.

62. Maeda, K., Diffusion of low energy auroral electrons in the atmosphere, J. Atm. Terr. Phys. 27, 259, 1965.

63. MacDonald, W.M., and M. Walt, Distribution function of magnetically confined electrons in a scattering atmosphere, Ann. Phys. 15, 44, 1961.

64. MacDonald, W.M. and M. Walt, Diffusion of electrons in the Van Allen radiation belt 2. Particles with mirroring points at low altitude, J. Geophys. Res., 67, 5025, 1962.

101/.....

65. McDiarmid, I.B., and E.E. Budzinski, Angular distributions and energy spectra of electrons associated with auroral events, Can. J. Phys. 42, 2048, 1964.

66. McIlwain, C.E. Direct measurements of protons and electrons in visible aurorae, Space Research 1, 715, 1960.

67. McIlwain, C.E., Co-ordinates for mapping the distribution of magnetically trapped particles, J.Geophys. Res. 66, 3681, 1961.

68. McIlwain, C.E., The radiation belts, natural and artificial, Science, 142, 355, 1963.

69. Meinel, A.B., Astrophys. J., 113, 50, 1951.

70. Mott, N.F. Proc. Roy. Soc. A124, 425, 1929.

71. Nakada, M.P. J.W. Dungey, and W.N. Hess, On the origin of the outer-belt protons, 1, J. Geophys. Res. 70, 3529, 1965.

72. Ness, N.F., C.S. Scearce, J.B. Seek, and J.M. Wilcox, A summary of results from Imp -I magnetic field experiment, Space Research VI, 1965.

73. Neugebauer, M., and C.W. Snyder, Jet Propulsion Lab. Tech. Memo. N. 33 - 111, 1962.

74. Nicolet, M., and A.C. Aikin, The formation of the D-region of the ionosphere, J. Geophys. Res., 65, 1469, 1960.

75. Nishida, A., and L.J. Cahill, Jr., Sudden impulses in the magnetosphere observed by Explorer 12, J. Geophys. Res., 69, 2243, 1964.

76. Northrup, T.G. and E. Teller, Stability of the adiabatic motion of charged particles in the earth's field, Phys. Rev., 117, 215, 1960.

77. O'Brien, B.J. Lifetimes of outer-zone electrons and their precipitation into the atmosphere, J. Geophys. Res., 67, 3687, 1962.

78. O'Brien, B.J., High-latitude geophysical studies with satellite Injun 3. 3. Precipitation of electrons into the atmosphere, J. Geophys. Res. 69, 13, 1964.

102/....

79. O'Brien, B.J. and H. Taylor, High-latitude geophysical studies with satellite Injun 3. 4. Auroras and their excitation, J. Geophys. Res., 69, 45, 1964.

80. Omholt, A., Astrophys. J. 126, 461, 1957.

81. Omholt, A. Geophys. Publikasjoner, 20, 1, 1959.

82. Parker, E.N. Geomagnetic fluctuations and the form of the outer zone of the Van Allen radiation belt, J. Geophys. Res., 65, 3117, 1960.

83. Parthasarathy, R., G.M. Lefold, and C.G. Little, Deviation of electron-density profiles in the lower ionosphere using radio absorption measurements at multiple frequencies, J. Geophys. Res., 68, 3581, 1963.

84. Piddington, J.H. J. Geophys. Res, 65, 93, 1960.

85. Ray, E.C. On the theory of protons trapped in the earth's magnetic field, J. Geophys. Res. 65, 1125, 1960.

86. Rees, M.H., Auroral ionization and excitation by incident energetic electrons, Planetary Space Sci., 11, 1209, 1963.

87. Roederer, J.G., and J.A. Welch, Calculations of longitude dependence of geomagnetically trapped electron fluxes, Part I. The general Fokker-Planck equation for electron diffusion, N.A.S.A. rept. X - 640 - 65, 149, 1965.

88. Rohrlich, F, and B.C. Carlson, Phys. Rev. 93, 38, 1954.

89. Rourke, G.F., Gross effect of electron precipitation events on magnetic bay disturbances, Research and Advanced Development Division, Avco Corporation Tech. Report, RAD - TR - 64 - 41, 1965.

90. Schmidt, A, Erdmagnetismus, Enzyklopadie der mathematischen Wissenschaften, Band VI, Leipzig, 1917.

91. Seward, F.D. and H.N. Kornblum, Jr., Near-earth charged-particle backgrounds measured with polar orbiting satellites, University of California, UCRL 6693, 1963.

92. Singer, S.F., A new model of magnetic storms and aurora, Trans. Am. Geophys Union, 38, 175, 1957.

103/.....

93. Sharp, G.W., W.L. Imhof, and R.G. Johnson. Direct evidence for corpuscular radiation effects on the ionosphere in the Southern Anomaly region, Cospar Conference, Buenos Aires, 1965.

94. Sharp,R.D., J.E. Evans, R.G. Johnson, and J.B.Reagan, Measurement of total energy flux of electrons precipitating on auroral zones, Space Research 5, 282, 1965.

95. Smith, L.G. Geophys. Corp. America Tech. Report, 63 - 19 - N, 1963.

96. Sonett, C.P., D.L. Judge, A.R. Sims, and J.M. Kelso, A radial rocket survey of the distant geomagnetic field, J. Geophys. Res. 65, 55, 1960.

97. Spencer, L.V. Nat. Bur. Stand. Monogr. No. 1. 1959.

98. Spitzer, L, Physics of fully ionized gases, Interscience Publishers Ltd., London, 1956.

99. Störmer, C., The Polar Aurora, Oxford Univ. Press, London and New York, 1955.

100. Swift, D.W., The effect of solar X-rays on the ionosphere, Radiowave Absorption in the Ionosphere (AGARDograph 53), Permagon Press, 29, 1962.

101. Taylor, H.E., and E.W. Hones, Jr. Adiabatic motion of auroral particles in a model of the electric and magnetic fields surrounding the earth, J.Geophys. Res., 70, 3605, 1965.

102. (a) Titheridge, J.E., J. Atmos. Terr. Phys. 17, 126, 1959.

102. Titheridge, J.E., J. Atmos. Terr. Phys. 24, 269, 1962.

103. Van Allen, J.A. Direct detection of auroral radiation with rocket equipment, Proc. Natl. Acad. Sci. U.S. 43, 57, 1957.

104. Van Allen, J.A. C.E. McIlwain, and G.H. Ludwig, Satellite observations of electrons artificially injected into the geomagnetic field, J. Geoph. Res. 64, 877, 1959.

105. Van Allen, J.A. Further investigations of the artificial radiation belts, State Univ. Iowa Rept. SUI 63-11, 1963.

104/.....

106. Vegard, L., Phil. Mag., 42, 47, 1921.

107. Vernov, S.N., A.E. Chudakev, P.V. Vakulov, and Yu. I. Logchev., Planetary Space Sci., 9, 855, 1962.

108. Walt, M. and W.M. MacDonald, Energy spectrum of electrons trapped in the geomagnetic field, J. Geophys. Res. 66, 2047, 1961.

109. Walt, M, and W.M. MacDonald, Diffusion of electrons in the Van Allen radiation belt. 1. Treatment of particles with mirroring points at high altitude, J. Geophys. Res., 67, 5013, 1962.

110. Walt M, G.E. Crane, and W.M. MacDonald, Analysis of atmospheric loss rates for geomagnetically trapped particles, Space Research IV, 631, 1963.

111. Walt, M., The effects of atmospheric collisions on geomagnetically trapped electrons, J. Geophys. Res., 69, 3947, 1964.

112. Welch, J.A. and W.A. Whitaker, Theory of geomagnetically trapped electrons from an artificial source, J. Geophys. Res., 64, 909, 1959.

113. Welch, J.A., R.L. Kaufmann, and W.N. Hess, Trapped electron. time histories for L = 1.18 to L = 1.30, J. Geophys. Res. 68, 685, 1963.

114. Wentworth, R.C., W.M. MacDonald and S.F. Singer, Lifetimes of trapped radiation belt particles determined by Coulomb scattering, Phys. Rev. Fluids 2, 499, 1959.

115. Williams, D.J., and J.W. Kohl, Loss and replenishment of electrons at middle latitudes and high B values, J. Chephys. Res., 70, 4139, 1965.

116. Wolfe, J.H., R.W. Silva, and M.A. Myers, Preliminary results from the Ames Research Centre plasma probe observations of the solar-wind - geomagnetic field interaction region on Imp II and Ogo I, Nasa report.